Chapter 9

Production, Fragmentation and Spectroscopy

G. Bodwin, E. Braaten, K. Byrum, R.K. Ellis, G. Feild, S. Fleming, W. Hao, B. Harris, V.V. Kiselev, E. Laenen, J. Lee, A. Leibovich, A. Likhoded, A. Maciel, S. Menary, P. Nason, E. Norrbin, C. Oleari, V. Papadimitriou G. Ridolfi, K. Sumorok, W. Trischuk, R. Van Kooten

The Tevatron is distinguished from the other current facilities involved in the study of particles containing heavy quarks by the size of the cross sections and the range of hadrons containing heavy quarks which are produced. The production of heavy quarks at the Tevatron and their subsequent fragmentation to a wide range of states is the subject of the present chapter. These processes offer a unique chance to study the dynamics of heavy quark systems in a region where perturbative methods can be applied.

9.1 Open beauty production

We outline the state of the art in theoretical calculations of B hadron production at a hadron collider. We refer to this as open beauty production to distinguish it from quarkonium production considered in Section 9.2. We follow up with some considerations of the experimental difficulties involved in measuring open beauty production at the Tevatron. We do not draw any firm conclusion beyond the fact that theory and experiment disagree by a factor of about 3. The discrepancy favors the experiments by providing three times as many b quarks as theory would expect.

9.1.1 The theory of b-quark production[†]

The cross section for the production of a b quark is calculable in perturbative QCD inasmuch as the heavy quark mass, m, is larger than Λ, the scale of the strong interactions. The results of the calculations are described in refs. [1–5].

[†]Author: R.K. Ellis

The cross section in the QCD improved parton model is

$$\sigma(S) = \sum_{i,j} \int \frac{dx_1}{x_1}\frac{dx_2}{x_2}\, \hat{\sigma}_{ij}(x_1 x_2 S, m^2, \mu^2) F_i(x_1, \mu^2) F_j(x_2, \mu^2) \,, \tag{9.1}$$

where the F_i are the momentum densities of the partons in the incoming hadrons. The quantity $\hat{\sigma}_{ij}$ is the short distance cross section

$$\hat{\sigma}_{ij}(\hat{s}, m^2, \mu^2) = \sigma_0 \; c_{ij}(\hat{\rho}, \mu^2) \,, \tag{9.2}$$

where $\sigma_0 = \alpha_s^2(\mu^2)/m^2$, $\hat{\rho} = 4m^2/\hat{s}$ and $\hat{s} = x_1 x_2 S$ is the parton total center-of-mass energy squared. The function c_{ij} has a perturbative expansion,

$$c_{ij}(\hat{\rho}, \mu^2/m^2) = c_{ij}^{(0)}(\hat{\rho}) + 4\pi\alpha_s \Big[c_{ij}^{(1)}(\hat{\rho}) + \ln(\frac{\mu^2}{m^2}) \bar{c}_{ij}^{(1)}(\hat{\rho}) \Big] + O(\alpha_s^2) \,. \tag{9.3}$$

The lowest order short distance cross section is calculated from the diagrams in Fig. 9.1. The results for the lowest order total cross sections derived from these diagrams are

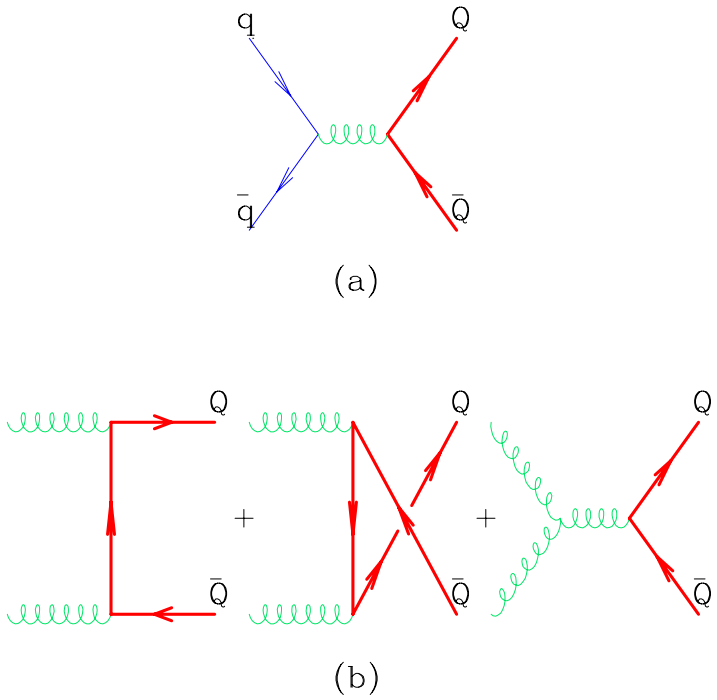

Figure 9.1: Diagrams for heavy quark production at lowest order.

$$\begin{aligned} c_{gg}^{(0)}(\rho) &= \frac{\pi\beta\rho}{12}\left\{ \frac{3}{N}\Big[(1+\rho-\frac{\rho^2}{2})L(\beta) - 1 - \rho\Big] + \frac{N}{2V}\Big[3\rho^2 L(\beta) - 4 - 5\rho\Big] \right\} \,, \\ c_{q\bar{q}}^{(0)}(\rho) &= \frac{V}{N^2}\frac{\pi\beta\rho}{24}[2+\rho] \,, \end{aligned} \tag{9.4}$$

where $V = N^2 - 1 = 8, N = 3$ and $\beta = \sqrt{1-\rho}, \rho = 4m^2/\hat{s}$ and

$$L(\beta) = \frac{1}{\beta}\log\Big[\frac{1+\beta}{1-\beta}\Big] \,. \tag{9.5}$$

The quantities $\bar{c}_{ij}^{(1)}$ and $c_{ij}^{(1)}$ are also known [1], the former analytically and the latter as a numerical fit. The results for these functions as a function of the incoming $\hat{s}$ are shown in Figs. 9.2, 9.3 and 9.4. Two features of $c_{ij}^{(1)}$ as shown in Figs. 9.2, 9.3 and 9.4 are worthy

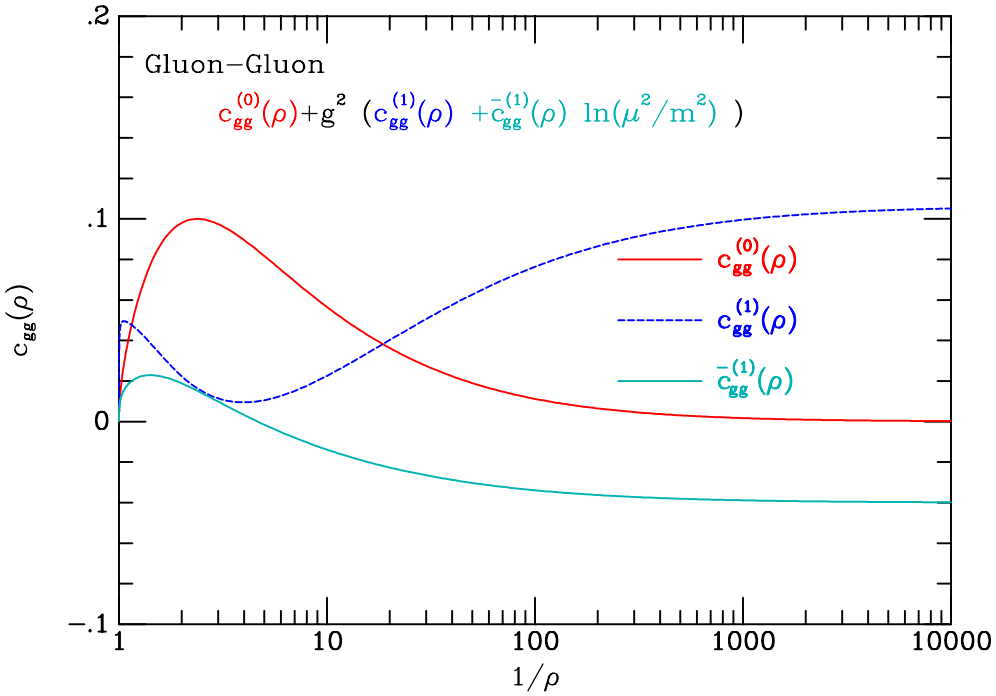

Figure 9.2: The parton level cross section for the gg process.

of note. The quark-antiquark and gluon-gluon initiated processes have a very rapid rise at threshold:

$$c_{q\bar{q}}^{(1)} \to \frac{c_{q\bar{q}}^{(0)}(\rho)}{8\pi^2}\left[-\frac{\pi^2}{6\beta}+\frac{16}{3}\ln^2(8\beta^2)-\frac{82}{3}\ln(8\beta^2)\right],$$
$$c_{gg}^{(1)} \to \frac{c_{gg}^{(0)}(\rho)}{8\pi^2}\left[\frac{11\pi^2}{42\beta}+12\ln^2(8\beta^2)-\frac{366}{7}\ln(8\beta^2)\right], \tag{9.6}$$

due to Coulomb $1/\beta$ singularities and to Sudakov double logarithms. Near threshold, these terms give large contributions and require special treatment, such as resummation to all orders. In addition the gg and gq contributions to $c_{ij}^{(1)}$, which involve spin-one gluon exchange in the t-channel, tend to a constant value at large $\hat{s}$. In agreement with the results in Figs. 9.2 and 9.4, the intercept at large s is given by

$$c_{gg} \to 6k \sim 0.1074\ , \tag{9.7}$$
$$c_{gq} \to \frac{4}{3}k \sim 0.02388\ , \tag{9.8}$$

where [6]

$$k = \frac{7291}{16200}\frac{1}{8\pi} \approx 0.01791\ . \tag{9.9}$$

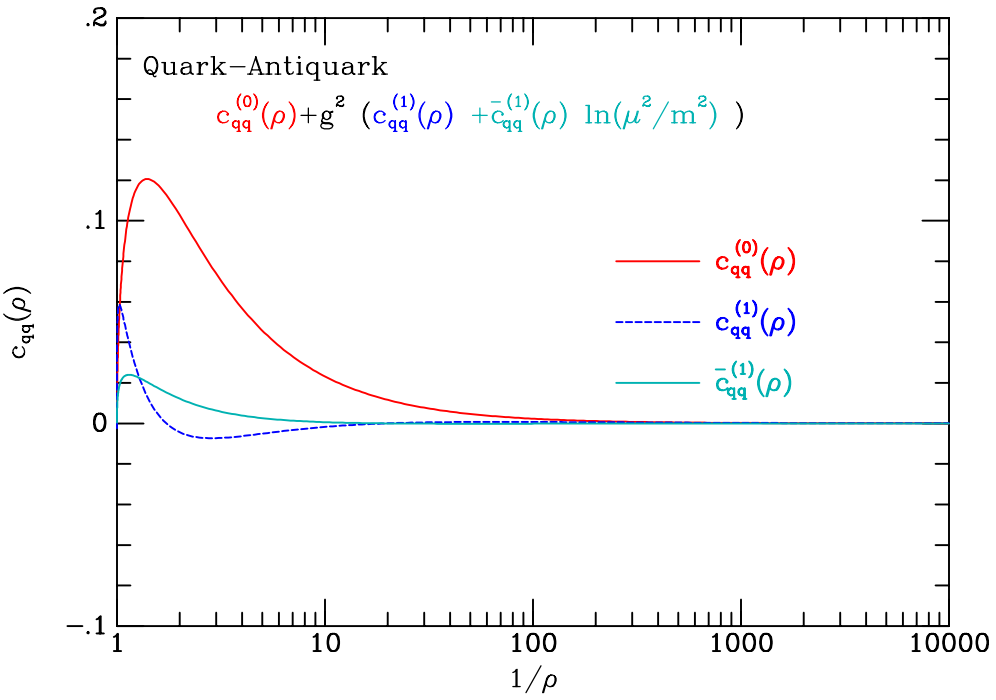

Figure 9.3: The parton level cross section for the $q\bar{q}$ process.

The significance of these results for the NLO cross section is shown in Fig. 9.5, illustrating that, at the energy of the Tevatron, both the threshold region and the large $\hat{s}$ region are important at NLO.

The resummation of the threshold soft gluon corrections is best carried out in ω-space, where ω is the moment variable after Mellin transform with respect to $\hat{s}$. In ω-space the threshold region corresponds to the limit $\omega \to \infty$ and the structure of the threshold corrections is as follows

$$\hat{\sigma} = \sigma^{LO}\Big\{1 + \sum_{j=1}^{\infty}\sum_{k=1}^{2j} b_{jk}\alpha_s^j \ln^k \omega\Big\} \ . \tag{9.10}$$

Detailed studies [7] indicate that such threshold resummation is of limited importance at the Tevatron where b-quarks are normally produced far from threshold. Resummation effects lead to minor changes in the predicted cross section and only a slight reduction in the scale dependence of the results.

At high energy, heavy quark production becomes a two scale problem, since $\hat{s} \gg m^2 \gg \Lambda^2$ and the short distance cross section contains logarithms of $\hat{s}/m^2$. As we proceed to higher energies such terms can only become more important, so an investment in understanding these terms at the Tevatron will certainly bear fruit at the LHC. At small ω the dominant terms in the heavy quark production short distance cross section are of the form

$$\hat{\sigma} \sim \frac{\alpha_s^2}{m^2}\sum_{j=0}^{\infty}\alpha_s^j\sum_{k=0}^{\infty}c_{jk}\Big(\frac{\alpha_s}{\omega}\Big)^k \ . \tag{9.11}$$

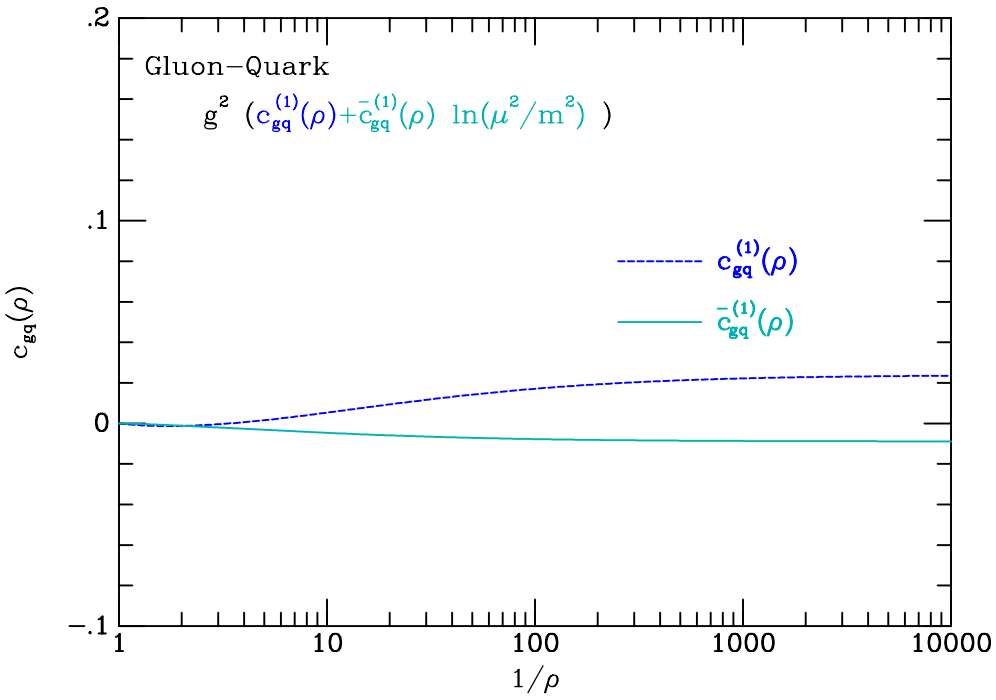

Figure 9.4: The parton level cross section for the gq process.

For $j = 0$ we obtain the leading logarithm series. Resummation of these terms has received considerable theoretical attention in the context of the k_T-factorization formalism [8–14].

In Ref. [15] an interpretation of the excess bottom-quark production rate at the Tevatron is proposed via the pair-production of light gluinos, of mass 12 to 16 GeV, with two-body decays into bottom quarks and light bottom squarks. Among the predictions of this SUSY scenario, the most clearcut is pair production of like-sign charged B mesons at the Tevatron collider.

9.1.2 Run II reach for b-quark production

We now consider some of the experimental boundary conditions on the determination of the cross-section for open beauty production at the Tevatron.

9.1.3 DØ Study of b Jet Production and Run II Projections [†]

The differential cross section for b-jet production as a function of jet transverse energy is obtained from a sample of muon tagged jets. We discuss b jets as an added tool for understanding b production, and use the present analysis to propose a follow up measurement in Run II. Focus on doubly tagged, two b-jet events should significantly reduce both theoretical and experimental uncertainties.

[†]Author: Arthur Maciel

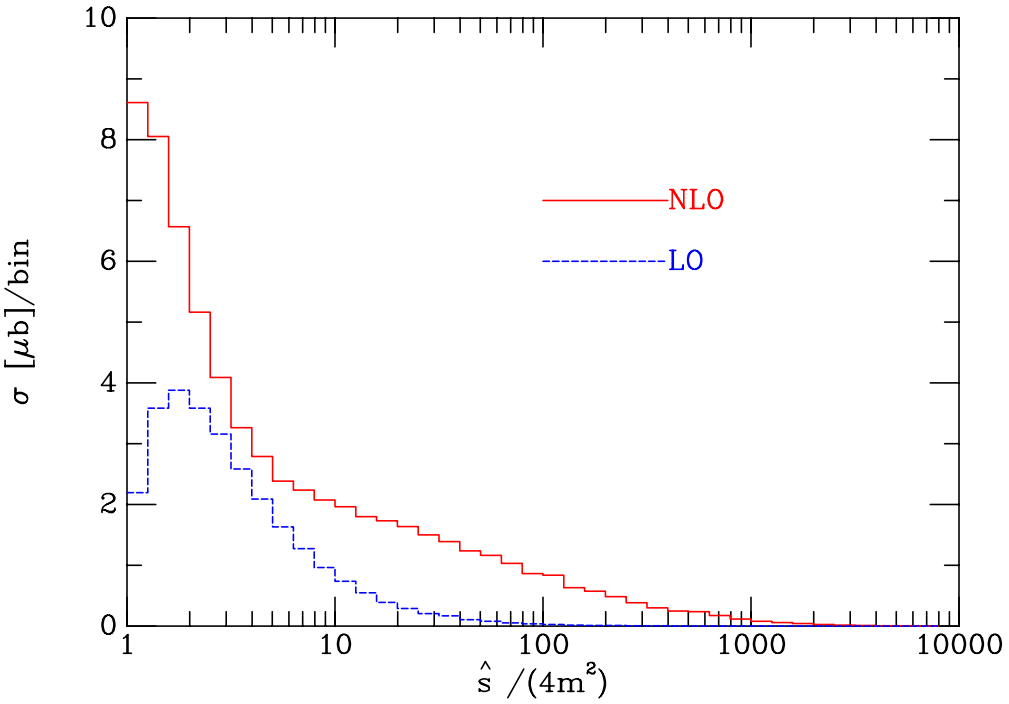

Figure 9.5: Contributions to the total cross section in LO and NLO.

9.1.3.1 Introduction

Previous studies on inclusive b production by the DØ collaboration have concentrated on the b quarks themselves, either as integrated production rates as a function of the b quark p_T^{min} [16], or the azimuthal correlations between the $b\overline{b}$ pair [17].

In contrast with such studies, we present a complementary measurement with the main focus on "b jets" rather than b quarks. "b jets" are defined as hadronic jets carrying b flavor. As such, the object of study is directly observable, and introduces less model dependence when the connection between observation and theory is made.

This measurement is in direct correspondence with a NLO-QCD calculation by S. Frixione and M. Mangano [19], who highlight the theoretical advantages of considering the cross section for producing jets rather than open quarks. For instance, large logarithms that appear at all orders in the open quark calculation (due to hard collinear gluons) are naturally avoided when all fragmentation modes are integrated and it no longer matters what portion of the jet energy is carried by heavy quarks or by radiation.

Following a brief presentation of our results, we try to assess what improvements over present measurements can be expected in Run II, taking into account the upgraded capabilities of the DØ detector. Moreover, we consider new experimental possibilities that might contribute to the ongoing process of understanding heavy quark production in the context of perturbative QCD.

9.1.3.2 The p_t Spectrum of b Jets

This measurement uses 5 pb^{-1} of Run I data from a muon plus jet trigger, from which an inclusive sample of muon tagged jets is extracted. Tagged jets have hadronic E_T above 20 GeV, pseudorapidity $\eta < 0.6$, and carry within their reconstruction cone ($\Delta R \equiv \sqrt{\Delta\eta^2 + \Delta\phi^2} = 0.7$) a muon track with p_T above 6 GeV and $\eta < 0.8$. About 36K events are thus selected, and less than 0.5% of them have either a second tagged jet or a doubly tagged one. This is because of the relatively high muon threshold, which also enriches the b flavor content of the sample.

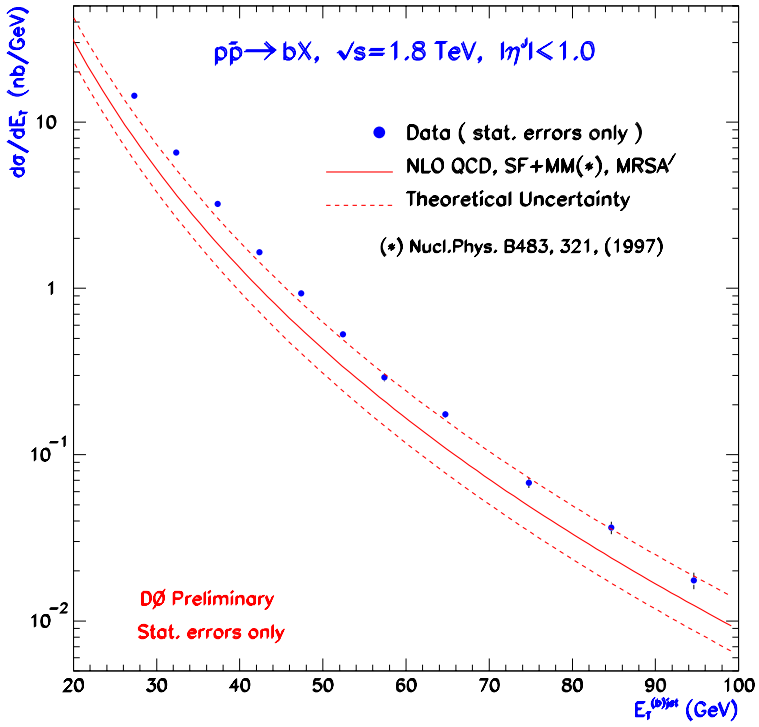

Figure 9.6: The differential b jet cross section and the next-to-leading order QCD prediction [19]. Data errors shown here are statistical only.

After detection efficiencies and resolution corrections are applied to the inclusive spectrum, the background of light flavors decaying to muons needs to be removed. This is done on a statistical basis, through fits of the distribution of muon transverse momentum with respect to the associated jet axis (P_T^{rel}). We use Monte Carlo templates representing light and heavy quark decay patterns. These templates are floated so as to fit the observed P_T^{rel} spectra in four different transverse energy ranges. Such fits determine the fraction of muons from b decay as a function of tagged jet E_T.

Tagging acceptance corrections are the last step towards a cross section. These stem from the tagging muon threshold, pseudorapidity ranges and the muon-jet association criterion.

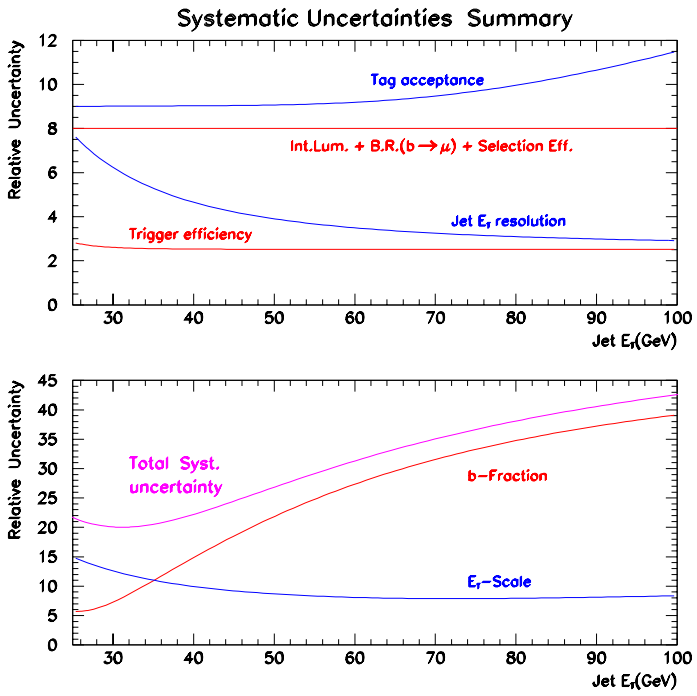

Figure 9.7: A summary of all systematic uncertainties expressed as a relative percentage.

The unseen lepton energy along the jet also needs to be added (statistically) to the hadronic portion registered in the calorimeter. After such corrections we obtain the b jet differential cross section shown in Fig. 9.6 and defined as the total number of jets carrying one or more b quarks in a given jet E_T bin, and within $|\eta| < 1$. ($\overline{b}$'s are not counted; technically we count tagging muons of either charge, and divide by twice the inclusive branching ratio of $b \to \mu + X$).

It is observed that this result repeats the general pattern of past b-production studies where data lies significantly above the central values of theory prediction, but not incompatibly so, considering both the experimental and theoretical uncertainties.

The measurement uncertainties are driven by the P_T^{rel} fits for the b-fraction, and to a lesser extent the tagging acceptance losses, and calorimeter energy scale at lower E_T. A summary of the systematic uncertainties (mostly correlated) in this measurement is shown in Fig. 9.7, and this leads us naturally to a discussion of Run II possibilities.

9.1.3.3 b Tagging for Run II

A detector with a precision vertex detector and a magnetic spectrometer should be able to study b jets. The measurement described above is limited in many directions by its tagging method. First, the b content of the sample decreases with jet E_T, and the P_T^{rel} fit

is not sensitive enough to extract a b signal reliably for jets above 100 GeV. Second, part of the advantage of studying b jets over b quarks is the removal of fragmentation model dependence. This dependence is partially reintroduced when corrections for muon tagging acceptances are performed.

The use of displaced vertex distributions for b tagging not only reduces the b fraction uncertainty to a secondary level in the analysis, but also removes the current upper limit on jet E_T imposed by the P_T^{rel} fits. Some fragmentation model dependence still remains associated with the determination of proper time distributions (decay lengths).

9.1.3.4 A Measurement Proposal

One puzzle that arises in the comparison of heavy flavor production data to theory is that despite the discrepancy in normalization, there is generally fair agreement in angular correlations [17,18,20]. This brings some conflict to the understanding of relative effects between the leading- and next-to-leading-order QCD amplitudes. The goal of resolving this puzzle, coupled with an interest in b jets, suggests a promising program for Run II.

In an attempt to minimize the current uncertainties on both theory and experiment, we consider a production measurement that is restricted to a limited kinematic regime to optimize uncertainties. We consider the cross section for pairs of b jets which are nearly back-to-back, have relatively high E_T and lie in the central rapidity region.

From the theoretical point of view, this experiment favors phase space regions that are far from production thresholds and have high x-values where PDF choices play a much reduced role. In addition, the back-to-back kinematics suppresses NLO amplitudes in the pQCD calculation [18].

From the experimental point of view there are many advantages. A muon plus jet trigger, very natural to the DØ architecture, (i) enhances the b-content of the sample, (ii) collects an ideal sample for a second tag by displaced vertex on the non-muon side and (iii) minimizes the bias towards soft b quarks inside hard jets because of the imposed muon p_T threshold.

9.1.3.5 Di-b-jets with DØ in Run II.

Inspection of Run I DØ data shows that over 70% of the muons in a muon plus jet trigger are naturally associated with a jet. Double tagging (of the b and $\overline{b}$ jets with muon and displaced vertex) improves b purity, and largely removes the limitations that are inherent to the P_T^{rel} fits method, in particular the limitation to low E_T because of increasing systematic uncertainties with b jet E_T.

For acceptance projections we take the Run I measurement as a starting point: 36K events in 5 pb^{-1} of data. The requirement of a recoil jet (central, opposite hemisphere) having $E_T \geq 20$ GeV reduces the sample to 15K muon tagged (p_T above 6 GeV) back-to-back dijet events. With a vertex tagging rate near 10% for the opposite jet, we can establish a rule of thumb of 300 events per pb^{-1}.

To access the transverse momentum of the b quark inside the muon tagged jet, we can focus on the tagging muon p_T spectrum (see next section). By applying the methods in reference [16] for determining the minimum b quark p_T compatible with our muon and jet thresholds, we find $p_T^{min}(b)$ around 20 GeV.

9.1.3.6 b Quark Production

A natural extension to the Run I b-jets study presented above is to use the same data sample and study b quarks rather than b jets. This offers a consistency check of our previous measurements [16,17], but also significantly extends the kinematic reach.

Starting from the data sample described in Section 9.1.3.2 we repeat the analysis steps of [16] to obtain the integrated b quark production cross section as a function of minimum b quark p_T. Our results are shown in Fig. 9.8 as the higher p_T^{min} points (triangles). In this figure, the present (and preliminary) measurement is confronted with previous results from DØ, CDF (resonant dimuons), and theory [5].

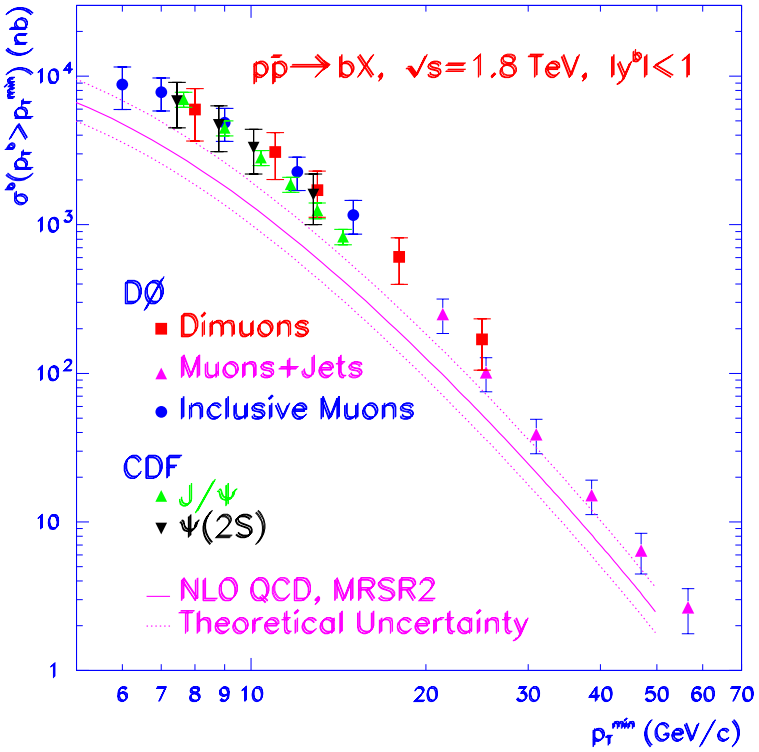

Figure 9.8: A summary of b production (integrated) cross section measurements, shown as a function of minimum b-quark p_T. The preliminary analysis described here is represented by the higher $p_T^{min}(b)$ triangles. The QCD prediction is also shown.

The consistency of the measurements is good. Our new results practically double the p_T^{min} reach to 60 GeV. A general trend that can be extracted from Fig. 9.8 is that data and theory agree better at higher p_T^{min}.

Of course this trend could be confirmed with extended and improved measurements in Run II. But the inclusive muon method described in this section has some limitations. Our uncertainties are dominated by systematics rather than statistics. Because the b-quark signal increases with muon p_T, b tagging with P_T^{rel} as a function of muon p_T is more precise than with jet E_T. It is the model dependence, introduced in relating the b-quark thresholds to the muon acceptance, that completely dominates the uncertainties in this type of measurement.

The full reconstruction of specific B-meson final states avoids some uncertainties. The CDF experiment [21] probes a lower B-meson p_T where the comparison of data to theory exhibits some of the same characteristics as the earlier measurements ($p_T^{min}(b) < 30$ GeV) in Fig. 9.8. It will be interesting to push fully reconstructed B-meson cross-sections to higher meson p_T. Various triggering and offline selection handles exist that could significantly extend meson p_T range. Such studies however lie beyond the scope of the present report.

9.1.3.7 Conclusion

We have presented a Run I cross-section measurement of jets carrying b flavor, and have illustrated the experimental advantages of studying b jets (which are complementary to b quarks). The b quark cross section extracted from the same data sample confirms previous measurements and significantly extends the b quark p_T reach, while hinting at improved agreement between data and theory at higher b p_T.

For Run II, a related measurement is envisaged that (i) focuses on dijets (doubly tagged) rather than single jets and (ii) restricts the kinematic region of the final states to reduce systematic uncertainties both in the theory and the measurements.

A muon plus jet(s) trigger is one of the strengths of the DØ experiment, and a center piece for various other physics projects. In Run II DØ will for the first time have an internal magnetic volume for precision tracking and vertexing. A muon tagged jets sample is an ideal starting point for the displaced vertex tagging of "other side" jets.

Our brief analysis demonstrates the possibility of a very useful and relatively fast measurement for early Run II.

9.1.4 CDF P_T Reach in the B Cross Section for Run II [†]

The differential cross section for $B \to D^0 + e + X$ as a function of B-hadron p_T is studied using Monte Carlo events. We predict the p_T reach for such a measurement in Run II.

The discrepancy between the next-to-leading order QCD predictions and the published Tevatron cross-sections remains unsolved. Recently, M. Cacciari, M. Greco and P. Nason [22] have presented a cross section formalism which is less sensitive to the renormalization and factorization scales at larger b-quark p_T ($p_T^b > 50$ GeV/c). We estimate the P_T reach for the B cross section using the exclusive decay $B \to D^0 + e + X$.

[†]Author: Karen Byrum

9.1.4.1 Run II P_T Reach

We use the PYTHIA Monte Carlo program to generate $b\bar{b}$ and use CLEO QQ [24] to decay the B mesons. The simulated sample is normalized to Run I data to provide a prediction of the cross section reach for Run II.

In Run II, CDF does not foresee low E_T inclusive single lepton triggers as were available in Run I. Still, we calculate Run II yields first using Run I trigger thresholds and then using the expected Run II higher thresholds. We include the following assumptions:

- an electron trigger similar to Run Ib with kinematic cuts on the electron of $E_T >$ 8 GeV and $p_T >$7.5 GeV/c or the proposed in Run II threshold of $E_T >$ 12 GeV;
- the Run Ib measured trigger efficiency;
- the electron selection efficiencies predicted by the CDF-II detector simulation;
- kinematic cuts on the D^0 decay products of $P^{\pi}_{Tot} > 0.5$ GeV/c, $P^{K}_{Tot} >$1.5 GeV/c, $\Delta(R) <$ 0.6 for both π, K; and
- a scale factor equal to the luminosity increase for Run I of 20.

Using the above assumptions, we estimate the number of $B \to D^0 eX$ events above some p_T^{min} and use this number to estimate the size for the statistical precision for a given p_T^{min}. The true statistical uncertainty will be larger than this and will depend on the signal-to-noise ratio of the D^0 mass peak. From the Run I data, we estimate that the statistical uncertainty will be a factor of two times greater than that determined from a signal-only Monte Carlo. This scale factor is conservative since we have not applied lifetime cuts to our Run I sample and these cuts are known to greatly increase the signal to noise ratio which would reduce the statistical uncertainty, approaching the predictions from a signal-only Monte Carlo.

We estimate the systematic uncertainty using the published $b \to eX$ measurement [23]. The uncertainties from that measurement are shown in Table 9.1. By measuring the B meson cross section as opposed to the b-quark cross section, we should be able to remove the systematics due to fragmentation of the b quark into a B meson from the measurement.

Source	Uncertainty
Models of B decays	10%
Underlying event contribution	8%
Hadron simulation	10%
B hadron semileptonic decay branching ratio	10%
Luminosity	7%
Total	20%

Table 9.1: Uncertainties in the published $b \to eX$ measurement [23] which are expected to contribute at the same level in Run II.

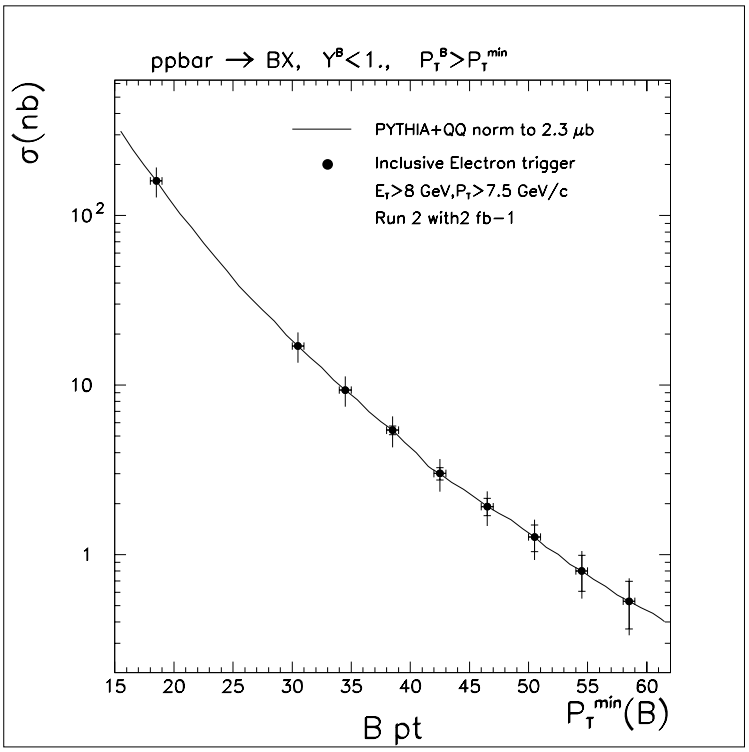

Figure 9.9: The predicted cross section reach as of function of B P_T for $B \to D^0 eX$ with the kinematic cut on the electron of $E_T > 8$ GeV and $P_T > 7.5$ GeV/c with 2 fb^{-1} of luminosity. The statistical errors are predicted from Monte Carlo and scaled by a factor of two to include the effect of background. A constant 20% systematic error is based on published results.

However there will still be an uncertainty on the theoretical prediction. The other uncertainties may be more difficult to reduce even with large statistics. For Run II we estimate a total systematic uncertainty of 20%.

9.1.4.2 Conclusions

The predicted p_T reach for $B \to D^0 eX$ with a kinematic cut on the electron of $E_T > 8$ GeV and $p_T > 7.5$ GeV/c for 2 fb^{-1} is shown in Figure 9.9. The statistical uncertainties come from our signal-only Monte Carlo simulation and scaled by a factor of two as an estimate of the influence of background. A flat 20% systematic error is based on published results [23].

We also show the predicted p_T reach for kinematic cut on the electron of $E_T > 12$ GeV for 2 fb^{-1} in Figure 9.10. The p_T requirement reduces the number of events in the largest B meson p_T bins by a modest 20%.

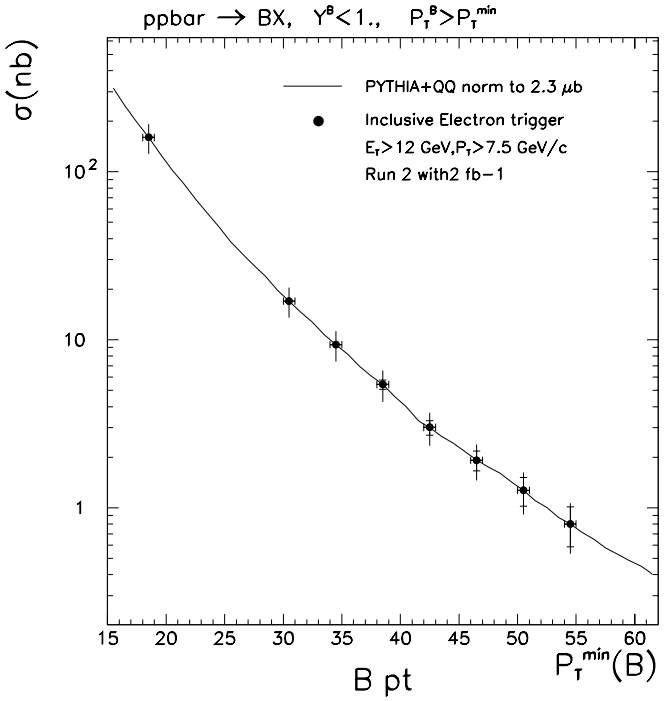

Figure 9.10: The predicted cross section reach as of function of B P_T for $B \to D^0 eX$ with the kinematic cut on the electron of $E_T > 12$ GeV/c with 2 fb^{-1} of luminosity. The statistical errors are predicted from Monte Carlo and scaled by a factor of two to include the effect of background. A constant 20% systematic error is based on published results.

9.2 Quarkonium production

The two heavy quarkonium systems provided by nature are bottomonium ($b\bar{b}$ bound states) and charmonium ($c\bar{c}$ bound states). The clean signatures provided by the $J^{PC} = 1^{--}$ quarkonium states make them a particularly clear window for studying the dynamics of heavy quarks. Although the major thrust of this report is bottom quark physics, we will discuss charmonium as well as bottomonium, since the physics of these two systems is very similar.

9.2.1 Spectroscopy †

The charmonium and bottomonium systems have rich spectra of orbital and angular-momentum excitations. The masses of these states can be predicted using potential models whose parameters are tuned to reproduce the spectrum of observed states. Some of the states that have not yet been discovered should be produced abundantly at the Tevatron. The obstacle to their discovery is finding a decay mode with a large enough branching fraction that can be used as a trigger.

†Author: Eric Braaten

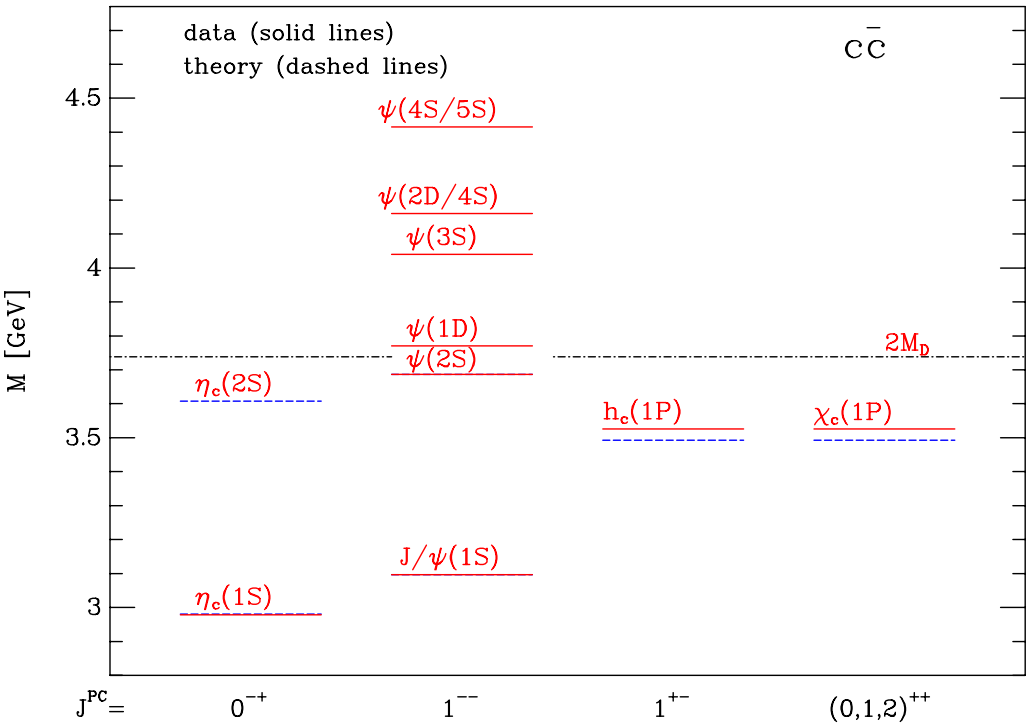

Figure 9.11: Spectrum of $c\bar{c}$ mesons: observed states (dotted red lines) and theoretical predictions (dashed blue lines). The $\chi_c(1P)$ lines are averaged over the spin states.

The charmonium spectrum is shown in Fig. 9.11. The observed states are shown as dotted (red) lines and the theory predictions are shown as dashed (blue) lines. The most prominent of the missing states are the spin-singlet states $\eta_c(2S)$ and $h_c(1P)$. A signal for $h_c \to J/\psi\pi^0$ has been observed in $p\bar{p}$ annihilation at resonance, but has not been confirmed. The states in the spectrum that were observed by the CDF collaboration in Run I of the Tevatron are the J/ψ and $\psi(2S)$, through their decays into $\mu^+\mu^-$, and the $\chi_{c1}(1P)$ and $\chi_{c2}(1P)$, through their decays into $J/\psi\gamma$. The χ_{c1} and χ_{c2}, which have a mass splitting of only 45.7 MeV, were resolved by conversions of the decay photon into e^+e^- in the material of the detector. The D0 collaboration also observed a $J/\psi/\psi(2S)$ signal, but they were unable to resolve the two states.

The charmonium state with the greatest prospects for discovery at the Tevatron is the $\eta_c(2S)$. One possibility is through the radiative decay $\eta_c(2S) \to J/\psi + \gamma$, whose branching fraction is estimated to be about 10^{-3} [25,26]. This is much smaller than the branching fraction for $\chi_{cJ}(1P) \to J/\psi+\gamma$, which is about 27% for $J = 1$ and 14% for $J = 2$. In Run Ia, CDF observed about 1200 $\chi_c(1P)$ or $\chi_c(2P)$ candidates in a data sample of about 18 pb^{-1}. The cross section for $\eta_c(1S)$ is probably a little larger than that for $\chi_c(1P) + \chi_c(2P)$. Thus the rate for $\eta_c(2S) \to J/\psi + \gamma$ should be large enough to observe in Run II.

It is also possible that the $\eta_c(2S)$ could be discovered through one of its annihilation decay modes. However a prerequisite would be the observation of the $\eta_c(1S)$, since it has a larger cross section and it probably has a larger branching fraction into any triggerable

decay mode. Of the measured decay modes of the $\eta_c(1S)$, the most promising for observation at the Tevatron is $\eta_c \to \phi\phi$, with one ϕ decaying into $\mu^+\mu^-$ to provide a trigger and the other decaying into K^+K^-. This decay path has a branching fraction of about 2×10^{-6}, which is small compared to the 6% branching fraction for $J/\psi \to \mu^+\mu^-$. The muons from the decay of the ϕ will typically be softer than those from the decay of a J/ψ with the same p_T as the $\eta_c(1S)$. The steep dependence of the acceptance of the muons on their transverse momentum could give a large reduction factor compared to the acceptance for $J/\psi \to \mu^+\mu^-$. In Run Ia, CDF observed about 2×10^5 J/ψ candidates in a data sample of about 15 pb^{-1}, and the cross section for $\eta_c(1S)$ is probably several times larger than that for J/ψ. Thus the rate for $\eta_c \to \phi\phi$ may be large enough to observe in Run II.

The bottomonium spectrum is shown in Fig. 9.12. The observed states are shown

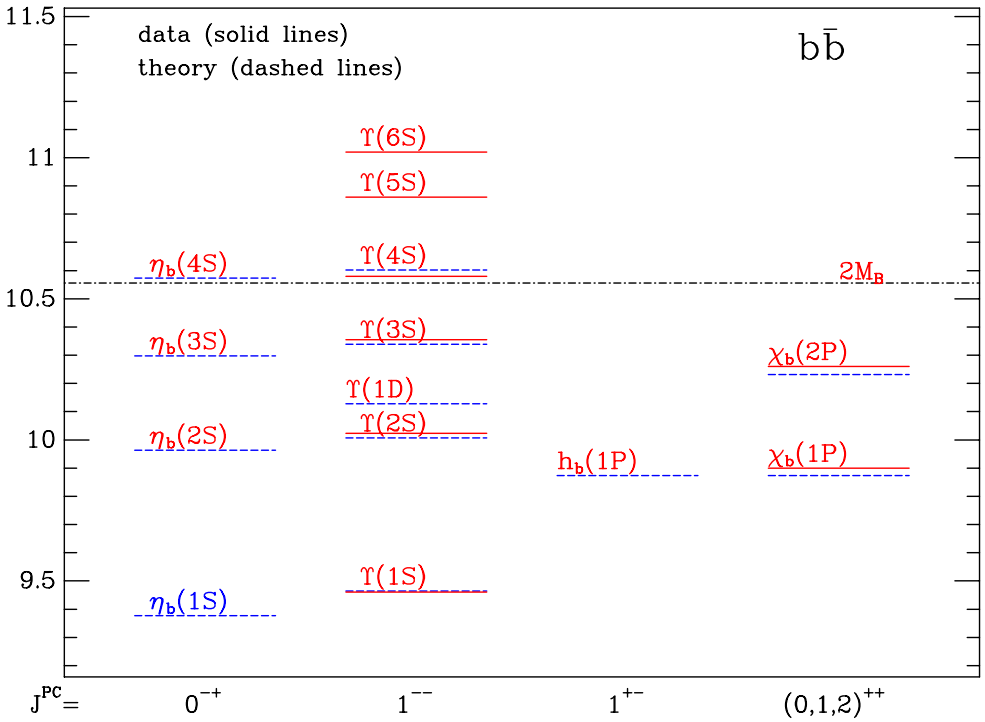

Figure 9.12: Spectrum of $b\bar{b}$ mesons: observed states (solid red lines) and theoretical predictions (dashed blue lines). The $\chi_b(1P)$ and $\chi_b(2P)$ lines are averaged over the spin states.

as dotted (red) lines and the theory predictions are shown as dashed (blue) lines. None of the spin-singlet states in the spectrum have been observed, not even the ground state $\eta_b(1S)$. The states in the spectrum that were observed by the CDF collaboration in Run I of the Tevatron are the $\Upsilon(1S)$, $\Upsilon(2S)$ and $\Upsilon(3S)$, (through their decays into $\mu^+\mu^-$), and the $\chi_{bJ}(1P)$ and $\chi_{BJ}(2P)$, (through their decays into $\Upsilon(nS)\gamma$). The $J = 0, 1, 2$ states of $\chi_{bJ}(nP)$ were not resolved. The D0 collaboration also observed a $\Upsilon(nS)$ signal, but they were unable to resolve the $n = 1, 2, 3$ states.

The bottomonium state with the greatest prospects for discovery at the Tevatron is the

ground state $\eta_b(1S)$. The discovery requires finding a triggerable decay mode with a large enough branching fraction. The branching fractions for exclusive decay modes of $\eta_b(1S)$ can not be predicted accurately. For final states containing light hadrons, a conservative estimate can be obtained by multiplying the corresponding branching fraction for $\eta_c(1S)$ by the appropriate suppression factor $(m_c/m_b)^n$ that would hold for asymptotically large quark masses. For the vector meson decay mode $\eta_b(1S) \to \rho\rho$, the appropriate factor is $(m_c/m_b)^4 \approx 10^{-2}$. A promising discovery mode at the Tevatron is $\eta_b(1S) \to J/\psi J/\psi$ [27], with one J/ψ decaying into $\mu^+\mu^-$ to provide a trigger and the other decaying into either $\mu^+\mu^-$ or e^+e^-. This decay has almost identical kinematics to $\eta_c(1S) \to \phi\phi$, whose branching fraction is 0.7%, except that all masses are scaled up by a factor of 3. The branching fraction for $\eta_b \to J/\psi J/\psi$ is probably smaller, but the suppression factor is probably not as severe as the asymptotic factor 10^{-2}. If the branching fraction for $\eta_b(1S) \to J/\psi J/\psi$ is greater than 10^{-4}, the prospects for the discovery of $\eta_b(1S)$ in Run II of the Tevatron look bright.

9.2.2 Theory of quarkonium production †

Heavy quarkonia (bottomonium and charmonium mesons) are to a good approximation nonrelativistic bound states consisting of a heavy quark and its antiquark. The bound-state dynamics involves both perturbative and nonperturbative aspects of QCD. Due to the large mass, m_Q, of the heavy quark, the bound-state dynamics can be described more simply using an effective field theory called *nonrelativistic QCD* (NRQCD) [28]. This effective field theory can be exploited to organize quarkonium production rates into systematic expansions in $\alpha_s(m_Q)$ and in v, the typical relative velocity of the heavy quark [29].

The physical picture of quarkonium production begins with a hard scattering that creates a heavy quark-antiquark pair in an angular momentum and color state that we will denote $b\bar{b}(n)$. The color state can be color-singlet ($b\bar{b}_1$) or color-octet ($b\bar{b}_8$). The angular momentum state is denoted by the standard spectroscopic notation $^{2S+1}L_J$. The $b\bar{b}$ subsequently evolves into the final state quarkonium H through nonperturbative dynamics that can be accurately described by the effective theory NRQCD.

The NRQCD factorization formula is the mathematical realization of the above picture. To be specific, we will focus on the production of spin-triplet bottomonium states. The inclusive differential cross section for producing a bottomonium state, H, in a proton-antiproton collision can be written as

$$d\sigma[p + \bar{p} \to H + X] \;=\; \sum_{ij} \int dx_1 dx_2 \; f_{i/p}(x_1) f_{j/\bar{p}}(x_2) \; d\sigma[ij \to H + X], \tag{9.12}$$

where the functions $f_{k/A}$ are parton distribution functions and the sum runs over the partons i and j in the initial state hadrons. The cross section $d\sigma[ij \to H + X]$ for the direct production of H by the collision of partons i and j can be written as the sum of products of short-distance cross sections and long-distance matrix elements:

$$d\sigma[ij \to H + X] \;=\; \sum_n d\hat{\sigma}[ij \to b\bar{b}(n) + X] \; \langle O^H(n) \rangle. \tag{9.13}$$

†Authors: Eric Braaten, Sean Fleming, Jungil Lee, Adam Leibovich

To obtain the completely inclusive cross section, one must also add the cross section for indirect production via the decay of higher bottomonium states. The short-distance cross section $d\hat{\sigma}$ can be calculated as a perturbative expansion in α_s evaluated at a scale of order m_Q or larger. The *NRQCD matrix element* $\langle O^H(n)\rangle$ encodes the probability for $b\bar{b}(n)$ to evolve into the quarkonium state H. Each of the NRQCD matrix elements scales as a definite power of v, allowing the sum over quantum numbers n in Eq. (9.13) to be truncated at some order in the v expansion. The approximate spin symmetry of NRQCD also implies relations between the matrix elements. Most of these matrix elements can be determined only by fitting them to production data. The exceptions are the color-singlet matrix elements with the same angular momentum quantum numbers as the bound state H, which can be related to the wavefunction of the meson. For the spin-triplet S-wave and P-wave bottomonium states, these color-singlet matrix elements can be expressed as

$$\langle O_1^{\Upsilon(nS)}(^3S_1)\rangle \simeq \frac{9}{2\pi}|R_{nS}(0)|^2, \tag{9.14}$$

$$\langle O_1^{\chi_{bJ}(nP)}(^3P_J)\rangle \simeq (2J+1)\frac{9}{2\pi}|R'_{nP}(0)|^2. \tag{9.15}$$

They can be extracted from data on annihilation decays, estimated from potential models, or calculated from first principles using lattice gauge theory simulations of NRQCD.

The NRQCD factorization formula provides a general framework for analyzing inclusive quarkonium production. Any model of quarkonium production that is consistent with QCD at short-distances must reduce to assumptions about the NRQCD matrix elements. For example, the *color-singlet model* assumes that only the color-singlet matrix elements with the same angular momentum quantum numbers as the bound state are important, namely $\langle O_1(^3S_1)\rangle$ for $\Upsilon(nS)$ and $\langle O_1(^3P_J)\rangle$ for $\chi_{bJ}(nP)$. To the extent that the *color-evaporation model* is consistent with QCD at short distances, it reduces to the assumption that the S-wave matrix elements $\langle O_1(^1S_0)\rangle$, $\langle O_1(^3S_1)\rangle$, $\langle O_8(^1S_0)\rangle$, and $\langle O_8(^3S_1)\rangle$ dominate and that they are equal up to color and angular momentum factors. However the color evaporation model is usually implemented by starting with the NLO cross section for producing $b\bar{b}$ pairs with invariant mass below the heavy meson threshold, imposing an ad hoc cutoff on the invariant mass of exchanged gluons, and multiplying by a phenomenological probability factor for each quarkonium state.

The effective field theory NRQCD also gives definite predictions for the relative importance of the NRQCD matrix elements, because they scale as definite powers of the typical relative velocity v. Given equal short-distance cross sections, the most important matrix element for direct $\Upsilon(nS)$ production should be the parameter $\langle O_1(^3S_1)\rangle$ of the color-singlet model. However the short-distance cross sections are not equal. From counting the color states, we expect the cross section for a color-octet $b\bar{b}$ pair to be about 8 times larger than the cross section for a color-singlet pair. There are also dynamical effects that enhance the color-octet cross section relative to that for $b\bar{b}_1(^3S_1)$ both at small p_T and at large p_T. At small p_T, the color-octet cross section is enhanced, because it can proceed through order-α_s^2 processes like $ij \to b\bar{b}$. At large p_T, the color-octet cross sections are enhanced because the leading order cross section for $b\bar{b}_1(^3S_1)$ is suppressed by m_b^4/p_T^4 relative to $b\bar{b}_8(^3S_1)$. According to NRQCD, the next most important matrix elements for direct $\Upsilon(nS)$ production

are suppressed by v^4 and can be reduced by spin-symmetry relations to three color-octet parameters $\langle O_8(^3S_1)\rangle$, $\langle O_8(^1S_0)\rangle$, and $\langle O_8(^3P_0)\rangle$ for each of the radial excitations $\Upsilon(nS)$. Including only these matrix elements, the NRQCD factorization formula (9.13) for direct $\Upsilon(nS)$ production reduces to

$$\sigma[\Upsilon(nS)] = \sigma[b\bar{b}_1(^3S_1)]\langle O_1^{\Upsilon(nS)}(^3S_1)\rangle + \sigma[b\bar{b}_8(^3S_1)]\langle O_8^{\Upsilon(nS)}(^3S_1)\rangle + \sigma[b\bar{b}_8(^1S_0)]\langle O_8^{\Upsilon(nS)}(^1S_0)\rangle + \left(\sum_J (2J+1)\sigma[b\bar{b}_8(^3P_J)]\right)\langle O_8^{\Upsilon(nS)}(^3P_0)\rangle. \quad (9.16)$$

NRQCD predicts that the most important matrix elements for the direct production of the P-wave states $\chi_{bJ}(nP)$ are suppressed by v^2 relative to $\langle O_1^{\Upsilon(nS)}(^3S_1)\rangle$. They can be reduced by spin symmetry relations to a color-singlet parameter $\langle O_1(^3P_0)\rangle$ and a single color-octet parameter $\langle O_8(^3S_1)\rangle$ for each radial excitation. Including only these matrix elements, the NRQCD factorization formula (9.13) for direct $\chi_{bJ}(nP)$ production reduces to

$$\sigma[\chi_{bJ}(nP)] = (2J+1)\left(\sigma[b\bar{b}_1(^3P_J)]\langle O_1^{\chi_{b0}(nP)}(^3P_0)\rangle + \sigma[b\bar{b}_8(^3S_1)]\langle O_8^{\chi_{b0}(nP)}(^3S_1)\rangle\right). \quad (9.17)$$

The factors of $2J+1$ comes from using spin-symmetry relations.

The NRQCD approach to quarkonium production is a phenomenologically useful framework only if the NRQCD expansion in (9.13) can be truncated after the matrix elements of relative order v^4. For S-waves, the truncation at order v^2 essentially reduces to the color-singlet model, which has been decisively ruled out by the CDF data on charmonium production in Run I [30,31]. Truncation at order v^6 introduces too many additional adjustable parameters to have any predictive power. In the NRQCD approach truncated at relative order v^4, the direct production of each S-wave radial excitation is described by four matrix elements $\langle O_1(^3S_1)\rangle$, $\langle O_8(^3S_1)\rangle$, $\langle O_8(^1S_0)\rangle$, and $\langle O_8(^3P_0)\rangle$. The production of each P-wave radial excitation is described by two matrix elements $\langle O_1(^3P_0)\rangle$ and $\langle O_8(^3S_1)\rangle$. The NRQCD framework has considerable flexibility, because the color-octet matrix elements are all adjustable parameters, but it is still restrictive enough to have predictive power. Since the color-octet matrix elements are predicted to dominate at large p_T, the NRQCD approach has sometimes been called the *color-octet model*. This terminology should be avoided, because NRQCD predicts that some production processes are dominated by color-singlet matrix elements. The phrase *NRQCD model* would more accurately reflect the theoretical assumptions that are involved.

The short-distance cross sections $d\hat{\sigma}$ in Eq. (9.13) can be calculated using perturbative QCD. Most of the parton cross sections required by the NRQCD approach have been calculated only to leading order in α_s. There are three regions of p_T that require somewhat different treatments: $p_T \ll 2m_b$, $p_T \sim 2m_b$, and $p_T \gg 2m_b$. The simplest region is $p_T \sim 2m_b$. Here the leading order cross sections are of order α_s^3 and come from the parton processes $ij \to b\bar{b} + k$. For lack of a better term, we refer to these as the *fusion cross sections*. The fusion cross sections are known only to leading order in α_s [32,33]. If they could be calculated to next-to-leading order, it would allow for more accurate predictions for quarkonium production in the region $p_T \sim 2m_b$.

That the region $p_T \gg 2m_b$ must be treated differently can be seen from the behavior of the fusion cross sections as $p_T \to \infty$. The order-α_s^3 cross sections $d\hat{\sigma}/dp_T^2$ fall like m_b^4/p_T^8 for $b\bar{b}_1(^3S_1)$, like m_b^2/p_T^6 for $b\bar{b}_1(^3P_J)$, $b\bar{b}_8(^1S_0)$, and $b\bar{b}_8(^3P_J)$, and like $1/p_T^4$ for $b\bar{b}_8(^3S_1)$. At higher orders in α_s, all the $b\bar{b}$ channels will exhibit the scaling behavior $d\hat{\sigma}/dp_T^2 \sim 1/p_T^4$. The scaling contributions can be expressed in the form

$$d\hat{\sigma}[ij \to b\bar{b}(n) + X] \;=\; \int_0^1 dz\, d\hat{\sigma}[ij \to k + X]\, D_{k\to b\bar{b}(n)}(z), \tag{9.18}$$

where $D_{k\to b\bar{b}(n)}(z)$ is the fragmentation function that specifies the probability for a parton k produced by a hard scattering to "decay" into a $b\bar{b}$ pair in the state n with a fraction z of the parton's longitudinal momentum. The fragmentation functions begin at order α_s for $b\bar{b}_8(^3S_1)$, at order α_s^2 for $b\bar{b}_1(^3P_J)$, $b\bar{b}_8(^1S_0)$, and $b\bar{b}_8(^3P_J)$, and at order α_s^3 for $b\bar{b}_1(^3S_1)$. They have all been calculated only to leading order in α_s, with the exception of the $b\bar{b}_8(^3S_1)$ fragmentation function, which has been calculated to next-to-leading order [34]. If they could all be calculated to order α_s^3, it would allow more accurate predictions for quarkonium production at large p_T.

That the region $p_T \ll 2m_b$ must be treated differently can be seen from the behavior of the fusion cross sections as $p_T \to 0$. The order-α_s^3 cross sections $d\hat{\sigma}/dp_T^2$ for $b\bar{b}_1(^3S_1)$ and for $b\bar{b}_1(^3P_1)$ are well-behaved in this limit, but those for $b\bar{b}_1(^3P_{0,2})$, $b\bar{b}_8(^3S_1)$, $b\bar{b}_8(^1S_0)$, and $b\bar{b}_8(^3P_J)$ diverge like $1/p_T^2$. These are precisely the channels in which a $b\bar{b}$ pair can be created at $p_T = 0$ by the order-α_s^2 parton process $ij \to b\bar{b}$. If the cross section is integrated over p_T, the singular term proportional to $1/p_T^2$ in the cross section for $ij \to b\bar{b} + g$ is canceled by a singular term proportional to $\delta(p_T^2)$ in the next-to-leading order correction to the cross section for $ij \to b\bar{b}$, so that the cross section integrated over p_T is finite. These next-to-leading order corrections have been calculated [35], and they allow the cross section integrated over p_T to be calculated to next-to-leading order. However what is really needed to compare with the Tevatron data is the differential cross section in p_T. To turn the naive perturbative prediction for $d\hat{\sigma}/dp_T^2$, which includes $1/p_T^2$ terms from $ij \to b\bar{b} + g$ and $\delta(p_T^2)$ terms from $ij \to b\bar{b}$, into a smooth p_T distribution requires taking into account multiple soft-gluon radiation. Reasonable prescriptions for doing this are available, but they have not yet been applied to this problem. This is the biggest obstacle to more quantitative analyses of quarkonium production at the Tevatron.

9.2.2.1 Bottomonium

A pioneering NRQCD analysis of the CDF data on bottomonium production in Run IA of the Tevatron was carried out by Cho and Leibovich [32]. An updated NRQCD analysis of the CDF data from Run Ib was recently carried out in Ref. [27]. An alternative analysis that uses PYTHIA to take into account some of the effects of soft gluon radiation has been presented in Ref. [37]. In the analysis of Ref. [27], the color-singlet matrix elements were extracted from Υ decay data or estimated using potential models. The color-octet matrix elements were extracted from the CDF cross sections for $\Upsilon(1S)$, $\Upsilon(2S)$, and $\Upsilon(3S)$ and the fractions of $\Upsilon(1S)$ coming from $\chi_b(1P)$ and $\chi_b(2P)$. To avoid the complications of soft-gluon re-summation at small p_T, the analysis used only the data for $p_T > 8$ GeV.

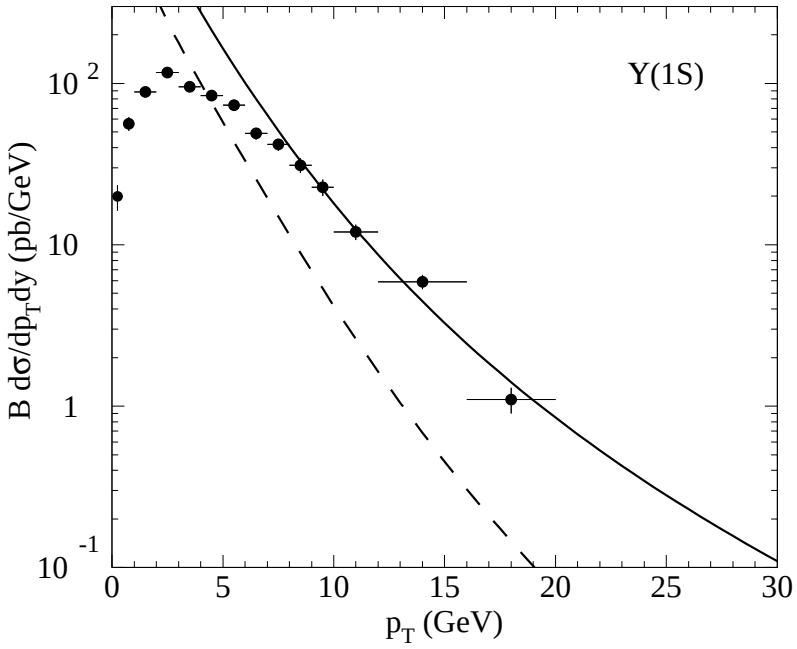

Figure 9.13: Inclusive cross section for $\Upsilon(1S)$ at Run I multiplied by its branching fraction into $\mu^+\mu^-$: CDF data, the NRQCD fit of Ref. [27] (solid line), and the color-singlet model prediction (dashed line).

Because the cross sections for $b\bar{b}_8(^1S_0)$ and $b\bar{b}_8(^3P_J)$ have similar dependences on p_T, only the linear combination $M_r = \langle O_8(^1S_0)\rangle + r\langle O_8(^3P_0)\rangle/m_b^2$ with $r \sim 5$ could be determined. Two different sets of parton distribution functions were used for the analysis: MRST98LO and CTEQ5L. The bottom quark mass was set to $m_b = 4.77 \pm 0.11$ GeV. The resulting color-octet matrix elements have large statistical error bars and many of them are consistent with zero. There are also large uncertainties due to the renormalization and factorization scales. The large errors limit the usefulness of these matrix elements for predicting bottomonium production in other high energy processes.

In Figs. 9.13, 9.14, and 9.15, we show the CDF data on the differential cross sections for $\Upsilon(1S)$, $\Upsilon(2S)$, and $\Upsilon(3S)$ at Run I of the Tevatron. The cross sections are integrated over the rapidity range $|y| \leq 0.4$ and then divided by 0.8. The solid curves are the central curves for the NRQCD fits. The dashed curves are the leading order predictions of the color-singlet model. The NRQCD curves agree with the data in the region $p_T > 8$ GeV used to fit the matrix elements, but the agreement deteriorates quickly at lower values of p_T. The data turns over and then approaches 0 at small p_T. This is to be expected, because the differential cross section $d\sigma/dp_T^2$ should be an analytic function of p_T^2, which implies that there is a kinematic zero in $d\sigma/dp_T = 2p_T d\sigma/dp_T^2$. In contrast with the data, the NRQCD curves for $\Upsilon(1S)$ and $\Upsilon(3S)$ diverge like $1/p_T$ as $p_T \to 0$. This unphysical behavior is an artifact of fixed-order perturbation theory and could be removed by carrying out the appropriate resummation of soft gluons. The NRQCD curve for $\Upsilon(2S)$ turns over and goes negative at small p_T. This unphysical behavior is an artifact of the fit, which gives a negative central value for M_5 that is consistent with zero to within the errors. The fact

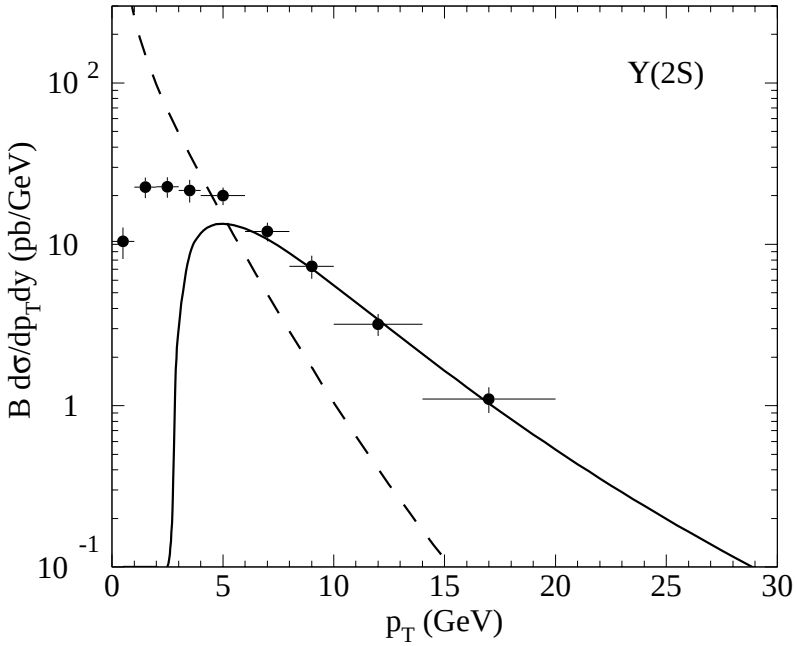

Figure 9.14: Inclusive cross section for $\Upsilon(2S)$ at Run I multiplied by its branching fraction into $\mu^+\mu^-$: CDF data, the NRQCD fit of Ref. [27] (solid line), and the color-singlet model prediction (dashed line).

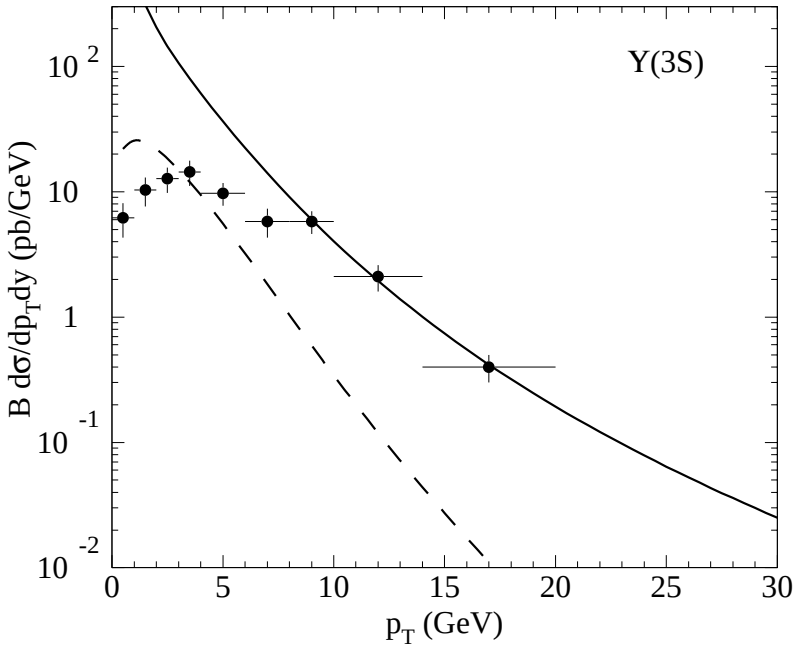

Figure 9.15: Inclusive cross section for $\Upsilon(3S)$ at Run I multiplied by its branching fraction into $\mu^+\mu^-$: CDF data, the NRQCD fit of Ref. [27] (solid line), and the color-singlet model prediction (dashed line).

H	$R^H(1.8\ \text{TeV})$	$R^H(2.0\ \text{TeV})$
$\Upsilon(3S)$	0.31 ± 0.14	0.36 ± 0.16
$\chi_{b2}(2P)$	0.44 ± 0.26	0.52 ± 0.30
$\chi_{b1}(2P)$	0.34 ± 0.16	0.39 ± 0.19
$\chi_{b0}(2P)$	0.20 ± 0.07	0.24 ± 0.08
$\Upsilon(2S)$	0.65 ± 0.35	0.76 ± 0.41
$\chi_{b2}(1P)$	0.57 ± 0.26	0.66 ± 0.31
$\chi_{b1}(1P)$	0.41 ± 0.17	0.48 ± 0.19
$\chi_{b0}(1P)$	0.23 ± 0.08	0.26 ± 0.09
$\Upsilon(1S)$	1	1.16 ± 0.02

Table 9.2: Inclusive cross sections for spin-triplet bottomonium states H at 1.8 TeV and 2.0 TeV divided by the inclusive cross section for $\Upsilon(1S)$ at 1.8 TeV. The cross sections are integrated over $p_T > 8$ GeV and $|y| < 0.4$.

that the NRQCD fit fails to describe the data below $p_T = 8$ GeV emphasizes the need for an analysis that takes into account soft gluon resummation at low p_T. Such an analysis could use the data from the entire range of p_T that has been measured, and it would therefore give matrix elements with much smaller error bars.

Because of the large uncertainties in the matrix elements, the only reliable predictions that can be made based on the NRQCD analysis of Ref. [27] are those for which the large errors cancel out. One such prediction is the increase in the cross section when the center-of-mass energy is increased from 1.8 TeV in Run I of the Tevatron to 2.0 TeV in Run II. In order to cancel out the large uncertainties in the matrix elements, it is convenient to normalize the cross section for the bottomonium state H at center-of-mass energy $\sqrt{s}$ to that for inclusive $\Upsilon(1S)$ at $\sqrt{s} = 1.8$ TeV. We therefore define the ratio

$$R^H(\sqrt{s}) = \frac{\sigma[H;\ \sqrt{s}]}{\sigma[\text{inclusive } \Upsilon(1S);\ \sqrt{s} = 1.8\ \text{TeV}]}, \tag{9.19}$$

where the cross sections are integrated over $p_T > 8$ GeV and $|y| < 0.4$. In Table 9.2, we give the ratios $R^H(\sqrt{s})$ for the inclusive production of spin-triplet bottomonium states, both at $\sqrt{s} = 1.8$ TeV and at $\sqrt{s} = 2.0$ TeV. When the center-of-mass energy is increased from 1.8 TeV to 2.0 TeV, all the cross sections increase by about the same amount. The increase depends on p_T, changing from about 15% at $p_T = 8$ GeV to about 19% at $p_T = 20$ GeV. The percentage increase for $\Upsilon(1S)$ is shown as a function of p_T in Fig. 9.16.

Another reliable application of the NRQCD analysis is to predict the cross sections for the spin-singlet bottomonium states $\eta_b(nS)$ and $h_b(nP)$. The most important matrix elements for $\eta_b(nS)$ and $h_b(nP)$ are related to those for $\Upsilon(nS)$ and $\chi_b(nP)$ by the spin symmetry of NRQCD. Thus, once the color-octet matrix elements are determined from the production of spin-triplet states, the NRQCD approach truncated at order v^4 predicts the cross sections for the spin-singlet states without any new nonperturbative parameters. The resulting expressions for the direct cross sections of $\eta_b(nS)$ and $h_b(nP)$ are

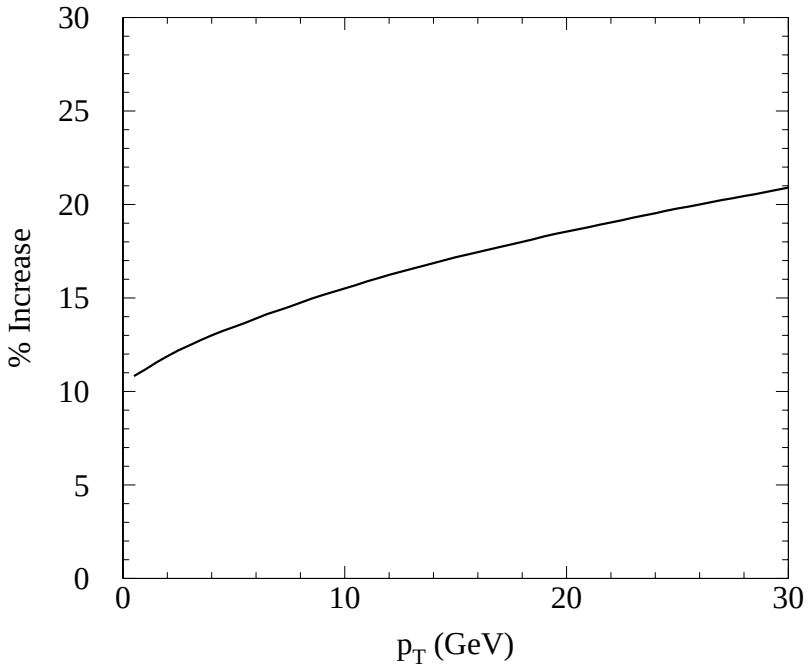

Figure 9.16: Percentage increase in the inclusive cross section for $\Upsilon(1S)$ at 2.0 TeV compared to 1.8 TeV. The cross sections are integrated over $p_T > 8$ GeV and $|y| < 0.4$.

$$\sigma[\eta_b(nS)] = \frac{1}{3}\sigma[b\bar{b}_1(^1S_0)]\langle O_1^{\Upsilon(nS)}(^3S_1)\rangle + \frac{1}{3}\sigma[b\bar{b}_8(^1S_0)]\langle O_8^{\Upsilon(nS)}(^3S_1)\rangle + \sigma[b\bar{b}_8(^3S_1)]\langle O_8^{\Upsilon(nS)}(^1S_0)\rangle + 3\sigma[b\bar{b}_8(^1P_1)]\langle O_8^{\Upsilon(nS)}(^3P_0)\rangle, \tag{9.20}$$

$$\sigma[h_b(nP)] = 3\left(\sigma[b\bar{b}_1(^1P_1)]\langle O_1^{\chi_{b0}(nP)}(^3P_0)\rangle + \sigma[b\bar{b}_8(^1S_0)]\langle O_8^{\chi_{b0}(nP)}(^3S_1)\rangle\right). \tag{9.21}$$

In Table 9.3, we give the ratios $R^H(\sqrt{s})$ defined in (9.19) for the direct production of the spin-singlet states, not including any effects from the feed down of higher bottomonium states. The cross sections for direct $h_b(nP)$ are significantly smaller than for inclusive $\Upsilon(1S)$. Since the h_b does not seem to have any distinctive decay modes that can be used as a trigger, its discovery at the Tevatron is unlikely. However the cross sections for direct

H	R^H(1.8 TeV)	R^H(2.0 TeV)
$\eta_b(3S)$	1.83 ± 0.54	2.13 ± 0.62
$h_b(2P)$	0.07 ± 0.07	0.08 ± 0.09
$\eta_b(2S)$	1.60 ± 0.59	1.87 ± 0.69
$h_b(1P)$	0.11 ± 0.08	0.13 ± 0.09
$\eta_b(1S)$	4.59 ± 0.83	5.34 ± 0.96

Table 9.3: Direct cross sections for spin-singlet bottomonium states H at 1.8 TeV and 2.0 TeV divided by the inclusive cross section for $\Upsilon(1S)$ at 1.8 TeV. The cross sections are integrated over $p_T > 8$ GeV and $|y| < 0.4$.

$\eta_b(nS)$, $n = 1, 2, 3$ are significantly larger than for inclusive $\Upsilon(1S)$. Thus it should be possible to discover the η_b if one can identify a suitable decay mode that can be used as a trigger. One promising possibility is the decay $\eta_b \to J/\psi + J/\psi$ [27].

9.2.2.2 Charmonium

The NRQCD factorization approach can be applied to charmonium production at the Tevatron as well as to bottomonium production. The differences are only quantitative. First, the coupling constant $\alpha_s(m_c) \approx 0.36$ is larger than $\alpha_s(m_b) \approx 0.22$, so the radiative corrections to the short-distance parton cross sections are larger for charmonium. Second, the typical relative velocity v of the heavy quark is significantly larger for charmonium ($v^2 \sim 1/4$) than for bottomonium ($v^2 \sim 1/10$). In the NRQCD approach truncated at relative order v^4, the terms that are neglected are suppressed only by an additional factor of v^2 and are therefore larger for charmonium than for bottomonium. A third difference is that the value of p_T above which fragmentation contributions become important is smaller by a factor of 3 for charmonium, simply because $m_c \approx m_b/3$.

An important experimental difference from bottomonium production is that charmonium is also produced by decays of B hadrons. We define the prompt cross section for a charmonium state to be the inclusive cross section excluding the contribution from B hadron decays. Thus the prompt cross section is the sum of the direct cross section and the indirect contributions from decays of higher charmonium states that were produced directly. The experimental signature of prompt production is the absence of a displaced vertex that would signal the weak decay of a B hadron.

NRQCD analyses of the CDF data on charmonium production from Run IA have been carried out by several groups [32,38–41]. We describe briefly the analysis of Ref. [41]. The color-singlet matrix elements were determined from annihilation decays of the charmonium states. The color-octet matrix elements were obtained by fitting the CDF cross sections for J/ψ, $\psi(2S)$, and χ_{cJ} and by imposing the constraint from a preliminary CDF measurement of the ratio of χ_{c1} to χ_{c2}. Because the cross sections for $c\bar{c}_8(^1S_0)$ and $c\bar{c}_8(^3P_J)$ have similar dependences on p_T, only the linear combination $M_r = \langle O_8(^1S_0)\rangle + r\langle O_8(^3P_0)\rangle/m_b^2$ with $r \sim 3.5$ could be determined. The sets of parton distribution functions that were used were MRST98LO and CTEQ5L. The charm quark mass was set to $m_c = 1.50 \pm 0.05$ GeV.

In Figs. 9.17 and 9.18, we show the CDF data on the differential cross sections for J/ψ and $\psi(2S)$ from Run IA [30,31]. The cross sections are integrated over the pseudorapidity range $|\eta| < 0.6$. The curves are the results of the NRQCD fit and the leading-order predictions of the color-singlet model. If the cross sections were measured at lower values of p_T, they would turn over and go to zero like the $\Upsilon(1S)$ cross section in Fig. 9.13. In contrast, the NRQCD curves continue rising and diverge like $1/p_T$ as $p_T \to 0$. In order to obtain the correct physical behavior at small p_T, it would be necessary to carry out an analysis that includes the effects of soft-gluon radiation. Neglecting these effects may introduce large systematic errors into the NRQCD matrix elements. In an analysis using a Monte Carlo event generator to take into account initial-state gluon radiation at the Tevatron, the values of some of the color-octet matrix were decreased by an order of magnitude [42]. One should

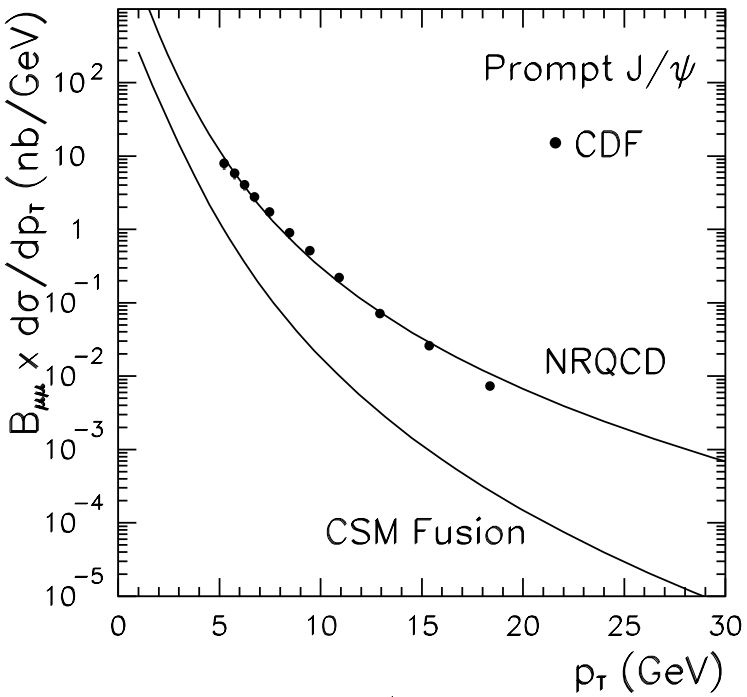

Figure 9.17: Prompt cross section for J/ψ at Run I multiplied by its branching fraction into $\mu^+\mu^-$: CDF data, the NRQCD fit of Ref. [41], and the color-singlet model prediction.

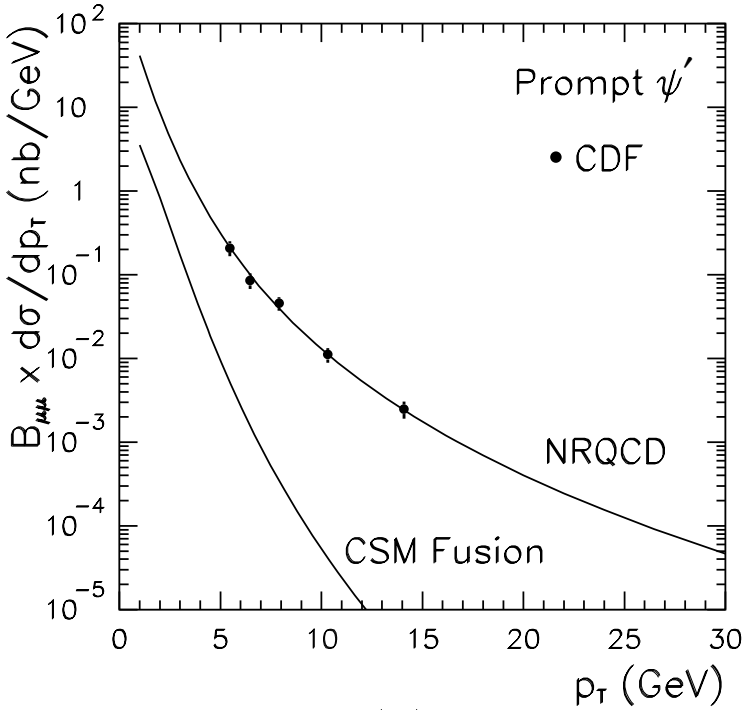

Figure 9.18: Prompt cross section for $\psi(2S)$ at Run I multiplied by its branching fraction into $\mu^+\mu^-$: CDF data, the NRQCD fit of Ref. [41], and the color-singlet model prediction.

H	$R^H(1.8\ \text{TeV})$	$R^H(2.0\ \text{TeV})$
$\psi(2S)$	0.21 ± 0.07	0.23 ± 0.08
$\chi_{c2}(1P)$	0.44 ± 0.08	0.50 ± 0.10
$\chi_{c1}(1P)$	0.40 ± 0.08	0.45 ± 0.09
$\chi_{c0}(1P)$	0.14 ± 0.03	0.16 ± 0.03
J/ψ	1	1.14 ± 0.08

Table 9.4: Prompt cross sections for spin-triplet charmonium states H at 1.8 TeV and 2.0 TeV divided by the prompt cross section for J/ψ at 1.8 TeV. The cross sections are integrated over $p_T > 5.5$ GeV and $|\eta| < 0.6$.

H	$R^H(1.8\ \text{TeV})$	$R^H(2.0\ \text{TeV})$
$\eta_c(2S)$	0.37 ± 0.11	0.42 ± 0.12
$h_c(1P)$	0.033 ± 0.006	0.037 ± 0.007
$\eta_c(1S)$	1.73 ± 0.15	1.97 ± 0.72

Table 9.5: Direct cross sections for spin-singlet charmonium states H at 1.8 TeV and 2.0 TeV divided by the prompt cross section for J/ψ at 1.8 TeV. The cross sections are integrated over p_T between 5 and 20 GeV and $|\eta| < 0.6$.

therefore be wary of using the matrix elements from existing analyses of the Tevatron data to predict production rates in other high energy processes.

The safest applications of the NRQCD analysis are to observables for which the errors associated with the extractions of the matrix elements tend to cancel out. One such observable is the increase in the cross section when the center-of-mass energy is increased from 1.8 TeV to 2.0 TeV. It is convenient to normalize the cross section for the charmonium state H at center-of-mass energy $\sqrt{s}$ to that for prompt J/ψ at $\sqrt{s} = 1.8$ TeV by defining the ratio (in analogy with Eq. (9.19))

$$R^H(\sqrt{s}) = \frac{\sigma[H;\ \sqrt{s}]}{\sigma[\text{prompt } J/\psi;\ \sqrt{s} = 1.8\ \text{TeV}]}, \tag{9.22}$$

where the cross sections are integrated over $p_T > 5.5$ GeV and over $|\eta| < 0.6$. In Table 9.4, we give the ratios $R^H(\sqrt{s})$ for the inclusive production of spin-triplet charmonium states, both at $\sqrt{s} = 1.8$ TeV and at $\sqrt{s} = 2.0$ TeV. When the center-of-mass energy is increased from 1.8 TeV to 2.0 TeV, all the cross sections increase by about the same amount. The increase depends on p_T, changing from about 13% at $p_T = 5.5$ GeV to about 18% at $p_T = 20$ GeV. The percentage increase for J/ψ is shown as a function of p_T in Fig. 9.19.

Another reliable application of the NRQCD analysis is to predict the cross sections for the spin-singlet bottomonium states $\eta_c(nS)$ and h_c. The most important matrix elements for $\eta_c(nS)$ and h_c are related to those for the spin-triplet states by the spin symmetry of NRQCD. Thus, once the color-octet matrix elements are determined from the production of spin-triplet states, the NRQCD approach predicts the cross sections for the spin-singlet states without any new nonperturbative parameters. In Table 9.5, we give the ratios $R^H(\sqrt{s})$ defined in (9.22) for the direct production of the spin-singlet states, not including

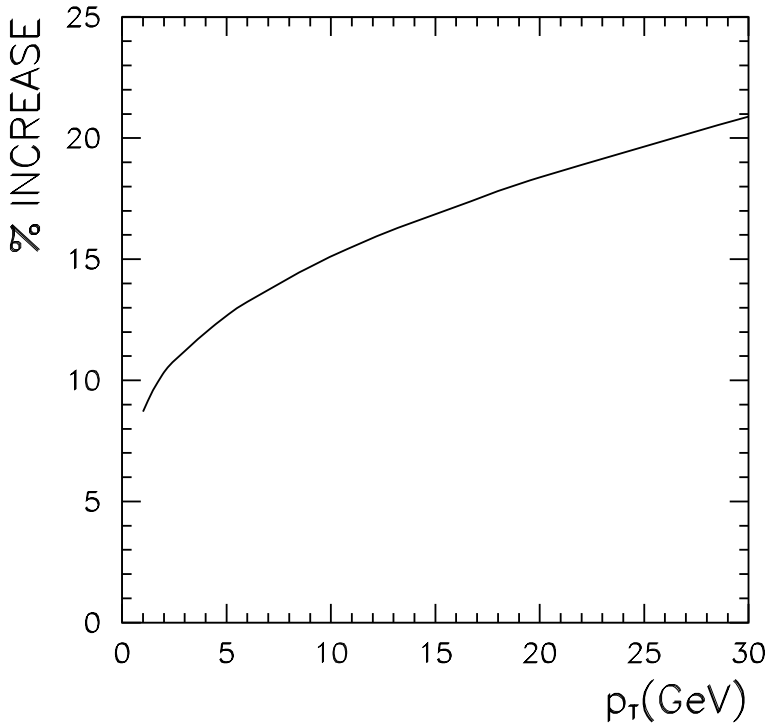

Figure 9.19: Percentage increase in prompt cross section for J/ψ at $\sqrt{s} = 2.0$ TeV compared to 1.8 TeV as a function of p_T. The cross sections are integrated over $p_T > 5.5$ GeV and $|\eta| < 0.6$.

any effects from the feed-down of higher charmonium states. The cross sections for direct h_c are significantly smaller than for prompt J/ψ, but the cross sections for direct $\eta_c(nS)$, $n = 1, 2$ are significantly larger. It may be possible to observe the $\eta_c(1S)$ and perhaps even discover the $\eta_c(2S)$ if one can identify a suitable decay mode that can be used as a trigger.

9.2.2.3 Quarkonium polarization

The most dramatic prediction of the NRQCD factorization approach for quarkonium production at the Tevatron is that the $J^{PC} = 1^{--}$ states like the J/ψ should be transversely polarized at sufficiently large p_T. This prediction follows from three simple features of the dynamics of heavy quarks and massless partons. (1) The inclusive production of quarkonium at large p_T is dominated by gluon fragmentation [43]. (2) At leading order in α_s, the $c\bar{c}$ pair produced by gluon fragmentation is in a color-octet $^3S_1$ state [44] with transverse polarization. (3) The approximate spin symmetry of NRQCD guarantees that the hadronization of a transversely polarized $c\bar{c}$ pair produces a J/ψ that is predominantly transversely polarized [45].

In the NRQCD approach truncated at relative order v^4, the cross sections for polarized quarkonium states can be calculated in terms of the matrix elements that describe unpolarized production. The only complication is that both the parton cross sections and the NRQCD matrix elements in the NRQCD factorization formula (9.13) become density

matrices in the angular momentum quantum numbers of the $c\bar{c}$ pairs. Thus the NRQCD approach gives definite predictions for polarized quarkonium cross sections, without any new nonperturbative parameters. In contrast, one of the basic assumptions of the color evaporation model is that quarkonium is always produced unpolarized. This model can therefore be ruled out by a measurement of nonzero polarization of quarkonium.

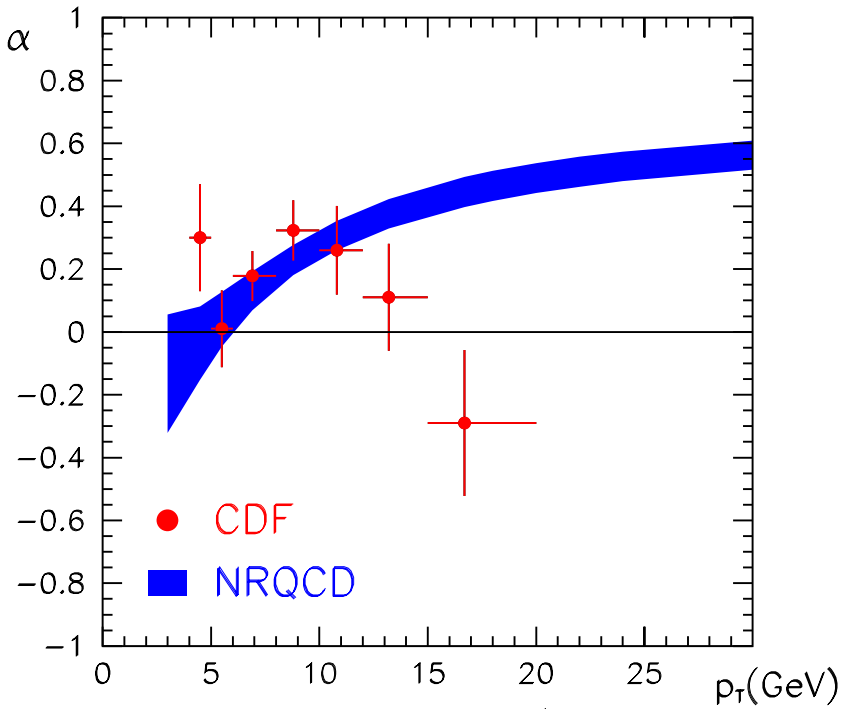

Figure 9.20: Polarization variable α for prompt J/ψ at Run I: CDF data and the NRQCD prediction of Ref. [41].

Defining the angle θ by the direction of the μ^+ with respect to the ψ direction in the ψ center of mass frame, the normalized angular distribution $I(\theta)$ is given by

$$I(\theta) = \frac{1}{\sigma_L + \sigma_T}\left[\frac{3}{8}(1+\cos^2\theta)\,\sigma_T + \frac{3}{4}\sin^2\theta\,\sigma_L\right]$$
$$\equiv \frac{3}{2(\alpha+3)}(1+\alpha\cos^2\theta). \qquad (9.23)$$

A convenient measure of the polarization of $J = 1$ quarkonium states is therefore the variable $\alpha = (\sigma_T - 2\sigma_L)/(\sigma_T + 2\sigma_L)$, where σ_T and σ_L are the cross sections for transversely and longitudinally polarized states, respectively. In Figs. 9.20 and 9.21, we show the CDF measurements of α for prompt J/ψ and prompt $\psi(2S)$ [46]. In Fig. 9.21 for $\psi(2S)$, the bands are the predictions from the NRQCD analyses of Leibovich [47], Beneke and Kramer [48] and Braaten, Kniehl and Lee [41]. The widths of the bands and the deviations between the predictions are indicators of the size of the theoretical errors. The calculation of α for prompt J/ψ is complicated by the need to take into account the feed-down from χ_{cJ}. The band in Fig. 9.20 is the prediction by Braaten, Kniehl and Lee [41]. For both prompt J/ψ and prompt $\psi(2S)$, the theoretical prediction for α is small around $p_T = 5$ GeV, but

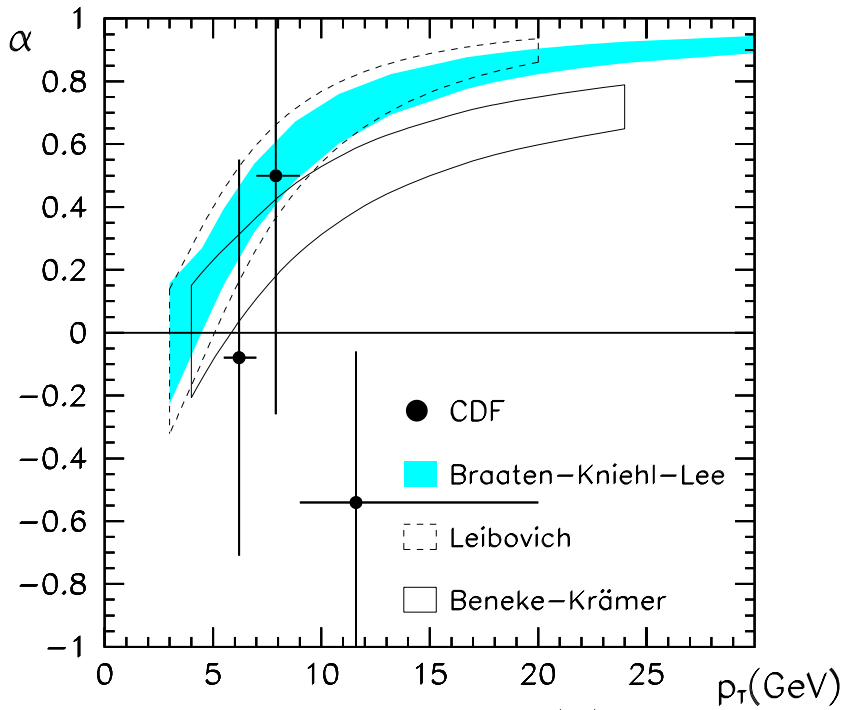

Figure 9.21: Polarization variable α for prompt $\psi(2S)$ at Run I: CDF data and the NRQCD predictions of Refs. [41] (shaded band), [47] (dashed box), and [48] (solid box).

then increases steadily with p_T. If the data is taken at its face value, it suggests exactly the opposite trend, decreasing at the largest values of p_T for which it has been measured. There are many effects, such as higher order corrections, that could dilute the polarization or delay the onset of the rise in α, but the basic conclusion that α should increase to a positive value at large p_T seems to follow inescapably from the NRQCD factorization approach. If this behavior is not observed in Run II, it will be a serious blow to this approach to quarkonium production.

In Ref. [49], the polarization variable α has also been calculated for inclusive $\Upsilon(nS)$ using the matrix elements from the NRQCD analysis of Ref. [27]. The prediction for inclusive $\Upsilon(1S)$ as a function of p_T is shown in Fig. 9.22. The variable α is predicted to be small for p_T less than 10 GeV, but it increases steadily with p_T. The prediction is compatible with the CDF measurement for p_T in the range from 8 GeV to 20 GeV, which is $\alpha = 0.03 \pm 0.28$. The data from Run II should allow the prediction to be tested.

9.2.3 Polarization in quarkonium production †

Measurements of the J/ψ and $\psi(2S)$ differential cross sections by CDF [30] separate the cross sections into those ψ mesons coming from b-flavored hadron production and those originating from prompt production mechanisms. This separation is made by reconstructing

†Authors: G. Feild, K. Sumorok, W. Trischuk

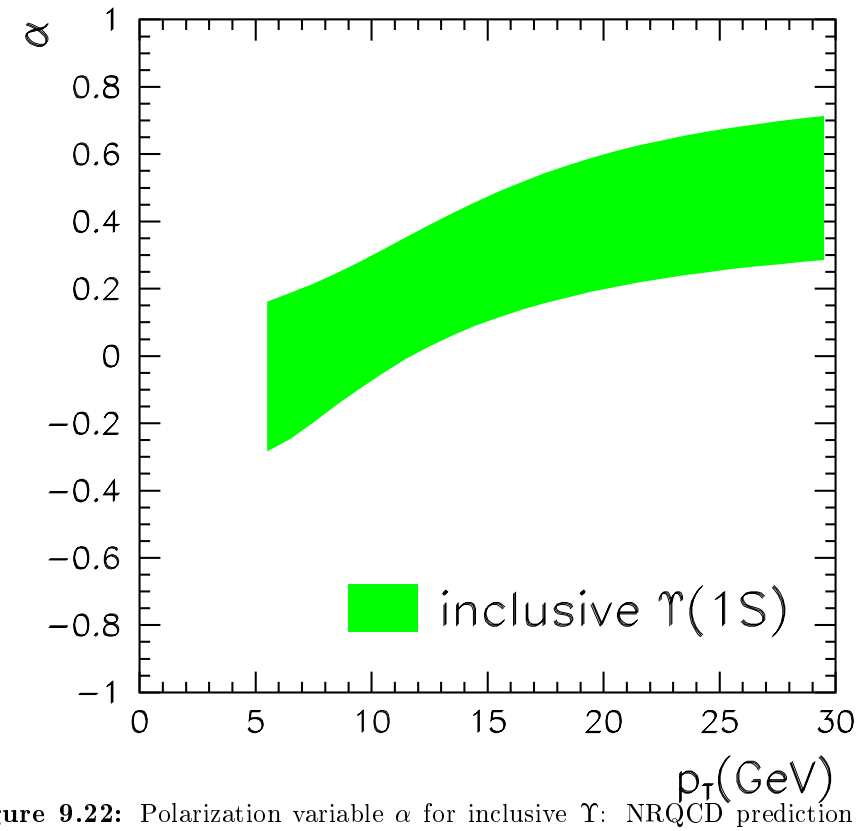

Figure 9.22: Polarization variable α for inclusive Υ: NRQCD prediction from Ref. [49].

the decay vertex of the J/ψ and $\psi(2S)$ mesons using the CDF Silicon Vertex detector (SVX). The fraction of J/ψ mesons coming from b-flavored hadron production increases from 15% at 5 GeV/c to 40% at 18 GeV/c $P_T^{J/\psi}$. For $\psi(2S)$ mesons, a similar increase is seen in the range from 5 to 14 GeV/c. The prompt production of J/ψ mesons has three components: a feed-down from χ_c production, a feed-down from $\psi(2S)$ and a direct component. Only the latter occurs in the production of $\psi(2S)$ mesons. CDF has measured the fraction of prompt J/ψ mesons coming from χ_c production to be $(29.7 \pm 1.7 \pm 5.7)\%$ of the total prompt production [31]. From the measured $\psi(2S)$ production cross section, the fraction of the prompt J/ψ's feeding down from $\psi(2S)$ meson decays is calculated to be $7 \pm 2\%$ at $P_T^{J/\psi} = 5$ GeV/c and $15 \pm 5\%$ at $P_T^{J/\psi} = 18$ GeV/c. The fraction of directly produced J/ψ mesons is $64 \pm 6\%$, independent of $P_T^{J/\psi}$ between 5 and 18 GeV/c.

Having separated out the prompt J/ψ mesons coming from χ_c, both direct/prompt J/ψ and $\psi(2S)$ production appear to be $\approx$ 50 times higher than color-singlet model (CSM) predictions [50].

9.2.3.1 NRQCD predictions for ψ meson polarization

Calculations based on the NRQCD factorization formalism are able to explain this anomalous production [32,38]. The model increases the prompt production cross section by includ-

ing color-octet $c\bar{c}$ states ${}^1S_0^{(8)}$, ${}^3P_0^{(8)}$ and ${}^3S_1^{(8)}$ in the hadronization process. At leading order in α_s, the color-singlet term in the parton cross section $d\hat{\sigma}/dp_T^2$ has a $1/p_T^8$ dependence at large p_T, the ${}^1S_0^{(8)}$ and ${}^3P_0^{(8)}$ terms have a $1/p_T^6$ dependence, and the ${}^3S_1^{(8)}$ term has a $1/p_T^4$ dependence. This last term, which corresponds to the fragmentation of an almost on-shell gluon into a $c\bar{c}$ pair, dominates at high P_T. An on-shell gluon is transversely polarized and NRQCD predicts this polarization is transfered to the J/ψ or $\psi(2S)$ mesons in the final state.

A consequence of this mechanism is that the direct prompt J/ψ mesons and the $\psi(2S)$ mesons will approach 100% transverse polarization at leading order in α_s for transverse momenta $p_T \gg m_c$ where m_c is the charm quark mass [45,51]. The observation of such a polarization would be an indication of the NRQCD hadronization mechanism.

9.2.3.2 CDF polarisation measurements from Run I

CDF has made a measurement of the production polarization of J/ψ and $\psi(2S)$ (collectively ψ) mesons by analyzing decays into $\mu^+\mu^-$ [46]. Defining the angle θ by the direction of the μ^+ with respect to the ψ direction in the ψ center of mass frame, the normalized angular distribution $I(\theta)$ is given by Eq. (9.23).

Unpolarized ψ mesons would have $\alpha = 0$, whereas $\alpha = +1$ and -1 correspond to fully transverse and longitudinal polarizations respectively. The polarization parameter for prompt ψ production can be separated from the B-hadron decay component by fitting the proper decay length distribution for ψ candidates with both muons reconstructed in the SVX. Fig. 9.23 shows the fitted polarization of J/ψ mesons obtained by CDF from prompt production and B-hadron decay compared with an NRQCD prediction for the prompt production [41]. The prediction for J/ψ meson polarization includes dilutions due to the contributions from χ_c and $\psi(2S)$ decays. Fig. 9.24 shows the fitted polarization for $\psi(2S)$ mesons obtained by CDF from prompt production and B-hadron decay compared with NRQCD predictions for prompt production from Refs. [48] and [41].

9.2.3.3 Polarization predictions for Run II

The measurements in Run I were based on a luminosity of 110 pb^{-1}. Estimates for Run II are made assuming a factor of 20 increase in integrated luminosity, or 2 fb^{-1}. CDF is also planning to increase the yield of its dimuon trigger by 50% by lowering the p_T threshold. In addition, the SVX will have increased coverage along the beam line leading to better acceptance for dimuons fully reconstructed in the SVX. This is crucial for separation of prompt and B hadron decay production in this measurement. Overall a factor of 50 increase in the effective statistics for Run II is assumed in our projections. We have extrapolated to higher p_T by using the fitted shape of the cross section below 20 GeV/c^2 in order to predict the number of events in a given p_T bin. We have estimated the errors by scaling the statistics from Run I measurements. In Run I, systematic uncertainties on the polarization measurement were small compared to the statistical errors. We anticipate that the systematics can be improved with the Run II data samples, but even if this is not the case systematics

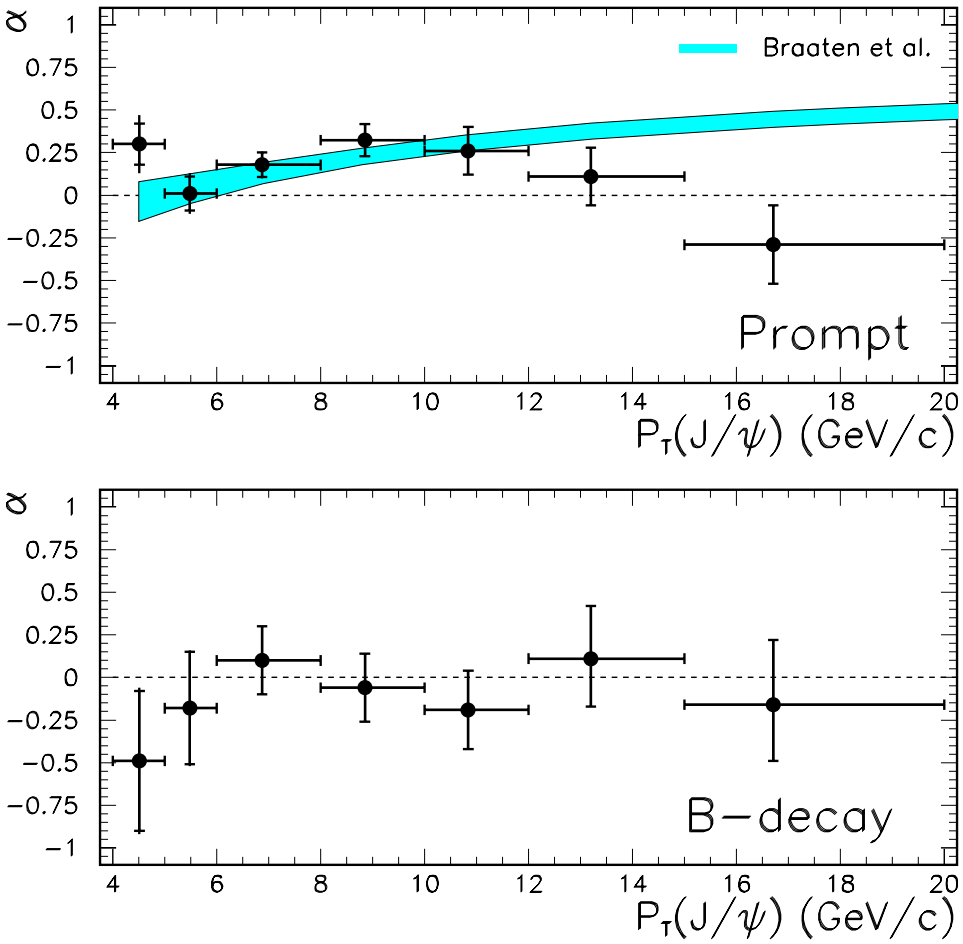

Figure 9.23: The fitted polarization of J/ψ mesons from prompt production and B-hadron decay. The shaded curve shows an NRQCD prediction from Ref. [41].

should still be negligible at the highest transverse momenta. Fig. 9.25 shows the expected precision for a polarization measurement in Run II of promptly produced J/ψ and $\psi(2S)$ mesons. Relative to Run I, the p_T range should be extended and the statistical precision on the measurement improved. The points are slightly scattered about zero to ease visibility.

9.2.3.4 Upsilon production and polarization in CDF Run II

The CDF Run IB Υ(1S) differential production cross section, measured as a function of transverse energy, is shown in Fig. 9.26. As discussed in section 9.2.2.1, this cross section can be described by including NRQCD color-octet matrix elements in the fit to the data. However, due to the free parameters in the fit, this compatibility alone is not enough to demonstrate that the NRQCD description is correct. As in the case of the J/ψ and ψ(2S) mesons, observation of transversely polarized Υ(1S) production due to gluon fragmentation at high p_T would provide further evidence in favor of the NRQCD framework over other proposed models, such as the color-singlet model and the color-evaporation model.

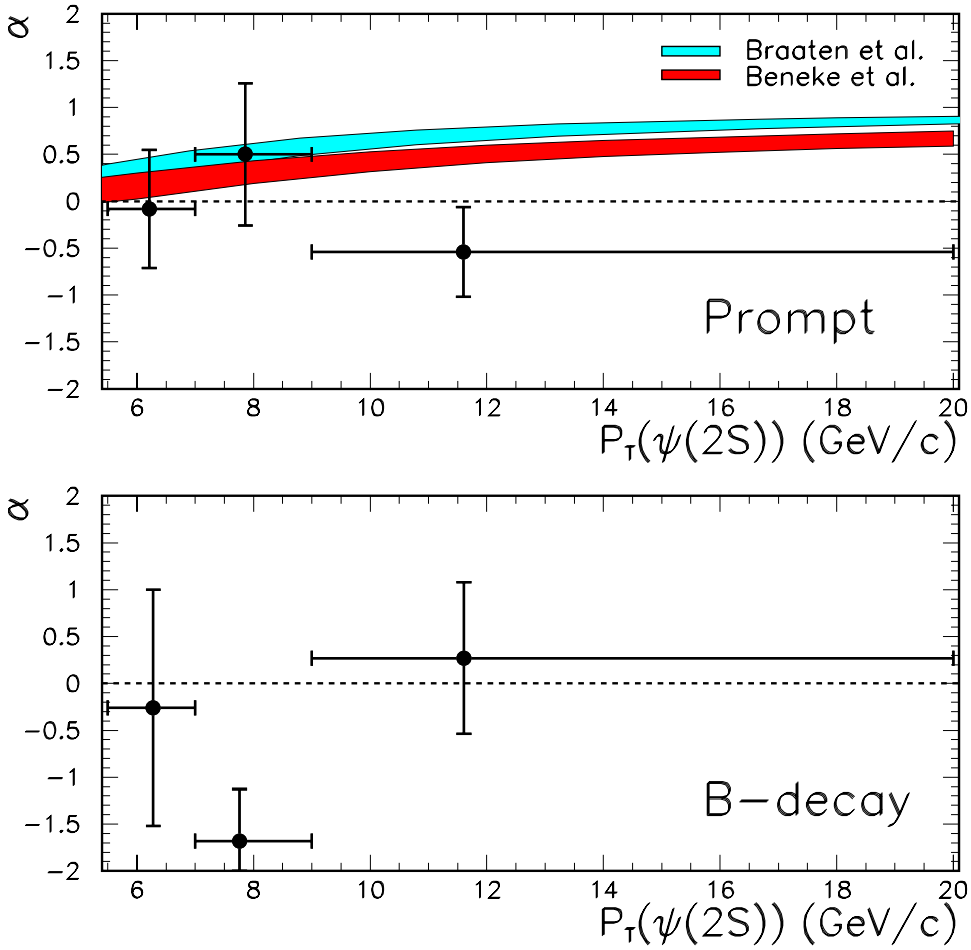

Figure 9.24: The fitted polarization of $\psi(2S)$ mesons from prompt production and B-hadron decay. The shaded curves are NRQCD predictions from Refs. [48] and [41].

The $\Upsilon(1S) \to \mu\mu$ production polarization for events in the transverse energy range 8 GeV/c $< p_T(\Upsilon) <$ 20 GeV/c has been determined in Run IB by measuring the muon decay angle in the Υ rest frame as described in section 9.2.3.2. This measurement is done by fitting longitudinally and transversely polarized Monte Carlo templates to the data shown in Fig. 9.27. In this case the longitudinal fraction Γ_L/Γ is measured to be 0.32 ± 0.11. The longitudinal fraction can be related to the usual polarisation parameter, α, by: $\Gamma_L/\Gamma = (1-\alpha)\ (3+\alpha)$. Thus our polarisation measurement in Υ decays yields a value of $\alpha = 0.03 \pm 0.25$. Our data is compatible with unpolarized production. This result does not contradict the predictions of NRQCD as the transverse polarisation is only expected to be large for transverse momenta $p_T \gg m_b$, where m_b is the b quark mass. We are probably not probing sufficiently high p_T with our current data.

An extrapolation of the Run IB cross section from Fig. 9.26 yields no appreciable cross section for $p_T(\Upsilon) > 20$ GeV. However, assuming a factor 20 increase in data for Run II, a polarization measurement statistically comparable to that from Run IB could be made in

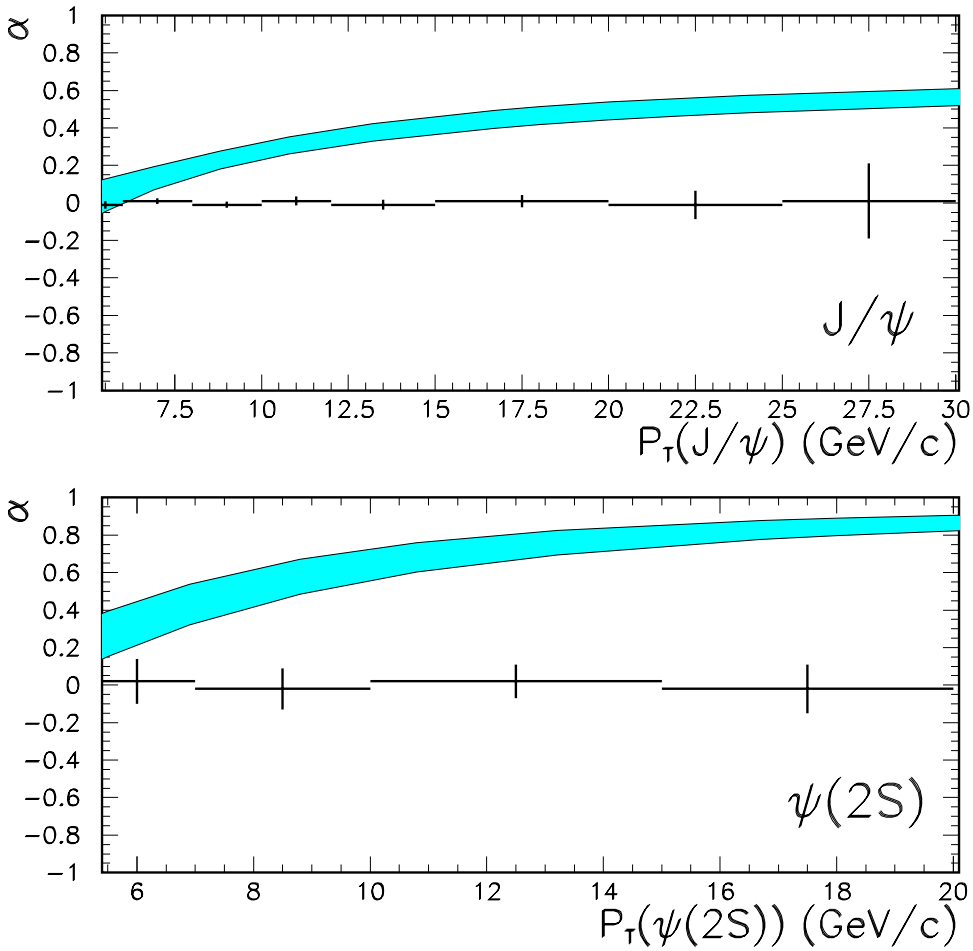

Figure 9.25: The expected precision for a polarization measurement in Run II of promptly produced J/ψ and $\psi(2S)$ mesons. The shaded curves are NRQCD predictions from [41].

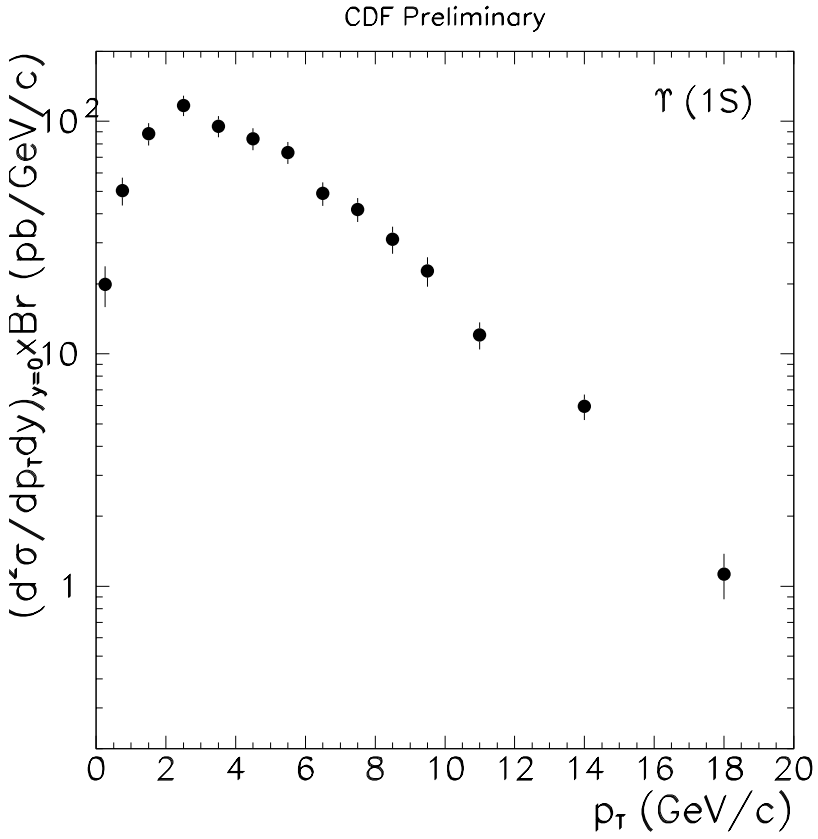

Figure 9.26: The differential cross-section for $\Upsilon(1S)$ production measured by CDF in Run I.

the transverse energy range 14 GeV $< p_T(\Upsilon) <$ 20 GeV. Conversely, the prediction from fits to the Run IB data shown in Fig. 9.13, predict a flattening of the cross section above 20 GeV. It will be quite interesting if such events are seen in Run II.

9.3 The B_c Meson

The B_c meson is the ground state of the $\bar{b}c$ system, which in many respects is intermediate between charmonium and bottomonium. However because $\bar{b}c$ mesons carry flavor, they provide a window for studying heavy-quark dynamics that is very different from the window provided by quarkonium. The observation of approximate 20 B_c events in the $B_c \to J/\psi l\nu$ decay mode by the CDF-collaboration [52] in Run I of the Tevatron demonstrates that the experimental study of the $\bar{b}c$ meson system is possible.

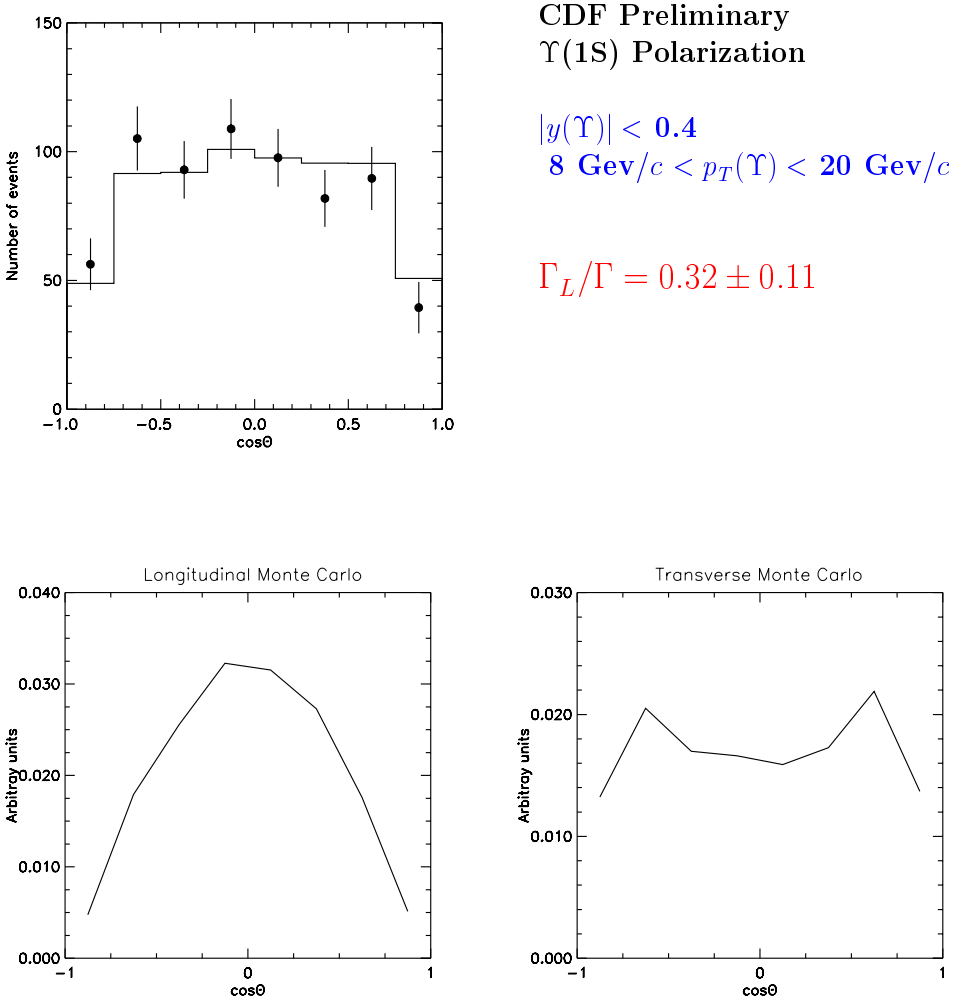

Figure 9.27: The polarisation measured in $\Upsilon(1S)$ decays by CDF in Run I.

9.3.1 Spectroscopy†

The $\bar{b}c$ system has a rich spectroscopy of orbital and angular-momentum excitations. The predicted spectrum is shown in Fig. 9.28. The only state that has been observed is the ground state B_c, which was discovered by the CDF collaboration in Run I of the Tevatron [52]. They measured the mass to be 6.4 ± 0.4 GeV. The masses of the B_c and the other states in the $\bar{b}c$ spectrum can be predicted using potential models whose parameters are tuned to reproduce the spectra of the observed charmonium and bottomonium states [53–58]. The range of the resulting predictions for the B_c mass is 6.24 ± 0.05 GeV. The first excited state is the spin-1 state B_c^*, which is predicted to be heavier by 78 ± 13 MeV. The mass of the B_c has also been calculated using lattice gauge theory to be 6.4 ± 0.1, where the uncertainty is dominated by the error from the omission of dynamical quarks [59].

†Authors: E. Braaten, R. K. Ellis

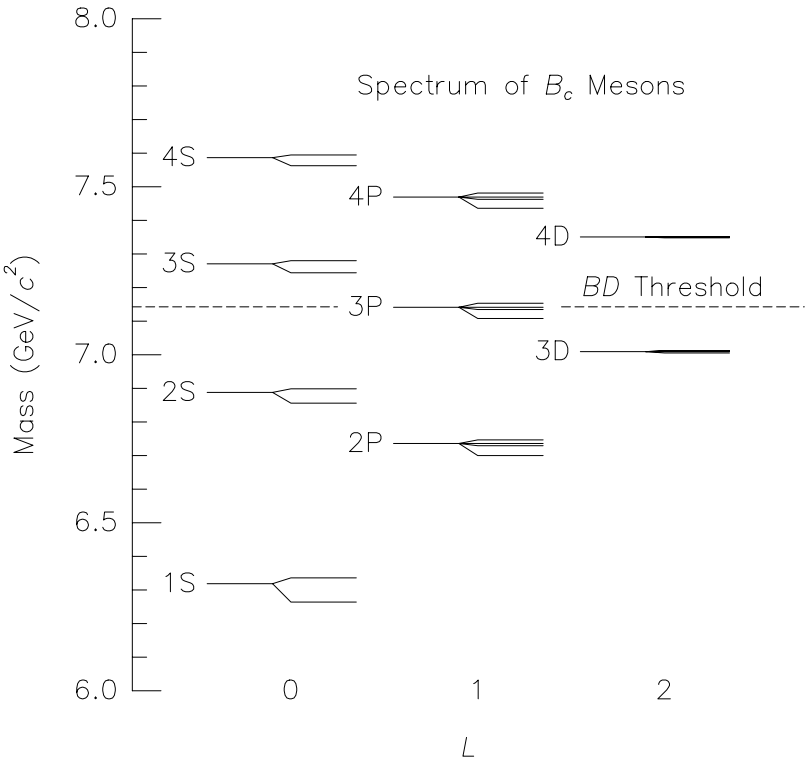

Figure 9.28: Predicted spectrum for the $\bar{b}c$ mesons [56].

The majority of the B_c mesons produced at the Tevatron are produced indirectly via the decay of excited $\bar{b}c$ mesons. The excited states cascade down through the spectrum via a sequence of hadronic and electromagnetic transitions, until they reach the ground state $B_c(1S)$, which decays via the weak interaction [56]. The $\bar{b}c$ states with the best prospects for discovery at the Tevatron are those that decay into $B_c + \gamma$. The discovery of the B_c^* is made difficult by the very low energy of the photon (~ 80 MeV). The first radial excitation $B_c^*(2S)$ decays into $B_c + \gamma$ with a much more energetic photon (~ 600 MeV), but a smaller fraction of the decay chains that end in B_c will have the $B_c^*(2S)$ as the next-to-last step. States in the $\bar{b}c$ spectrum could also be discovered via 2-pion transitions into the B_c. The most promising is the first radial excitation $B_c(2S)$, whose mass is higher than that of the B_c^* by about 600 MeV.

9.3.2 Production[1]

One can think of the production of a B_c as proceeding in three steps. First, a $\bar{b}$ and c with small relative momentum are created by a parton collision. Second, the $\bar{b}$ and c bind to form the B_c or one of its excited states below the BD threshold. Third, the excited states all cascade down to the ground state B_c via hadronic or electromagnetic transition. Thus,

[1] Authors: Eric Braaten, A. Likhoded

the total production cross section for B_c is the sum of the direct production cross sections for B_c and its excited states.

The direct production of the B_c and other $\bar{b}c$ mesons can be treated within the NRQCD factorization framework described in Section 9.2.2. The cross section for the direct production of a $\bar{b}c$ meson H can be expressed in the form of Eqs. (9.12) and (9.13), with $b\bar{b}(n)$ replaced by $\bar{b}c(n)$. The short-distance cross section $d\hat{\sigma}[ij \to \bar{b}c(n)+X]$ for creating the $\bar{b}c$ in the color and angular-momentum state n can be calculated as a perturbative expansion in α_s at scales of order m_c or larger. The nonperturbative matrix element $\langle O^H(n)\rangle$ encodes the probability for a $\bar{b}c$ in the state n to bind to form the meson H. The matrix element scales as a definite power of the relative velocity v of the charm quark. For S-wave states, the leading color-octet matrix element is suppressed by v^4 relative to the leading color-singlet matrix element. For P-wave states, the leading color-singlet matrix element and the leading color-octet matrix element are both suppressed by v^2 relative to the leading color-singlet matrix element for S-waves.

The production mechanisms for $\bar{b}c$ differ in an essential way from those for $b\bar{b}$, because two heavy quark-antiquark pairs must be created in the collision. While a $b\bar{b}$ pair can be created at order α_s^2 by the parton processes $q\bar{q}, gg \to b\bar{b}$, the lowest order mechanisms for creating $\bar{b}c$ are the order-α_s^4 processes $q\bar{q}, gg \to (\bar{b}c) + b\bar{c}$. At the Tevatron, the gg contribution dominates. The parton process $gg \to (\bar{b}c) + b\bar{c}$ can create the $\bar{b}c$ in either a color-singlet or color-octet state. We expect the cross section for color-octet $\bar{b}c$ to be about a factor of 8 larger than for color-singlet $\bar{b}c$, just from counting the color states. This factor of 8 can partially compensate any suppression factors of v from the probability for the color-octet $\bar{b}c$ to bind to form a meson. However, unlike the case of $\bar{b}b$, there is no dynamical enhancement of color-octet $\bar{b}c$ at low p_T or at high p_T. Color-octet production processes should therefore be less important for $\bar{b}c$ mesons than for quarkonium.

All existing calculations for the cross sections of $\bar{b}c$ mesons have been carried out within the color-singlet model. The $\bar{b}c$ is assumed to be created in a color-singlet state with the same angular-momentum quantum numbers as the meson. The appropriate long-distance matrix elements can be determined from the radial wavefunctions of the mesons as in Eqs. (9.14) and (9.15). For the B_c and the first excited state B_c^*, the matrix element is proportional to $|R_{1S}(0)|^2$. Since the wavefunctions are known from potential models, the cross sections for $b\bar{c}$ mesons in the color-singlet model are absolutely normalized.

The production of $\bar{b}c$ mesons in the color-singlet model at leading order in α_s was studied in detail in the series of papers [60]. The cross sections are proportional to $\alpha_s^4(\mu)$ and to a wavefunction factor, which is $|R_{nS}(0)|^2$ for S-waves and $|R'_{nP}(0)|^2$ for P-waves. The largest uncertainties in the theoretical predictions arise from the factor $\alpha_s^4(\mu)$. There is a large ambiguity in the choice of the scale μ, since the short-distance process involves several scales, including m_c, m_b, and p_T. For example, if the scale μ is varied from m_c up to $2(m_c + m_b)$, the $\bar{b}c$ cross-section changes by a factor of 7. There are additional ambiguities from the wave function factors and from the c-quark mass, but the resulting uncertainties are less than a factor of 2.

The result of the order-α_s^4 color-singlet model calculation for $d\sigma/dp_T$ of the B_c meson at the Tevatron at 1.8 TeV are presented in Fig. 9.29. The cross section integrated over p_T

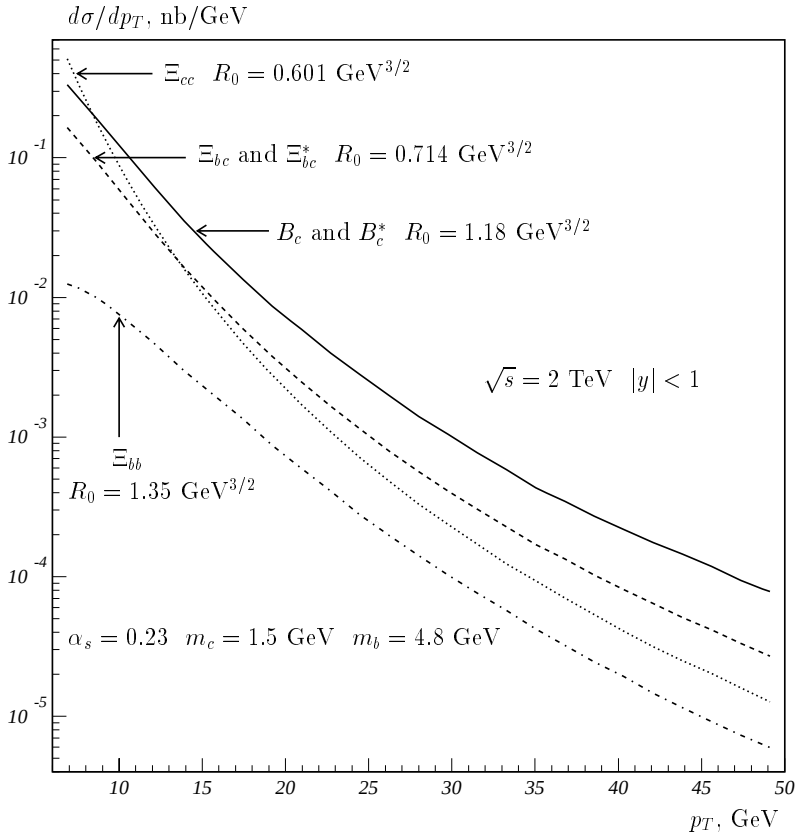

Figure 9.29: Differential cross sections for the B_c meson and doubly-heavy baryons.

greater than $p_{T\,min}$ is shown in Fig. 9.30. The prediction includes the feeddown from B_c^*, but not from any of the higher $\bar{b}c$ states. The cross sections are integrated over $|y| < 1$. In our calculations we used the following values of parameters. The quark masses were taken to be $m_c = 1.5$ GeV and $m_b = 4.8$ GeV. The QCD coupling constant was frozen at the value $\alpha_s = 0.23$, which describes the experimental data of the OPAL Collaboration on the production of additional $c\bar{c}$-pairs in e^+e^--annihilation [60]. The radial wavefunction at the origin for the B_c and B_c^* was taken to be $R_{1S}(0) = 1.18$ GeV$^{3/2}$. The cross-section for B_c mesons is roughly three orders of magnitude smaller than that for B mesons due to the presence of two heavy quark-antiquark pairs in the final state.

To estimate the inclusive B_c cross section, we must take into account the feeddown from all the $\bar{b}c$ mesons below the BD threshold, all of which eventually cascade down into the B_c via hadronic or electromagnetic transitions. Including the feeddown from all the higher $\bar{b}c$ states and integrating over $p_T > 6$ GeV and $|y| < 1$, the inclusive cross section for B_c is predicted to be

$$\sigma_{th}(B_c^+) = 2.5 \text{ nb}, \tag{9.24}$$

with an error that is roughly a factor of 3. This should be compared with the cross section obtained from the experimental result [52], using the value $(2.5\pm0.5)\times10^{-2}$ for the branching

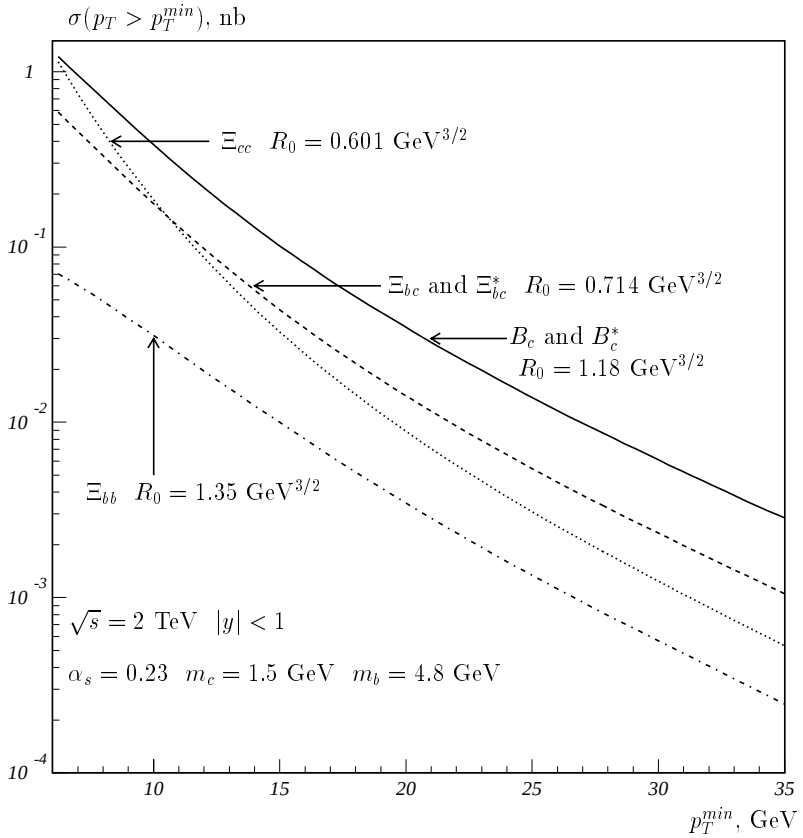

Figure 9.30: Integrated cross sections for the B_c meson and doubly-heavy baryons.

fraction for $B_c^+ \to J/\psi + l\nu$,

$$\sigma_{exp.} \sim 10 \pm 6 \text{ nb} . \tag{9.25}$$

The B_c cross section should be measured much more accurately in Run II. If the cross section proves to be significantly higher than predicted by the color-singlet model, it may indicate that color-octet production mechanisms are also important.

9.3.3 Theory of B_c Decays[2]

Decays of the long-lived heavy meson B_c, which contains two heavy quarks of different flavors, were considered in the pioneering paper written by Bjorken in 1986 [61]. Bjorken's report gave a unified view of the decays of hadrons with heavy quarks: mesons and baryons with a single heavy quark, the B_c meson, and baryons with two and three heavy quarks. A major effort was recently directed to study the long-lived doubly-heavy hadrons using modern understanding of QCD dynamics in the weak decays of heavy flavors. The modern theoretical tools are the Operator Product Expansion, sum rules of QCD and NRQCD, and potential models adjusted using data from hadrons with a single heavy quark. Surprisingly,

[2]Authors: V.V.Kiselev, A.K.Likhoded

Bjorken's estimates of total widths and various branching fractions are close to what is evaluated in a more strict manner.

Various hadronic matrix elements enter in the description of weak decays. Measuring the lifetimes and branching ratios therefore provides information about nonperturbative QCD interactions. This is important in the determination of electroweak parameters, such as the quark masses and the mixing angles in the CKM matrix, which enter into constraints on the physics beyond the Standard Model. The accumulation of more data on hadrons with heavy quarks will provide greater accuracy and confidence in our understanding of the QCD dynamics that is necessary to isolate the electroweak parameters.

A new laboratory for such investigations is the doubly-heavy long-lived quarkonium B_c recently observed for the first time by the CDF Collaboration [52]. The measured B_c lifetime is equal to

$$\tau[B_c] = 0.46^{+0.18}_{-0.16} \pm 0.03 \text{ ps} . \tag{9.26}$$

In studying the B_c meson, we can take advantage of two features that it has in common with the $\bar{b}b$ and $\bar{c}c$ quarkonia: the nonrelativistic motion of the $\bar{b}$ and c quarks and the suppression of the light quark-antiquark sea. These two physical conditions imply two small expansion parameters for B_c: the relative velocity v of quarks and the ratio Λ_{QCD}/m_Q of the confinement scale to the heavy quark mass. The double expansion in v and $1/m_Q$ generalizes the HQET approach [62,63] to what is called NRQCD [64]. The energy release in heavy quark decays determines the $1/m_Q$ parameter to be the appropriate quantity for the operator product expansion (OPE) and also justifies the use of potential models (PM) in the calculations of hadronic matrix elements. The same arguments ensure the applicability of sum rules (SR) of QCD and NRQCD.

The B_c decays were first calculated using potential models [65]. Various models gave similar estimates after adjusting parameters to reproduce the semileptonic decay rates of B mesons. The OPE evaluation of inclusive decays gave values for the lifetime and inclusive widths that agreed with the sum of the dominant exclusive modes predicted by the potential models. Quite unexpectedly, QCD sum rules gave values for the semileptonic B_c widths [66] that were an order of magnitude smaller than predicted by the potential models and by the OPE. The reason for this was that Coulomb-like α_s/v corrections had been neglected in the sum rule calculations. These corrections can be taken into account by summing up α_s/v corrections to all orders. They are significant both for heavy quarkonia and for the B_c [67,68]. At present, all three approaches give similar results for the lifetime and inclusive decay modes of the B_c for similar sets of parameters. Nevertheless, various dynamical questions remain open:

- What is the appropriate renormalization scale for the nonleptonic weak Lagrangian, which basically determines the lifetime of the B_c?
- What are the values of masses for the charmed and beauty quarks?
- What are the implications of NRQCD symmetries for the form factors of B_c decays and partial widths?

- How consistent is our understanding of the hadronic matrix elements that characterize B_c decays with the data on the other heavy hadrons?

In the present short review of B_c decays, we summarize the theoretical predictions and discuss how direct experimental measurements can answer the questions above.

9.3.3.1 Lifetime and inclusive decay rates

The B_c-meson decay processes can be subdivided into three classes:

- the $\bar{b}$-quark decay with a spectator c-quark,
- the c-quark decay with a spectator $\bar{b}$-quark and
- the annihilation decays $\bar{b}c \to l^+\nu_l, c\bar{s}, u\bar{s}$, where $l = e,\ \mu,\ \tau$.

In the $\bar{b} \to \bar{c}c\bar{s}$ decays, one separates also the *Pauli interference* with the c-quark from the initial state. In accordance with the given classification, the total width is the sum over the partial widths from $\bar{b}c$ annihilation, $\bar{b}$ decay, c decay, and Pauli interference.

The annihilation width is the sum of the widths from the annihilation of the $\bar{b}c$ into leptons and quarks. In the width from annihilation into quarks, one must take into account the hard-gluon corrections to the effective four-quark interaction of weak currents, which give an enhancement factor $a_1 = 1.22 \pm 0.04$. The nonperturbative effects of QCD can be absorbed into the leptonic decay constant $f_{B_c} \approx 400$ MeV. This estimate of the contribution from annihilation into quarks does not depend on a hadronization model, since a large energy release of the order of the meson mass takes place. Because of helicity suppression, the decay width is proportional to the square of the masses of leptons or quarks in the final state. Thus the only important annihilation channels are $\bar{b}c \to \tau^+\nu_\tau$ and $\bar{b}c \to c\bar{s}$.

B_c decay mode	OPE, %	PM, %	SR, %
$\bar{b} \to \bar{c}l^+\nu_l$	3.9 ± 1.0	3.7 ± 0.9	2.9 ± 0.3
$\bar{b} \to \bar{c}u\bar{d}$	16.2 ± 4.1	16.7 ± 4.2	13.1 ± 1.3
$\sum \bar{b} \to \bar{c}$	25.0 ± 6.2	25.0 ± 6.2	19.6 ± 1.9
$c \to sl^+\nu_l$	8.5 ± 2.1	10.1 ± 2.5	9.0 ± 0.9
$c \to su\bar{d}$	47.3 ± 11.8	45.4 ± 11.4	54.0 ± 5.4
$\sum c \to s$	64.3 ± 16.1	65.6 ± 16.4	72.0 ± 7.2
$B_c^+ \to \tau^+\nu_\tau$	2.9 ± 0.7	2.0 ± 0.5	1.8 ± 0.2
$B_c^+ \to c\bar{s}$	7.2 ± 1.8	7.2 ± 1.8	6.6 ± 0.7

Table 9.6: Branching ratios of B_c decay modes calculated using the operator product expansion (OPE) approach, by summing up the exclusive modes from potential models (PM) [65,67], and by using sum rules (SR) of QCD and NRQCD [67].

For the non-annihilation contributions to the width of the B_c, one can apply the *operator product expansion* (OPE) for the quark currents of weak decays [69]. One takes into account the α_s-corrections to the free quark decays and uses quark-hadron duality for the final states.

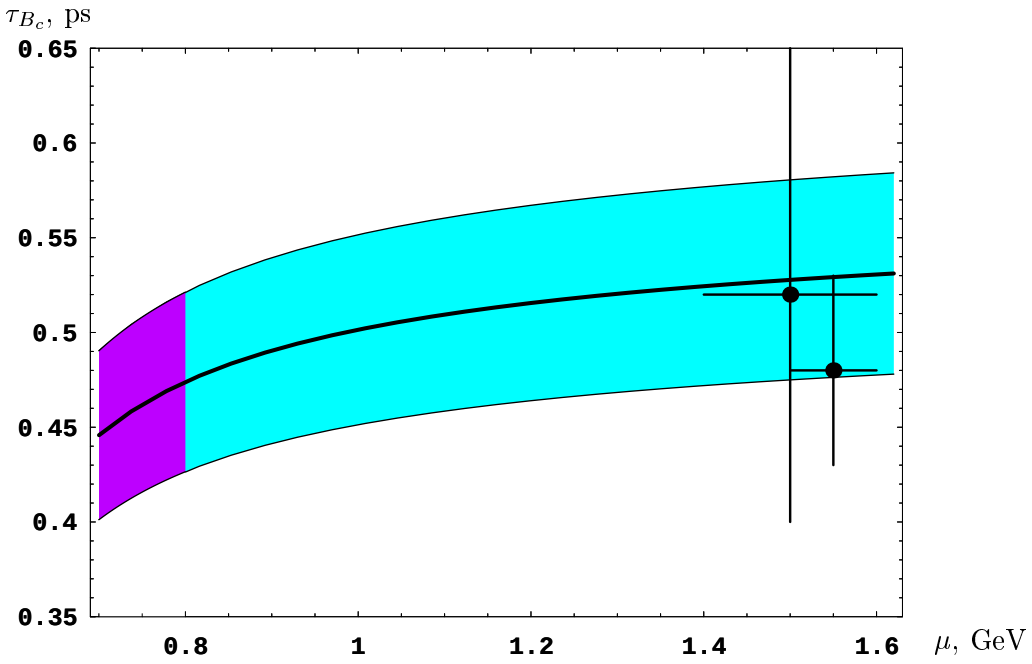

Figure 9.31: The B_c lifetime calculated in QCD sum rules versus the scale of hadronic weak Lagrangian. The shaded region shows the uncertainty of estimates, the dark shaded region is the preferable choice as given by the lifetimes of charmed mesons. The points represent the values in OPE approach taken from Ref. [69].

Then one considers the matrix element for the transition operator in the bound meson state. The latter allows one also to take into account the effects caused by the motion and virtuality of decaying quark inside the meson because of the interaction with the spectator. In this way the $\bar{b} \to \bar{c}c\bar{s}$ decay mode turns out to be suppressed almost completely due to the Pauli interference with the charm quark from the initial state. The c-quark decays with a spectator $\bar{b}$ are also suppressed compared to the decay of a free c-quark, because of the large binding energy of the initial state. Possible effects of interference between the leading-order weak amplitudes and the penguin corrections in B_c decays were considered in the framework of OPE in Ref. [70], and these corrections were estimated to be about 4%.

To calculate inclusive widths in the potential model approach, it is necessary to sum up the widths of exclusive decay modes [65]. For semileptonic decays via the transition $\bar{b} \to \bar{c}l^+\nu_l$, one finds that the hadronic final state is almost completely saturated by the most deeply bound states in the $\bar{c}c$ system, *i.e.* by the $1S$ states η_c and J/ψ. For semileptonic decays via the transition $c \to sl^+\nu_l$, one finds that the only $\bar{b}s$ states that can enter the accessible energy gap are the B_s and B_s^*. Furthermore, the $\bar{b} \to \bar{c}u\bar{d}$ channel, for example, can be calculated by multiplying the decay width for $\bar{b} \to \bar{c}l^+\nu_l$ by a color factor and by taking into account hard-gluon corrections to the four-quark interaction. It can be also obtained as a sum over the widths of decays involving specific $u\bar{d}$ bound states.

The calculations of the total B_c width in the inclusive OPE approach and the exclusive potential model approach give consistent values, if one takes into account the largest uncer-

tainty, which comes from the quark masses (especially the charm quark). The final result is

$$\tau(B_c) = 0.55 \pm 0.15 \text{ ps}, \tag{9.27}$$

which agrees with the measured value of the B_c lifetime.

The OPE estimates of inclusive decay rates agree with recent calculations in the sum rules of QCD and NRQCD [67], where one assumed the saturation of hadronic final states by the ground levels in the $c\bar{c}$ and $b\bar{s}$ systems as well as the factorization that allows one to relate the semileptonic and hadronic decay modes. The Coulomb-like corrections in the heavy quarkonia states play an essential role in the B_c decays and allow one to remove the disagreement between the estimates in sum rules and OPE. In contrast to OPE, where the basic uncertainty is given by the variation of heavy quark masses, these parameters are fixed by the two-point sum rules for bottomonia and charmonia, so that the accuracy of sum rule calculations for the total width of B_c is determined by the choice of scale μ for the hadronic weak Lagrangian in decays of charmed quark. We show this dependence in Figure 9.31, where $m_c/2 < \mu < m_c$ and the dark shaded region corresponds to the scales preferred by data on the charmed meson lifetimes. Taking the preferred scale in the $c \to s$ decays of B_c to be equal to $\mu^2_{B_c} \approx (0.85 \text{ GeV})^2$ and setting $a_1(\mu_{B_c}) = 1.20$ in the charmed quark decays, we predict the lifetime to be [67]

$$\tau(B_c) = 0.48 \pm 0.05 \text{ ps}. \tag{9.28}$$

9.3.3.2 Semileptonic and leptonic modes

The semileptonic decay rates were underestimated in the QCD sum rule approach of Ref. [66], because large Coulomb-like corrections were not taken into account. The recent sum rule analysis in [67,68] decreased the uncertainty, so that the estimates agree with the calculations in the potential models. The widths and branching fractions calculated using QCD sum rules are presented in Table 9.7. The expected accuracy is about 10%. In practice, the most important semileptonic decay mode is to the J/ψ which is easily detected in experiments via its leptonic decays [52].

The estimates for exclusive semileptonic decay rates of the B_c into $1S$ charmonium states obtained from QCD sum rules agree with the values obtained from potential models in Ref. [65], which also considered the contributions of decays to the excited $2S$ and $1P$ states. The direct decay rate into P-wave charmonium states is about 20% of the direct decay rate into the $1S$ states. The radiative decay of the χ_c states increases the total semileptonic decay rate of B_c to J/ψ by about 5%. The exclusive semileptonic decay rates of the B_c into the P-wave states χ_c and h_c have also been calculated within a framework that involves overlap integrals of the wavefunctions of the B_c and the charmonium states [71].

The dominant leptonic decay of B_c is given by the $\tau\nu_\tau$ mode (see Table 9.6). However, it has a low experimental efficiency of detection because of hadronic background in the τ decays and missing energy. Recently, in Refs. [72] the enhancement of muon and electron channels in the radiative modes was studied. The additional photon allows one to remove the helicity suppression for the leptonic decay of a pseudoscalar particle, which leads to an increase of the muonic decay rate by a factor of 2.

mode	Γ, 10^{-14} GeV	BR, %
$B_s e^+ \nu_e$	5.8	4.0
$B_s^* e^+ \nu_e$	7.2	5.0
$\eta_c e^+ \nu_e$	1.1	0.75
$\eta_c \tau^+ \nu_\tau$	0.33	0.22
$J/\psi e^+ \nu_e$	2.8	2.1
$J/\psi \tau^+ \nu_\tau$	0.7	0.51

Table 9.7: Widths and branching fractions for the semileptonic decay modes of the B_c meson calculated using QCD sum rules. (For the branching fractions, we set $\tau_{B_c} = 0.46$ ps.)

9.3.3.3 Nonleptonic modes

The inclusive nonleptonic width of the B_c can be estimated in the framework of quark-hadron duality (see Table 9.6). However, calculations of exclusive nonleptonic modes usually involve the approximation of factorization [73]. This approximation is expected to be quite accurate for the B_c, since the light quark-antiquark sea is suppressed in $\bar{b}c$ mesons. Thus, the important parameters are the factors a_1 and a_2 in the nonleptonic weak Lagrangian, which depend on the renormalization scale for the B_c decays. The QCD SR estimates for the widths of exclusive modes involving the nonleptonic decay of the charmed quark in B_c are presented in Table 9.8 [67]. They agree with the values predicted by the potential models.

For decays involving large recoils as in $B_c^+ \to \psi\pi^+(\rho^+)$, the spectator picture of the transition breaks down due to hard gluon exchanges. Taking these nonspectator effects into account increases the estimates of potential models by a factor of 4 [74]. The corresponding estimates in the factorization approach are determined by the leptonic decay constants and by the QCD coupling constant at the scale of the virtuality of the hard gluon. Numerically, one finds the values represented in Table 9.9. Due to the contribution of a t-channel diagram, the matrix element is *enhanced* by a factor of 2 compared to the potential model value. The spin effects in such decays were studied in [75]. The relative yield of excited charmonium states can be also evaluated. For example, the branching fraction for $B_c^+ \to \psi(2S)\pi^+$ should be smaller than that for $B_c^+ \to \psi\pi^+$ by about a factor of 0.36. The contributions to two-particle hadronic decays of B_c from P-wave states of charmonium were considered in Refs. [76] and [71] using methods that involve the hard-scattering of constituents with large recoil and the overlap of wave functions, respectively. In Ref. [76], the form factors have power-law tails that come from one-gluon exchange, and they therefore obtain larger values for the widths than Ref. [71], in which the form factors fall exponentially. The ratios of the widths for $B_c^+ \to \psi(2S)\pi^+$ in these two approaches agree with each other. The estimates of $B_c^+ \to \psi(2S)\rho^+$ modes are more model dependent. The cascade electromagnetic transitions of the χ_c states increase the inclusive $B_c \to J/\psi\pi(\rho)$ decay rates by about 8%. Finally, suppressed decays caused by flavor-changing neutral currents have been studied in Ref. [77].

CP-violation in B_c decays can be investigated in the same manner as for B decays, although it is very difficult in practice because of the low relative yield of B_c compared to

mode	Γ, 10^{-14} GeV	BR, %
$B_s\pi^+$	15.8 a_1^2	17.5
$B_s\rho^+$	6.7 a_1^2	7.4
$B_s^*\pi^+$	6.2 a_1^2	6.9
$B_s^*\rho^+$	20.0 a_1^2	22.2

Table 9.8: Widths and branching fractions of nonleptonic decay modes of the B_c meson. (For the branching fractions, we set $\tau_{B_c} = 0.46$ ps and a_1=1.26.)

mode	BR, %
$\psi\pi^+$	0.67 ± 0.07
$\eta_c\pi^+$	0.87 ± 0.09
$\psi\rho^+$	1.96 ± 0.20
$\eta_c\rho^+$	2.43 ± 0.24

Table 9.9: Widths and branching fractions of charmonium decay modes of the B_c meson. (For the branching fractions, we set $\tau_{B_c} = 0.46$ ps and a_1=1.26.)

ordinary B mesons: $\sigma(B_c)/\sigma(B) \sim 10^{-3}$. The expected CP-asymmetry of $\mathcal{A}(B_c^\pm \to J/\psi D^\pm)$ is about $4 \cdot 10^{-3}$, but this decay mode has a very small branching ratio of about 10^{-4} [78]. Another possibility is lepton tagging of the B_s in $B_c^\pm \to B_s^{(*)} l^\pm \nu$ decays for the study of mixing and CP-violation in the B_s sector [79].

9.3.3.4 Discussion and conclusions

We have reviewed the current status of theoretical predictions for the decays of B_c meson. We have found that the operator product expansion, potential models, and QCD sum rules all give consistent estimates for inclusive decay rates. The sum rule approach, which has been explored for the various heavy quark systems, leads to a smaller uncertainty due to the quite accurate knowledge of the heavy quark masses. The dominant contribution to the B_c lifetime is given by the charmed quark decays ($\sim 70\%$), while the b-quark decays and the weak annihilation add about 20% and 10%, respectively. The Coulomb-like α_s/v corrections play an essential role in the determination of exclusive form factors in the QCD sum rules. The form factors are expected to obey the relations dictated by the spin symmetry of NRQCD and HQET with quite good accuracy.

The accurate direct measurement of the B_c lifetime can provide us with the information on both the masses of charmed and beauty quarks and the normalization point of the nonleptonic weak Lagrangian that is responsible for the B_c decay (the a_1 and a_2 factors). The experimental study of semileptonic decays and the extraction of ratios for the form factors can test the spin symmetry derived in the NRQCD and HQET approaches. It can also decrease the theoretical uncertainties in the theoretical evaluation of quark parameters as well as the hadronic matrix elements that take into account nonperturbative effects caused by quark confinement. The measurement of branching fractions for the semileptonic and nonleptonic modes can give information on the values of factorization parameters, which

depend again on the normalization of the nonleptonic weak Lagrangian. The counting of charmed quarks in B_c decays is also sensitive to nonperturbative effects, because it is determined not only by the contribution from b quark decays, but also by the suppression of $\bar{b} \to c\bar{c}\bar{s}$ transitions due to destructive Pauli interference.

Thus, progress in measuring the B_c lifetime and decays should enhance the theoretical understanding of what really happens in heavy quark decays.

9.3.4 DØ Study of B_c: Triggering and Reconstruction [3]

9.3.4.1 Introduction

The B_c meson is a particularly interesting system to study since it contains two different heavy quarks that are often in competition regarding subsequent decays. As a result, measurements of its properties such as mass, lifetime, and decay branching ratios offer a unique window into heavy quark hadrons. Since it has nonzero flavor, it has no strong or electromagnetic annihilation decay channels, and it is the heaviest such meson predicted by the Standard Model. Its weak decay is expected to yield a large branching fraction to final states containing a J/ψ which is a useful experimental signature. The B_c meson (like the single-b baryons and doubly-heavy baryons) is too massive to produce at the B factories running at the $\Upsilon(4S)$. LEP has only a few B_c candidates, while CDF isolated a sample of 23 B_c decays in approximately 100 pb^{-1} of data [52] in Run I resulting in the estimate that $\sigma(B_c)/\sigma(b) \approx 2 \times 10^{-3}$.

9.3.4.2 DØ simulations

To examine DØ prospects for Run II, simulations were made of B_c production using PYTHIA and reweighting the resulting spectrum to match the differential $d\sigma/dp_T$ cross section calculated using code supplied by the authors of Ref. [80]. After reweighting, the production spectrum of produced B_c mesons is shown in Fig. 9.32. The mass of the B_c meson was set to 6.40 GeV and the lifetime to 0.50 ps, consistent with CDF and LEP measurements [52,81]. The fraction of $b \to B_c$ was increased to 0.5 while the fractions of $b \to B_d^0$, B^+, B_s^0, and Λ_b were scaled down appropriately. Any events containing two B_c mesons were discarded in order to get the hadron composition of the "away-side" B hadron correct. Events with $p_T(B_c) > 3$ GeV and $|\eta(B_c)| < 3$ were retained.

The CLEO QQ package was used to force the semileptonic decay $B_c \to J/\psi\ell\nu$ (Br $\approx$ 2.5% [82]) and $B_c \to J/\psi\pi$ (Br $\approx$ 0.2% [82]) followed by the subsequent decays of $J/\psi \to e^+e^-$ or $J/\psi \to \mu^+\mu^-$. The distinctive trilepton signature of the first decay mode was used to allow efficient triggering, from the presence of at least two electrons or muons with significant transverse momentum, with reasonable background rates.

Detector simulations were performed at a number of different levels of sophistication: MCFAST [83], PMCS (a DØ parameterized fast Monte Carlo), and full GEANT simulated

[3] Author: R. Van Kooten

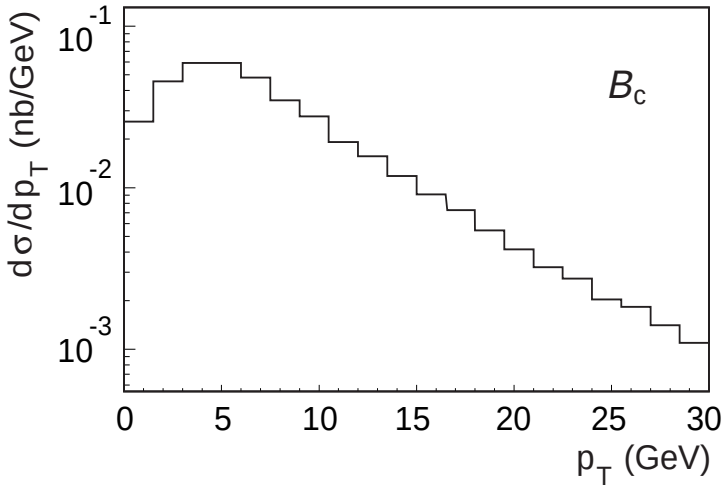

Figure 9.32: The differential cross section for the B_c meson used in the following studies.

events to allow the use of a more realistic trigger simulator and reconstruction resolution determination. Typical distributions of B_c decay products from the MCFAST simulation are shown in Fig. 9.33.

9.3.4.3 Results

MCFAST simulations could be used to determine kinematic and trigger efficiencies; however, the DØ trigger simulator was run on GEANT fully simulated events for a more sophisticated and reliable treatment. Starting with the case of a semileptonically decaying B_c where all three leptons are muons, Table 9.10 gives the DØ muon trigger efficiency for the indicated criteria. "Medium" and "Tight" muon identification refers to the correspondingly tighter requirements of coincidence of greater number of muon detector layers.

The status of the simulation of triggering on electrons is less complete, and trigger efficiencies in this case were extrapolated from prior studies [84] for the decay $B_d^0 \to J/\psi K_S^0$. At Level 1, information from the electromagnetic calorimeter, the fiber tracker, and matches between these and hits in the central preshower detector are expected to lead to a trigger efficiency of approximately 30%, but with a substantial background rate. This background rate is expected to be lowered to a reasonably low value with invariant mass cuts on the electrons from the $J/\psi \to e^+e^-$ decay applied at Level 2 of the trigger. An overall efficiency for triggering on states with di-electrons from the J/ψ decay is estimated to be 12.8%.

Although DØ will initially be running without a vertex silicon track trigger, studies were made of the potential for such a trigger to help isolate a large sample of B_c mesons. Note that the events were generated with a B_c lifetime set to 0.50 ps rather than the usual lifetimes of 1.5–1.6 ps of the other B mesons. A decay length resolution of 116 μm has been measured in MCFAST simulated events. A vertex silicon track trigger would operate by

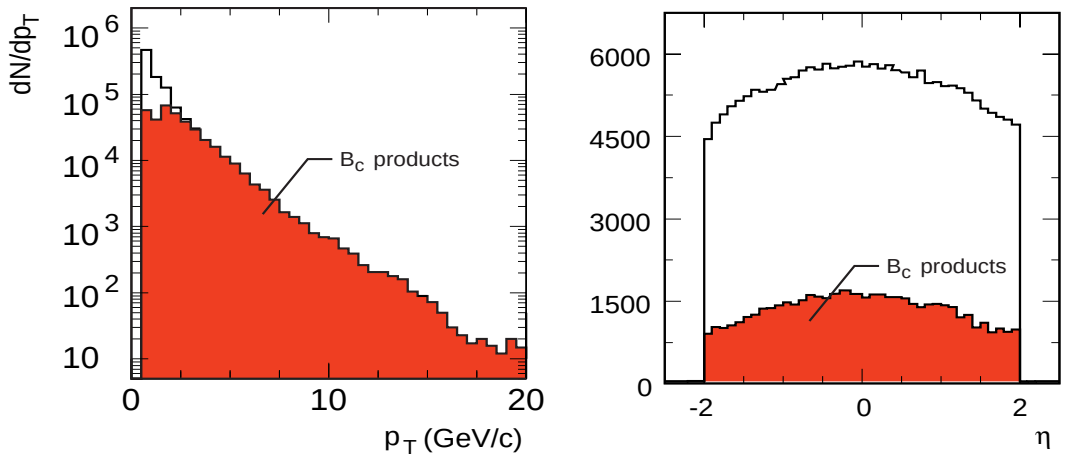

Figure 9.33: Kinematic distributions of (a) p_T and (b) η for all particles (open histograms) and for B_c semileptonic decay products (dark histograms)

examining the impact parameter significance, i.e., b/σ_b, where b is the impact parameter of a track and σ_b its error. The distribution of this quantity for tracks from B_c decay is shown in Fig. 9.34(a). This distribution is substantially narrower than for tracks from other B meson decays due to the shorter lifetime of the B_c. The trigger efficiency obtained by cutting on the presence of one or more tracks with large impact parameter significance is shown in Fig. 9.34(b). For the same background rate, the efficiency is about a factor of 2.5 times smaller than the comparable rate for $B_d^0 \to J/\psi K_S^0$ decays.

In the $B_c \to J/\psi\ell\nu$ channel, a typical mass reconstruction of the J/ψ through its decay into $\mu^+\mu^-$ is shown in Fig. 9.35(a) indicating a mass resolution σ_m of 29 MeV. Events are required to have the invariant mass of the two leptons assigned to the J/ψ within $2\sigma_m$ of the J/ψ mass. To reduce backgrounds, the p_T of the combined (J/ψ plus lepton) system was required to be greater than 8 GeV, and the decay length of the J/ψ-lepton vertex was required to be greater than 50 μm. Kinematic quantities such as the trilepton invariant mass yield information on the mass of the decaying state (Fig. 9.35).

Similar studies were extended to the $B_c \to J/\psi\pi$ decay channel that would allow an exclusive reconstruction of the B_c meson but with smaller statistics due to the small (0.2%) branching ratio for this final state. With only two leptons to trigger on, the overall trigger efficiency for the di-muon final state analogous to that shown in Table 9.10 is found to be slightly lower with a value of 0.24. The mass resolution of the reconstructed B_c without constraints on the J/ψ mass is found to be 52 MeV.

We proceed to estimate the expected number of B_c events reconstructed by DØ in Run II with an integrated luminosity of 2 fb^{-1}. One could use the estimate of $\sigma(B_c^+)/\sigma(\bar{b}) = 1.3 \times 10^{-3}$ compared to the measurement of $\sigma(B^+)/\sigma(\bar{b}) = 0.378 \pm 0.022$. It is more straightforward to use the CDF measurement [52] of

$$\frac{\sigma(B_c^+) \cdot \mathrm{B}r(B_c^+ \to J/\psi\ell\nu)}{\sigma(B^+) \cdot \mathrm{B}r(B^+ \to J/\psi K^+)} \tag{9.29}$$

and comparisons of DØ's trigger and reconstruction efficiency with the corresponding CDF

Criteria	Efficiency	DØ Designation
Single Muon		
$p_T^\mu > 4$ GeV $\|\eta^\mu\| < 1.5$ "Medium"	0.23	MTM5, MUO(1,4,A,M)
$p_T^\mu > 4$ GeV $\|\eta^\mu\| < 1.5$ "Tight"	0.08	MTM6, MUO(1,4,A,T)
Di-Muon		
Both $p_T^\mu > 2$ GeV $\|\eta^\mu\| < 1.5$ "Medium"	0.16	MTM10, MUO(2,2,A,M)
Both $p_T^\mu > 4$ GeV $\|\eta^\mu\| < 2.0$ "Medium"	0.15	MTM12, MUO(2,4,A,M)
"Or" of above	0.28	

Table 9.10: DØ Level 1 muon trigger efficiencies for trilepton final states from semileptonic decay of B_c mesons with $p_T(B_c) > 3$ GeV and $|\eta(B_c)| < 3$.

efficiencies. This leads to an estimate that approximately 600 identified $B_c^+ \to J/\psi\ell\nu$ would be produced. This sample is large enough to make improvements in the lifetime and mass measurements that would significantly increase our understanding of the B_c system. In addition, samples of 30–40 fully exclusive decays such as $B_c^+ \to J/\psi\pi$ can also be expected that would clearly supplement the semileptonic decay measurements which suffer from the escaping neutrino. Of course, proportionally much larger samples would be expected in subsequent runs of the Tevatron beyond Run IIa.

9.3.5 CDF Projections for B_c^+ yield in Run II[†]

9.3.5.1 Introduction

We present here the CDF projections for the B_c^+ yield in Run II by performing studies with Run I data and with Monte Carlo simulation and by using theoretical expectations for the branching ratios of various B_c^+ decay channels. We are making some simple projections for the decays $B_c^+ \to J/\psi\pi^+$, $B_c^+ \to B_s^0\pi^+$ and $B_c^+ \to J/\psi l^+\nu$. Please keep in mind for the rest of this section that references to a specific state imply the charge-conjugate state as well.

[†]Authors: Wei Hao, Vaia Papadimitriou

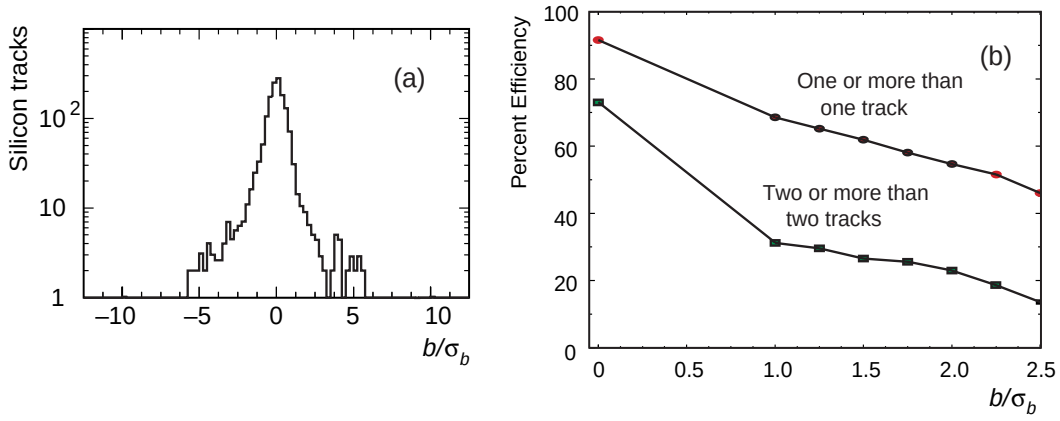

Figure 9.34: (a) Impact parameter divided by its error for track from $B_c \to J/\psi\ell\nu$; (b) efficiency of future silicon track trigger as a function of cut on b/σ_b.

9.3.5.2 Monte Carlo generation and simulation

B_c^+ Monte Carlo events were generated with a "toy" Monte Carlo using the P_t spectrum from a full α_s^4 perturbative QCD calculation of hadronic production of the B_c^+ meson [98] and assuming a flat rapidity y distribution (see Fig. 9.36). The B_c^+ mesons were generated with the mass set to 6.2 GeV/c^2, lifetime set to 0.3335 ps and in the region $P_t(B_c^+) >$ 3.0 GeV/c and $|y(B_c^+)| < 1.5$. The B_c^+ mesons were decayed to $J/\psi\pi^+$ or other decay channels using the CLEO decay table (QQ) and then they were simulated by the CDF Run I simulation package QFL′.

B^+ events, for comparison, were generated with a Monte Carlo which is generating b quarks according to the next-to-leading order QCD predictions [99], using a scale $\mu = \mu_0/2 \equiv \sqrt{(P_t)^2 + (m_b)^2}/2$ where P_t is the transverse momentum of the b quark and m_b its mass. m_b is set to 4.75 GeV/c^2. The b quark is fragmented into b hadrons using Peterson fragmentation [100] with the fragmentation parameter, ϵ_b, set to 0.006 . In Fig. 9.37 we show the P_t spectrum of the B^+, at the generation level, for $P_t(min)$ of the b-quark equal to 5.0 GeV and in the rapidity region $-1.3 < Y_{RANGE} < 1.3$. The B^+ events were decayed to $J/\psi K^+$ using QQ and then they were simulated by QFL′.

The theoretical cross sections used for the Monte Carlo generations were calculated for $\sqrt{s} = 1.8$ TeV.

9.3.5.3 Selection Criteria for the $B_c^+ \to J/\psi\pi^+$ decay channel

To select $J/\psi \to \mu^+\mu^-$ candidates, we require that the transverse momentum, P_t, of each muon is greater than 2.0 GeV/c. The CMU muon chambers, at a radius of 3.5 m from the beam axis, cover the pseudorapidity region $|\eta| < 0.6$. These chambers are complemented by the central muon upgrade system (CMP) which consists of four layers of drift tubes behind two feet of steel. In addition we have the CMX muon chambers covering the pseudorapidity

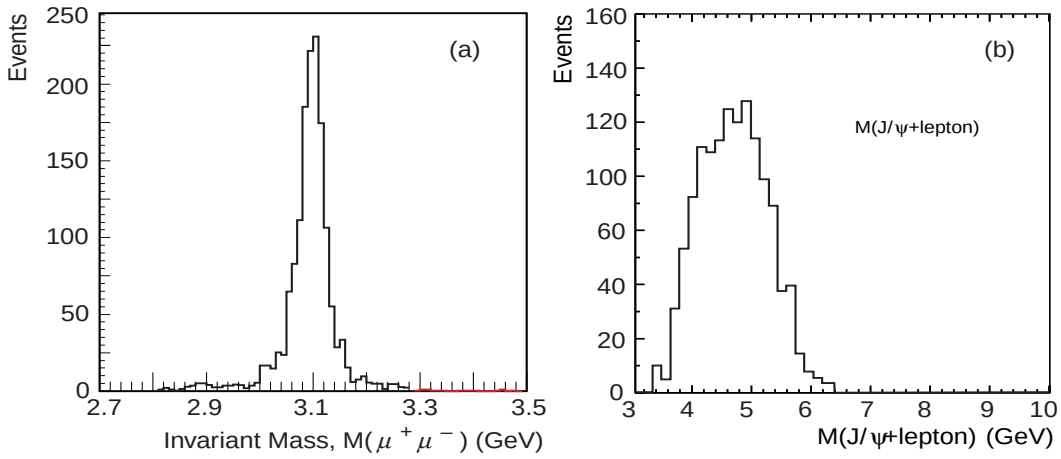

Figure 9.35: (a) $\mu^+\mu^-$ invariant mass distribution in $B_c \to J/\psi\ell\nu$ events; (b) tri-lepton invariant mass distribution that can be used to extract the B_c mass.

region $0.6 < |\eta| < 1.0$. The position matchings between muon chamber track and the track as measured in the Central Tracking Chamber (CTC) are required to have $\chi^2 < 9.0$ in r-ϕ and $\chi^2 < 12$ in r-z. There is no requirement on a specific trigger path. We require that at least one muon is reconstructed in the Silicon VerteX detector (SVX) (*i.e.* at least 3 associated SVX hits were found). We then keep the J/ψ candidates so that the muon pair passes a vertex constrained fit and the mass of the pair is within 50 MeV of the known value [101] of the J/ψ mass.

After the J/ψ candidates are found, events are scanned for other daughter particle candidates, π^+'s in this case, from B_c^+ decays. We reconstruct the B_c^+ by performing a vertex-constrained fit. The tracks with more than 3 associated SVX hits are considered to be SVX tracks, and all others are considered to be CTC tracks. We apply no further quality cuts to the SVX tracks. In the vertex constrained fit the invariant mass of the $\mu^+\mu^-$ pair is constrained to the known J/ψ mass [101]. For each B_c^+ candidate, we require that the χ^2 probability of the fit be greater than 1%.

After the B_c^+ is reconstructed, the following cuts are applied: all the B_c^+ candidates are required to have transverse momentum $P_t(B_c^+)$ greater than 6.0 GeV/c; proper lifetime $ct(B_c^+)$ greater than 80 μm; impact parameter with respect to the beam line $|I_{xy}(B_c^+)|$ less than 80 μm. We also require that the π^+ is reconstructed in the SVX and that $P_t(\pi^+) > 2.5$ GeV/c.

9.3.5.4 Acceptance Calculation using QFL′

Using the QFL′ Monte Carlo we find that the geometric/kinematic acceptance for $B_c^+ \to J/\psi\pi^+$ is equal to ∼0.018 while the same acceptance, and with the same selection criteria, for $B^+ \to J/\psi K^+$ is equal to ∼0.04 [102]. These acceptances are calculated in the region $6.0 < P_t < 30.0$ and $|y| < 0.9$ where P_t and y are the transverse momentum and rapidity, respectively, of the B_c^+ or B^+ mesons. The acceptances are calculated with the default kine-

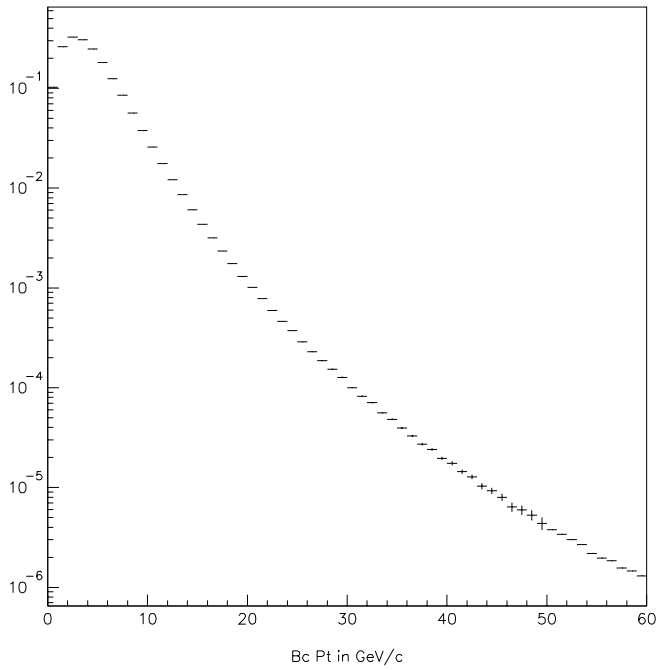

Figure 9.36: P_t distribution of B_c^+ mesons in GeV/c, at the generation level.

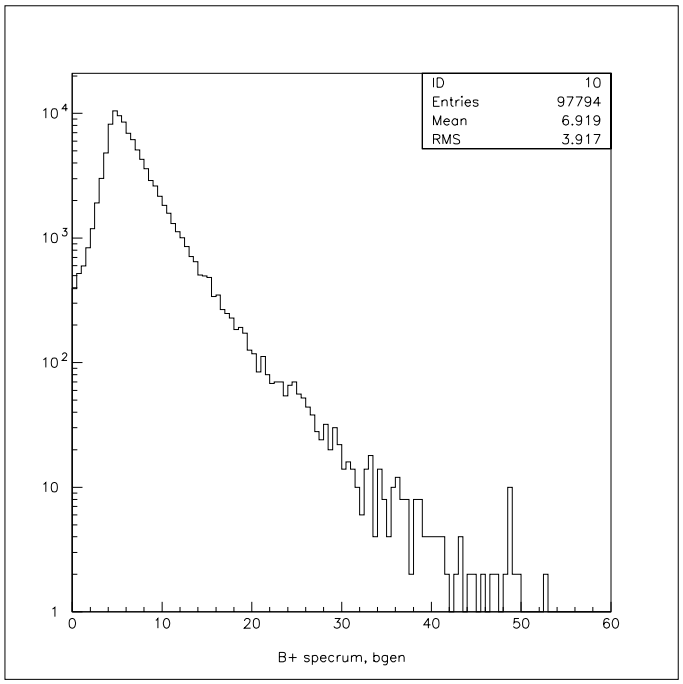

Figure 9.37: P_t distribution of B^+ mesons in GeV/c, at the generation level.

matic cuts of $P_t(B_c^+, B^+) > 6.0 GeV/c$, $P_t(\pi^+, K^+) > 2.5 GeV/c$, $|I_{xy}(B_c^+, B^+)| < 80\mu m$ and $ct(B_c^+, B^+) > 80\mu m$. At least one of the two muons forming the J/ψ has to be reconstructed in the SVX. These acceptances do not include any trigger efficiency corrections.

9.3.5.5 Yield estimate for the $B_c^+ \to J/\psi\pi^+$ decay channel

We know that $\sigma(B_c^+) \cdot BR(B_c^+ \to J/\psi\pi^+)$ is equal to:

$$R_l \cdot \sigma(B^+) \cdot BR(B^+ \to J/\psi K^+) \cdot \frac{BR(B_c^+ \to J/\psi\pi^+)}{BR(B_c^+ \to J/\psi l^+\nu)},$$

where

$$R_l = \frac{\sigma(B_c^+) \cdot BR(B_c^+ \to J/\psi l^+\nu)}{\sigma(B^+) \cdot BR(B^+ \to J/\psi K^+)} \tag{9.30}$$

and σ stands for production cross section and BR stands for branching ratio. We get the ratio R_l from [52], $\sigma(B^+)$ from [103] and $BR(B^+ \to J/\psi K^+)$ from [101]. We tabulate the theoretical expectations for the value of the ratio

$$R = \frac{BR(B_c^+ \to J/\psi\pi^+)}{BR(B_c^+ \to J/\psi l^+\nu)} \tag{9.31}$$

in Table 1. These values cover a wide spectrum from 0.06 to 0.32 according to References [104]- [61]. For this study we use as a default value the one from Reference [104]. $\sigma(B_c^+) \cdot BR(B_c^+ \to J/\psi\pi^+)$ is equal to $(0.132^{+0.061}_{-0.052}) \cdot (3.52 \pm 0.61\mu b) \cdot (9.9 \pm 1.0) \times 10^{-4} \cdot (0.091) =$ $(4.6 \pm 2.3) \cdot 10^{-4} \cdot 0.091$ μb. Then we multiply the calculated value of $\sigma(B_c^+) \cdot BR(B_c^+ \to J/\psi\pi^+)$, which is the cross section times the branching ratio of either positively charged or negatively charged B_c's, by the branching ratio of the decay $J/\psi \to \mu^+\mu^-$ [101], by the total integrated luminosity (100 pb^{-1}) and by the kinematic/geometric acceptance of the decay $B_c^+ \to J/\psi\pi^+$ (0.018). This way we get the number, S, of $B_c^+ \to J/\psi\pi^+$ events expected in our Run I sample. Then we multiply that number by 2 to account for both positively and negatively charged particles. S is approximately equal to 9 events. If we consider the variations in R discussed above, then the expected number of $B_c^+ \to J/\psi\pi^+$ events in Run I varies between 6 and 32.

One could think that we could possibly exclude the possibility of an R in the range of 0.3 based on the number of events we currently observe or based on the limit we set on

$$R_\pi = \frac{\sigma(B_c^+) \cdot BR(B_c^+ \to J/\psi\pi^+)}{\sigma(B^+) \cdot BR(B^+ \to J/\psi K^+)} \tag{9.32}$$

in [108] using Run I data. As can be seen from Fig. 9.38, which is taken from Reference [108], $R_\pi < 0.10$ for a B_c^+ lifetime of 0.33 ps and $R_\pi < 0.07$ for a B_c^+ lifetime of 0.50 ps. We can write R_π as equal to:

$$R_l \cdot \frac{BR(B_c^+ \to J/\psi\pi^+)}{BR(B_c^+ \to J/\psi l^+\nu)}.$$

We get the ratio R_l from ref. [52] to be equal to 0.132 and the ratio $\frac{BR(B_c^+ \to J/\psi\pi^+)}{BR(B_c^+ \to J/\psi l^+\nu)}$ to be in the range 0.06-0.32. This results in R_π in the range 0.008-0.04. We see that we cannot really exclude the value 0.32 for R based on our published limit for R_π.

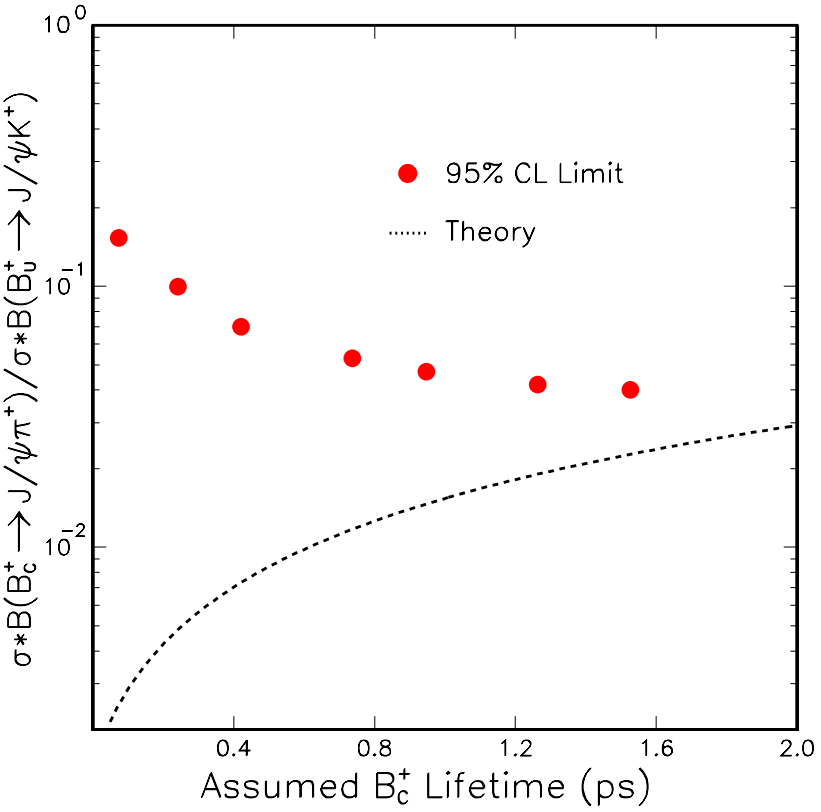

Figure 9.38: The circular points show the different 95% CL limits on the ratio of cross section times branching fraction for $B_c^+ \to J/\psi\pi^+$ relative to $B^+ \to J/\psi K^+$ as a function of the B_c^+ lifetime. The dotted curve represents a calculation of this ratio based on the assumption that the B_c^+ is produced 1.5×10^{-3} times as often as all other B mesons and that $\Gamma(B_c^+ \to J/\psi\pi^+) = 4.2 \times 10^9$ s^{-1}.

For Run IIa we expect to have an integrated luminosity of 2 fb^{-1}, that is an increase by a factor of 20 in comparison with Run I. In Run II we will take data with an upgraded silicon detector that has extended coverage in comparison to Run I by a factor of 1.4. We also plan to run with extended muon coverage for muons of type CMP (x1.2) and CMX (x1.3) and with lower muon P_t thresholds. For CMU type muons we plan to lower the thresholds from 2.0 GeV/c to 1.5 GeV/c. If we lower our P_t muon thresholds from 2.0 GeV/c to 1.5 GeV/c in our current Run I analysis we get an increase of acceptance by a factor of 1.43. According to reference [109] there will be a factor of 2 increase in the $B^0 \to J/\psi K_s^0$ yield due to the extended muon coverage and due to the lowering of the muon P_t threshold from 2.0 GeV/c to 1.5 GeV/c. Assuming conservatively an increase in yield in Run IIa by a factor of 40 in comparison to Run I we expect to have approximately 360 events in the decay channel $B_c^+ \to J/\psi\pi^+$.

In Fig. 9.39 we show the distribution of the B_c^+ mass from Monte Carlo after the selection requirements described above. Here we have lowered the muon P_t threshold to 1.5 GeV/c. The mass resolution is 17.9±0.3 MeV.

Reference	$B_c^+ \to J/\psi\pi^+$	$B_c^+ \to J/\psi l^+\nu$	R
Chang, Chen (1994) [104]	$\Gamma = 3.14 \cdot 10^{-6}$ eV	$\Gamma = 34.4 \cdot 10^{-6}$ eV	0.091
Gershtein et al (1998) [106]	BR = 0.2%	BR = 2.5%	0.08
Gershtein et al (1995) [105]	$\Gamma = 3.14 \cdot 10^{-6}$ eV	$\Gamma = 38.5 \cdot 10^{-6}$ eV (ISGW1)	0.08
	$\Gamma = 3.14 \cdot 10^{-6}$ eV	$\Gamma = 53.1 \cdot 10^{-6}$ eV (ISGW2)	0.06
Kiselev et al. (1999) [107]	BR = 0.67%	BR = 2.1%	0.32
Bjorken (1986) [61]	BR = 0.6%	BR = 2.0%	0.29

Table 9.11: Theoretical estimations of the branching ratios of two B_c^+ decay modes and of their ratio R.

9.3.5.6 Yield estimate for the $B_c^+ \to B_s^0\pi^+$ decay channel

From Reference [104] we see that $\Gamma = 73.3 \cdot 10^{-6}$ eV for the decay channel $B_c^+ \to B_s^0\pi^+$ and that $\Gamma = 34.4 \cdot 10^{-6}$ eV for the decay channel $B_c^+ \to J/\psi l^+\nu$. Using the fact that from References [61,106,107] the branching ratio of $B_c^+ \to J/\psi l^+\nu$ is expected to be ~2.2%, we derive the branching ratio for $B_c^+ \to B_s^0\pi^+$ to be equal to 4.7%.

According to Reference [110] we had 58 ± 12 $B_s^0 \to J/\psi\phi$ events in Run I and if we multiply the yield by a factor of 40 for Run IIa we will have ~ 2,400 events.

From Reference [109] we see that we expect 23,400 fully reconstructed B_s^0 events in the decay channels $B_s^0 \to D_s^-\pi^+$ and $B_s^0 \to D_s^-\pi^+\pi^-\pi^+$ for scenario A and 15,300 events for scenario C. Scenario A corresponds to a Tevatron running with bunch spacing of 396 ns and instantaneous luminosity of 0.7×10^{32} cm^{-2}s^{-1} and scenario C corresponds to a Tevatron running with bunch spacing of 396 ns and instantaneous luminosity of 1.7×10^{32} cm^{-2}s^{-1}. Based on these we conservatively assume a total of 25,000 fully reconstructed B_s^0 events in Run IIa.

From the CDF measurement of R_l [52], from the branching ratios of $B_c^+ \to J/\psi l^+\nu = 2.2\%$ and $B^+ \to J/\psi K^+ = 0.099\%$ [101] and from the fact that 39.7% of b quarks fragment into B^+ mesons [101] we get that $\sigma(B_c^+)/\sigma(b)$ is equal to $2.3 \cdot 10^{-3}$. On the other hand we know that $\sigma(B_s^0)/\sigma(b)$ is equal to 10.5% [101], that is, $\sigma(B_s^0)/\sigma(B_c^+)$ is equal to 45.6. Therefore the observed number of $B_c^+ \to B_s^0\pi^+$ events in Run IIa will be equal to $25,000/45.6 \cdot 4.7\% \cdot A_\pi$ where A_π is the acceptance for finding the pion in $B_c^+ \to B_s^0\pi^+$ after having found the B_s^0. For $A_\pi = 100\%$, we would observe 26 such decays.

If we wanted to estimate how many of the expected 25,000 fully reconstructed B_s^0 events in Run IIa will originate from B_c^+ decays, we would have to multiply $25,000/45.6 = 548.2$ by the branching ratio $BR(B_c^+ \to B_s^0/B_s^{0*}X)$ and the acceptance of reconstructing X in the presence of the B_s^0/B_s^{0*}.

In Table 9.12 we show the widths of various B_c^+ decays involving a B_s^0 or a B_s^{0*} meson from Reference [104]. If this is a complete list of the B_c^+ decays involving a B_s^0 or a B_s^{0*} and if we use the fact (as in the beginning of this section) that $\Gamma = 34.4 \cdot 10^{-6}$ eV for the decay $B_c^+ \to J/\psi l^+\nu$ and the corresponding branching ratio is expected to be ~2.2%, then $BR(B_c^+ \to B_s^0/B_s^{0*}X)$ is expected to be equal to 29.5%. It will be very useful to measure the above branching ratios. If the expectations are correct though, the above discussion

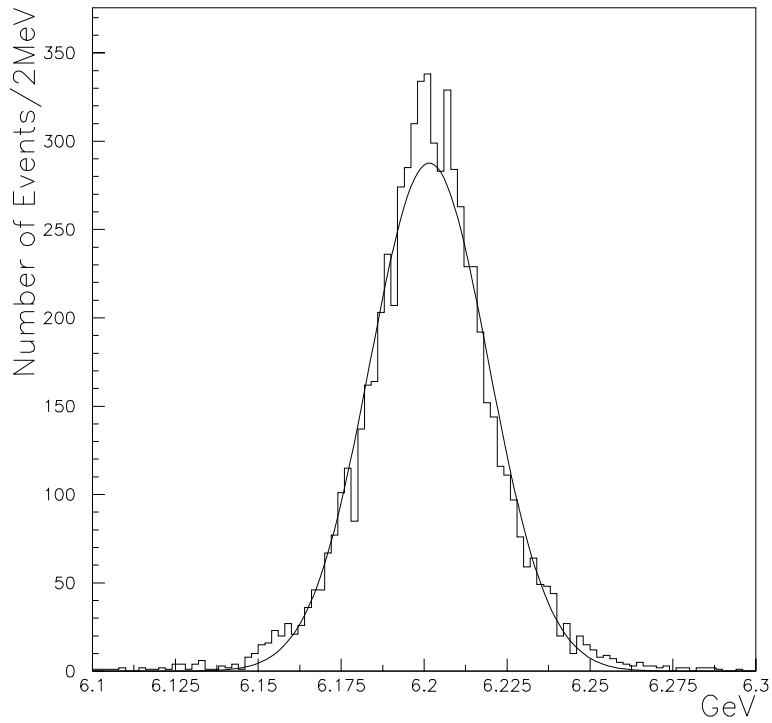

Figure 9.39: Mass distribution of B_c^+ mesons in GeV/c^2.

indicates that we will not have many B_c^+ candidates decaying to a B_s^0 or a B_s^{0*}. We have to also take into account that it will not be easy to detect the photon from the B_s^{0*} decay or to reconstruct the ρ meson in some of the above decays.

9.3.5.7 Yield estimate for the $B_c^+ \to J/\psi l^+ \nu$ decay channel

For the decay channel $B_c^+ \to J/\psi l^+ \nu$ we expect to observe ~ 800 events in Run IIa based on the 20.4 candidates of Run I [52] and the factor of 40 expected increase in the yield.

9.3.5.8 Conclusion

In Run IIa we expect to see ~ 800 $B_c^+ \to J/\psi l^+ \nu$ events, ~ 360 $B_c^+ \to J/\psi \pi^+$ events and maybe a small number of events from other exclusive decay channels. We can use these events to measure accurately the B_c^+ mass and lifetime as well as ratios of various B_c^+ branching ratios.

Decay Mode	Width in 10^{-6} eV [104]
$B_c^+ \to B_s^0 e^+ \bar{\nu}_e$	26.6
$B_c^+ \to B_s^{0*} e^+ \bar{\nu}_e$	44.0
$B_c^+ \to B_s^0 \pi^+$	73.3
$B_c^+ \to B_s^0 \rho^+$	56.1
$B_c^+ \to B_s^{0*} \pi^+$	64.7
$B_c^+ \to B_s^{0*} \rho^+$	188.0
$B_c^+ \to B_s^0 K^+$	5.27
$B_c^+ \to B_s^{0*} K^+$	3.72
Total	461.69

Table 9.12: Theoretical estimates of the width of B_c^+ decay modes involving B_s^0 or B_s^{0*} in the final states.

9.4 Doubly-heavy Baryons

Doubly-heavy baryons are baryons that contain two heavy quarks, either cc, bc or bb. These hadrons provide yet another window onto the dynamics of heavy quarks. Doubly-heavy baryons are expected to be produced at respectable rates at the Tevatron; the basic production cross sections are in the nanobarn range. Also of interest are the states formed from three heavy quarks: bbb, bbc, bcc or ccc. We do not provide cross section estimates for these triply-heavy baryons.

9.4.1 Spectroscopy[†]

The spectroscopy of baryons containing two heavy quarks QQ is of interest because of similarities both to a quarkonium state, $Q\bar{Q}$ and to a heavy-light meson, $\bar{Q}q$. On the one hand, the slow relative motion of the two heavy quarks is similar to quarkonium. On the other hand, the lighter degree of freedom moves relativistically around the slowly moving QQ. Since the QQ is in a color antitriplet state, in the heavy quark limit the system is very similar to a $\bar{Q}q$ system.

A rich spectrum of excitations is expected, both excitations of the QQ system as well as the light degrees of freedom. However from the experimental point of view, a detailed discussion of the excited states is probably premature. We will limit our discussion here to the estimates of the masses of the lowest lying states, $\Xi_{QQ'} = (QQ'q)$, $\Omega_{QQ'} = (QQ's)$ containing two heavy quarks and the states $\Xi_{QQQ'} = (QQQ')$, $\Omega_{QQQ} = (QQQ)$ containing three heavy quarks. Where the corresponding $J = \frac{1}{2}$ state exists, the $J = \frac{3}{2}$ states are unstable decaying to the ground state by photon emission. The hyperfine splittings with the spin-$\frac{1}{2}$ states are calculated using the procedure of De Rujula et al. [125]. Ignoring electromagnetism we have that

$$H = H_0 + \alpha \sum_{i<j} \frac{s_i \cdot s_j}{m_i m_j} \,, \tag{9.33}$$

[†]Author: R.K. Ellis

where the sum runs over the three pairs of quarks and α is a constant fixed using the normal decuplet-octet splitting.

Estimates for the masses and spectra of the baryons containing two or more heavy quarks have been considered by many authors [111]- [124]. We are not aware of a reference which gives the masses of all the states we are interested in. This is of some importance since the separation between states may be more reliable than the absolute energy scale. We have therefore created a complete list, using the simple procedure suggested by Bjorken [111]. The mass of the spin-$\frac{3}{2}$, QQQ baryons are calculated by scaling from the $Q\bar{Q}$ state,

$$\frac{M_{QQQ}}{M_{Q\bar{Q}}} = \frac{3}{2} + \frac{k}{m^{\frac{4}{3}}} + \frac{k'}{\ln^2 m/m_0} \; . \tag{9.34}$$

Experience from the Δ, ρ and Ω, ϕ systems suggest the values

$$M_{ccc} = (1.59 \pm 0.03) M_{c\bar{c}}, \quad M_{bbb} = (1.56 \pm 0.02) M_{b\bar{b}} \; . \tag{9.35}$$

The other spin-$\frac{3}{2}$ baryons are estimated using an equal spacing rule to interpolate between the QQQ state and normal $J = \frac{3}{2}$ baryons. This results in the rule that replacing a b-quark by a c-quark costs 3.280 GeV, a c-quark by an s-quark costs 1.085 GeV, and an s-quark by a u-quark costs 0.145 GeV. Finally the masses of the spin-$\frac{1}{2}$ baryons are calculated using the procedure and mass values of DGG [125]. The results for the hyperfine splitting are

$$\begin{aligned}
E(abc, J = \frac{3}{2}) &= E_0 + \frac{\alpha}{4}\Big(\frac{1}{m_a m_b} + \frac{1}{m_b m_c} + \frac{1}{m_c m_a}\Big), \\
E(bbc, J = \frac{1}{2}) &= E_0 + \frac{\alpha}{4}\Big(\frac{1}{m_b^2} - \frac{3}{m_b m_c}\Big), \\
E(abc, J = \frac{1}{2}) &= E_0 + \frac{\alpha}{4 m_a m_b m_c}\Big(- \Sigma - 2\sqrt{\Delta}\Big), \\
E'(abc, J = \frac{1}{2}) &= E_0 + \frac{\alpha}{4 m_a m_b m_c}\Big(- \Sigma + 2\sqrt{\Delta}\Big) \; ,
\end{aligned} \tag{9.36}$$

where $\Sigma = m_a + m_b + m_c, \Delta = \Sigma^2 - 3(m_a m_b + m_b m_c + m_c m_a)$. The values found using this procedure are compared with the results of other authors in Table 9.13. We quote only the central values and refer the reader to the original publications for the estimated errors. There is substantial agreement between all estimates if these errors are taken into account.

9.4.2 Production[†]

The direct production of a doubly-heavy baryon can be treated within the NRQCD factorization framework described in Section 9.2.2. The cross section for the direct production of a bc baryon H can be expressed in the form (9.1) and (9.13), except that $b\bar{b}(n)$ is replaced by $bc(n)$. The short-distance cross section $d\hat{\sigma}[ij \to bc(n) + X]$ for creating the bc in the color and angular-momentum state n can be calculated as a perturbative expansion in α_s at scales of order m_c or larger. The nonperturbative matrix element $\langle O^H(n) \rangle$ encodes the

[†]Authors: E. Braaten, A. Likhoded

State	Mass ref. [113]	Mass ref. [112]	Mass ref. [114]	Mass
$\Xi_{cc}^{++}(ccu, J=\frac{3}{2})$	3.735	3.81	3.746	3.711
$\Omega_{cc}^{+}(ccs, J=\frac{3}{2})$	3.84	3.89	3.851	3.848
$\Omega_{ccc}^{++}(ccc, J=\frac{3}{2})$				4.925
$\Xi_{cc}^{++}(ccu, J=\frac{1}{2})$	3.70	3.66	3.676	3.651
$\Omega_{cc}^{+}(ccs, J=\frac{1}{2})$	3.72	3.76	3.787	3.811
$\Xi_{bc}^{+}(bcu, J=\frac{3}{2})$	7.02	7.02	7.083	7.000
$\Omega_{bc}^{0}(bcs, J=\frac{3}{2})$	7.105	7.11	7.165	7.128
$\Xi_{bcc}^{+}(bcc, J=\frac{3}{2})$				8.202
$\Xi_{bc}^{+}(bcu, J=\frac{1}{2})$	6.93	6.95	7.029	6.938
$\Xi_{bc}^{\prime +}(bcu, J=\frac{1}{2})$		7.00	7.053	6.971
$\Omega_{bc}^{0}(bcs, J=\frac{1}{2})$	7.00	7.05	7.126	7.095
$\Omega_{bc}^{\prime 0}(bcs, J=\frac{1}{2})$		7.09	7.148	7.115
$\Xi_{bcc}^{+}(bcc, J=\frac{1}{2})$				8.198
$\Xi_{bb}^{0}(bbu, J=\frac{3}{2})$	10.255	10.28	10.398	10.257
$\Omega_{bb}^{-}(bbs, J=\frac{3}{2})$	10.315	10.36	10.483	10.399
$\Xi_{bbc}^{0}(bbc, J=\frac{3}{2})$				11.481
$\Omega_{bbb}^{-}(bbb, J=\frac{3}{2})$				14.760
$\Xi_{bb}^{0}(bbu, J=\frac{1}{2})$	10.21	10.23		10.235
$\Omega_{bb}^{-}(bbs, J=\frac{1}{2})$	10.27	10.32		10.385
$\Xi_{bbc}^{0}(bbc, J=\frac{1}{2})$				11.476

Table 9.13: Mass estimates in GeV for low-lying baryons with two or more heavy quarks. The last column shows our values derived using the methods of Ref [111].

probability for a bc in the state n to bind to form the baryon H. The matrix element scales as a definite power of the relative velocity v of the charm quark.

The production mechanisms for bc are similar to those for $\bar{b}c$, because two heavy quark-antiquark pairs must be created in the collision. The lowest order mechanisms for creating bc are the order-α_s^4 processes $q\bar{q}, gg \to (bc) + \bar{b}\bar{c}$. The color state of the quark-quark system can be either color-antitriplet or color-sextet. From counting the color states, we expect the color-sextet cross section to be about a factor of 2 larger than the color-antitriplet cross section. Thus the relative importance of the two color states should be determined primarily by the probability for the b and c to bind with a light quark to produce a doubly-heavy baryon.

In the ground state Ξ_{bc} of the bc baryon system, the bc is in a color-antitriplet S-wave state that is relatively compact compared to the size of the baryon. The bc diquark behaves very much like the heavy antiquark in a heavy-light meson. The probability that b and c quarks that are created with small relative momentum in a parton collision will hadronize into the Ξ_{bc} is therefore expected to be greatest if the bc is in a color-antitriplet S-wave state. All other NRQCD matrix elements are suppressed by powers of v. If we keep only the color-antitriplet S-wave contribution, the formula for the cross section of Ξ_{bc} is very similar to that for the B_c in the color-singlet model. The short-distance cross section for creating

a color-singlet $\bar{b}c$ is replaced by the cross section for creating a color-antitriplet bc. The long-distance factor for B_c, which is proportional to the square of the radial wavefunction at the origin $R_{1S}(0)$, is replaced by a color-antitriplet matrix element for the Ξ_{bc}. This matrix element can be treated as a phenomenological parameter analogous to the color-octet matrix elements for quarkonium production. It can also be estimated using a quark potential model for the doubly-heavy baryon, in which case it is proportional to the square of an effective radial wavefunction at the origin $R^{bc}_{1S}(0)$ for the bc diquark. The quark model estimate is probably much less reliable than the potential model estimate of $R_{1S}(0)$ for B_c. We will refer to the cross sections obtained by using the leading order bc cross section and a quark model estimate for the S-wave color-antitriplet matrix element as the *diquark model* for doubly-heavy baryon production.

The production of doubly-heavy baryons in the diquark model at order α_s^4 was studied in detail in the series of papers [60]. The resulting differential cross sections $d\sigma/dp_T$ for Ξ_{cc}, Ξ_{bc} and Ξ_{bb} baryons are presented in Fig. 9.29 and compared to that of the B_c meson. The cross sections integrated over p_T greater than ${p_T}^{min}$ are shown in Fig. 9.30. The cross sections are evaluated at 2.0 TeV and integrated over $|y| < 1$. The quark masses were set to $m_c = 1.5$ GeV and $m_b = 4.8$ GeV. The QCD coupling constant was fixed at $\alpha_s = 0.23$. The radial wave functions at the origin for the heavy diquarks were taken to be $R^{cc}_{1S}(0) = 0.601$ GeV$^{3/2}$, $R^{bc}_{1S}(0) = 0.714$ GeV$^{3/2}$, and $R^{bb}_{1S}(0) = 1.35$ GeV$^{3/2}$ [86]. The largest uncertainties come from the choice of scale in the overall factor $\alpha_s^4(\mu)$ and from the radial wave functions at the origin for the heavy diquarks. The production rates for Ξ_{cc} and Ξ_{bc} are predicted to be as large as 50% of the production rate for $(B_c + B_c^*)$ for ${p_T}^{min} = 10$ GeV.

The uncertainties in the prediction of the Ξ_{bc} cross section can be greatly reduced by normalizing the cross section to that of the B_c. The reason is that the short-distance cross sections come from exactly the same Feynman diagrams, except that the color-singlet $\bar{b}c$ is replaced by a color-antitriplet bc. Regions of phase space with various gluon virtualities μ are weighted in almost the same way, so the factor of $\alpha_s^4(\mu)$ that gives the largest uncertainty in the B_c cross section cancels in the ratio $\sigma(\Xi_{bc})/\sigma(B_c)$ given that $\mu_{bc} = \mu_{b\bar{c}}$. The largest remaining uncertainty comes from the radial wave function at the origin $R^{bc}_{1S}(0)$ for the heavy diquark in the Ξ_{bc}. Using the value $R^{bc}_{1S}(0) = 0.714$ GeV$^{3/2}$, one gets the estimate

$$\sigma(\Xi_{bc})/\sigma(B_c) \simeq 0.5\,. \tag{9.37}$$

Taking into account the cascade decays of excited bc baryon states, the inclusive Ξ_{bc} cross-section integrated over $p_T > 6$ GeV and $|y| < 1$ is predicted to be

$$\sigma(\Xi_{bc}) = 1.5\ nb\,. \tag{9.38}$$

Alternatively, taking the experimental value for the B_c cross section [52], we get

$$\sigma(\Xi_{bc}) = 5 \pm 3\ nb\,. \tag{9.39}$$

With an integrated luminosity of about 100 pb^{-1} in Run I, this corresponds to more than 10^5 events with Ξ_{bc} baryons in the considered kinematical region.

The predicted cross sections for bb and cc baryons have larger uncertainties than those for bc baryons. The large uncertainties from the $\alpha_s^4(\mu)$ factor can not be removed by normalizing

to $b\bar{b}$ or $c\bar{c}$ quarkonium cross sections, since they arise from very different short-distance parton processes. However, from the predictions in Fig. 9.29, one can expect roughly the same number of Ξ_{cc} and Ξ_{bc} events in the kinematical region of $p_T > 10$ GeV and $|y| < 1$. The total number of Ξ_{bb} events will be about a factor of 10 smaller.

9.4.3 Decays[†]

Since the major thrust of this report is B-physics, we may be tempted to limit discussion to baryons containing b quarks. However, such baryons often decay by cascades into baryons containing c quarks and identification of the latter may be an important first step in reconstructing doubly-heavy baryons containing b quarks.

The lifetimes for the ground states of the doubly-heavy baryons have been calculated in the framework of the operator product expansion, which involves an expansion in inverse powers of the heavy quark mass [87]. In leading order of $1/m_Q$, the inclusive widths are determined by the spectator approximation with QCD corrections. The next order in $1/m_Q$ takes into account corrections connected with quark motion in the doubly-heavy baryon and with the chromomagnetic quark interaction. In doubly-heavy baryons, there is Pauli interference (PI) of quark decay products with identical quarks from the initial state, as well as weak scattering (WS, or weak exchange) where exchange of a $W^{\pm}$ occurs between quarks. Both effects play important roles in the mechanism of doubly-heavy baryon decay. For example, Pauli interference leads to the increase of the b-quark decay contribution to bc-baryon by a factor of two. In this case, the sign is basically determined from the interference of the charm quark of the initial state with the charm quark from the b-quark decay. The antisymmetric color structure of the baryon wave function leads to the positive sign for the Pauli interference. The overall effect of the corrections to the spectator mechanism can reach 40–50%. In Tables 9.14 and 9.15, we show the contributions of the different modes to the total decay widths of cc and bc baryons. One can see from these tables that the weak scattering contributions are comparable with the spectator contributions. The estimates of the lifetimes of the Ξ_{cc} and Ξ_{bc} baryons from the operator product expansion are [90–92]:

$$\begin{aligned} \tau_{\Xi_{cc}^{++}} &= 0.43 \pm 0.1 \text{ ps}, \\ \tau_{\Xi_{cc}^{+}} &= 0.12 \pm 0.1 \text{ ps}, \\ \tau_{\Xi_{cc}^{0}} &= 0.28 \pm 0.07 \text{ ps}, \\ \tau_{\Xi_{bc}^{+}} &= 0.33 \pm 0.08 \text{ ps}. \end{aligned} \tag{9.40}$$

We proceed to discuss exclusive decay modes of the doubly-heavy baryons that may be observable. Let us first consider spectator decay modes, in which the doubly-heavy baryon decays into either a lighter doubly-heavy baryon or a baryon containing a single heavy quark. In Table 9.16, we give branching fractions for exclusive spectator decay modes that were calculated in the framework of QCD sum rules [88]. Some of the decay modes have surprisingly large branching fractions, particularly $\Xi_{cc}^{+} \to \Xi_{cs}^{0}\pi^{+}(\rho^{+})$, $\Xi_{cc}^{++} \to \Xi_{cs}^{+}\pi^{+}(\rho^{+})$

[†]Authors: A. Likhoded, R. Van Kooten

Mode	width, ps^{-1}	Fraction of Ξ_{cc}^{++} width	Fraction of Ξ_{cc}^{+} width
$c \to sdu$	2.894	1.24	0.32
$c \to s\ell^+\nu$	0.760	0.32	0.09
PI	-1.317	-0.56	–
WS	5.254	–	0.59
$\Gamma_{\Xi_{cc}^{++}}$	2.337	1	–
$\Gamma_{\Xi_{cc}^{+}}$	8.909	–	1

Table 9.14: Fractional contributions of different modes to the total decay width of doubly-charmed baryons, Ξ_{cc}. PI and WS are Pauli interference and weak scattering effects, respectively.

Mode	Fraction of Ξ_{bc}^{+} width	Fraction of Ξ_{bc}^{0} width
$b \to c + X$	0.120	0.17
$c \to s + X$	0.37	0.31
PI	0.23	0.20
WS	0.20	0.31

Table 9.15: Fractional contributions of different modes to the total decay width of Ξ_{bc} baryons. PI and WS are Pauli interference and weak scattering effects, respectively.

and semileptonic decays. A recent work from Onishchenko calculating these branching ratios including results from three-point NRQCD sum rules [93] give even larger values.

We also consider another class of exclusive decay modes for doubly-heavy baryons that may be observable. As pointed out above, the contribution from weak scattering to the Ξ_{bc}^{+} and Ξ_{bc}^{0} decay width is about 20%. This type of decay is characterized by specific kinematics. In the rest frame of the Ξ_{bc} baryon, the c and s quarks from the scattering process $bc \to cs$ move in the opposite directions with a high momentum of about 3.2 GeV. Both the c and s quarks then fragment, producing multiparticle final states. These states include the 3-particle states $D^{(*)}K^{(*)}N$. The $D^{(*)}$ and $K^{(*)}$ can be produced by fragmentation processes: $c \to D^{(*)} + X_q$ and $s \to K^{(*)} + X_q$. However, in order for only one additional particle N to be produced in the decay of Ξ_{bc}, the $D^{(*)}$ and $K^{(*)}$ must be in the hard part of fragmentation spectrum with $z > 0.8$. We can use a well-known parametrization of the fragmentation functions to estimate the probability for such a decay:

$$\begin{aligned} Br(\Xi_{bc} \to D^{(*)}K^{(*)}N) &\approx Br(WS) \times W(z_D > 0.8) \times W(z_K > 0.8) \\ &= 0.2 \times 0.2 \times 0.04 \, . \end{aligned} \tag{9.41}$$

The resulting rough estimate of the branching fraction for $\Xi_{bc} \to D^{(*)}K^{(*)}N$ is 0.2%. We conclude that the branching fractions for these modes may be large enough to be observed.

Baryon	Mode	Br (%)	Baryon	Mode	Br (%)
$\Xi_{bb}^{\diamond}$	$\Xi_{bc}^{\diamond}\ l^-\bar{\nu}_l$	11.2			
	$\Xi_{bc}^{\diamond}\ \pi^-$	0.3			
	$\Xi_{bc}^{\diamond}\ \rho^-$	3.4			
Ξ_{bc}^0	$\Xi_{cc}^+\ l^-\bar{\nu}_l$	3.3	Ξ_{bc}^+	$\Xi_{cc}^{++}\ l^-\bar{\nu}_l$	3.5
	$\Xi_{bs}^-\ l^+\nu_l$	2.8		$\Xi_{bs}^0\ l^+\nu_l$	3.0
	$\Xi_{cc}^+\ \pi^-$	0.55		$\Xi_{cc}^{++}\ \pi^-$	0.6
	$\Xi_{cc}^+\ \rho^-$	1.4		$\Xi_{cc}^{++}\ \rho^-$	1.5
	$\Xi_{bs}^-\ \pi^+$	12.3		$\Xi_{bs}^0\ \pi^+$	13.1
	$\Xi_{bs}^-\ \rho^+$	5.2		$\Xi_{bs}^0\ \rho^+$	5.6
Ξ_{cc}^+	$\Xi_{cs}^0\ l^+\nu_l$	6.9	Ξ_{cc}^{++}	$\Xi_{cs}^+\ l^+\nu_l$	14.9
	$\Xi_{cs}^0\ \pi^+$	4.2		$\Xi_{cs}^+\ \pi^+$	8.1
	$\Xi_{cs}^0\ \rho^+$	24.8		$\Xi_{cs}^+\ \rho^+$	45.1

Table 9.16: Exclusive (spectator) decay modes of doubly-heavy baryon calculated in the framework of QCD sum rules. The symbol $^\diamond$ represents electric charge, i.e., $^{\diamond=\pm,0}$.

9.4.4 Experimental Observability[†]

To set the scale for observability of doubly-heavy baryons, we note that CDF has observed [52] about 20 events of the type $B_c \to J/\psi\ell^\pm\nu$ in 0.11 fb^{-1} using the $\mu^+\mu^-$ decay of the J/ψ. We take this process to have a total branching ratio of 0.3%. We assume comparable trigger and reconstruction efficiencies for the B_c and typical doubly-heavy baryon decay modes. In Section 9.4.3, the cross sections for baryons containing cc or bc were predicted to be within about a factor of 2 of the cross section for B_c for $p_T > 10$ GeV. With data samples of 3, 10, and 30 fb^{-1}, we are therefore initially restricted to doubly-heavy baryon decay modes with branching ratios greater than of order 10^{-4}, 5×10^{-5}, and 1.5×10^{-5} respectively. Special purpose detectors with better triggering abilities (such as BTeV) will be able to investigate rarer modes.

Historically, larger samples of rarer b-quark states are available for measuring properties such as lifetimes and polarization through "semi-exclusive" decays where not all the decay products are reconstructed and/or there is an escaping neutrino from semileptonic decay. As an example, the Λ_b state was first observed at LEP [85] through an excess of "correct-sign" Λ-ℓ^- and Λ-ℓ^+ correlations over the "wrong-sign" correlations. A similar situation will exist for doubly-heavy baryons, but now there can be two leptons in the decay chain exhibiting charge correlations.

If a doubly-heavy baryon decays semileptonically into either a lighter doubly-heavy baryon or a baryon containing a single heavy quark, and if the second baryon also decays semileptonically, they will give rise to two leptons associated with the same jet. Due to the large masses of the heavy baryons, both of these leptons tend to be at large values of p_T relative to the jet axis. It is also interesting to note that cascading semileptonic decays in the case of Ξ_{bb} or Ξ_{cc} can result in same-sign leptons in the same jet, a process with

[†]Authors: R.K. Ellis, R. Van Kooten

very little background. The largest irreducible background comes from a gluon splitting into $b\bar{b}$ to produce a jet containing two b-hadrons, one of which decays semileptonically and the other mixes before decaying semileptonically. Another background is the decay of one b quark semileptonically along with a same-sign lepton from the cascade decay through charm of the other $\bar{b}$ quark. However, this background level can be reduced by appropriate kinematic cuts on the lepton from the cascade decay. More problematic in this case would be lepton misidentification faking the same-sign lepton signal.

Other doubly-heavy baryon decays resulting in two opposite-sign leptons may still be distinctive due to the kinematics of the decay, but can suffer from a large physics background due to generic $b \to c \to s$ decays. Typical branching ratios for both types of decays are collected in Table 9.17 using the semileptonic rates predicted in ref. [93].

Mode			Br (%)	Lepton charge correlation
Ξ_{bb}^-	$\to \Xi_{bc}^0 \ell^- \nu$	$\to \Xi_{cc}^+ \ell^- \nu$	0.69%	same-sign
		$\to \Xi_{bs}^- \ell^+ \nu$	0.61%	opp-sign
Ξ_{bb}^0	$\to \Xi_{bc}^+ \ell^- \nu$	$\to \Xi_{cc}^{++} \ell^- \nu$	0.73%	same-sign
		$\to \Xi_{bs}^- \ell^+ \nu$	0.61%	opp-sign
Ξ_{bc}^0	$\to \Xi_{cc}^+ \ell^- \nu$	$\to \Xi_{cs}^0 \ell^+ \nu$	0.35%	opp-sign
	$\to \Xi_{bs}^- \ell^+ \nu$	$\to \Xi_{cs}^0 \ell^- \nu$	0.37%	opp-sign
Ξ_{bc}^+	$\to \Xi_{cc}^{++} \ell^- \nu$	$\to \Xi_{cs}^+ \ell^+ \nu$	0.82%	opp-sign
	$\to \Xi_{bs}^0 \ell^+ \nu$	$\to \Xi_{cs}^+ \ell^- \nu$	0.40%	opp-sign
Ξ_{cc}^{++}	$\to \Xi_{cs}^+ \ell^+ \nu$	$\to \Xi \ell^+ X$	1.5%	same-sign
Ξ_{cc}^+	$\to \Xi_{cs}^0 \ell^+ \nu$	$\to \Xi \ell^+ X$	0.68%	same-sign

Table 9.17: Decay rates of cascading semileptonic decays from doubly-heavy baryons.

For fully exclusive decays, decay diagrams involving either spectator decays or W-exchange (including Cabibbo-suppressed decays) were considered. For a doubly-heavy baryon of the form bbq or bcq, the decays into J/ψ's are the favored decay modes, because of the ease of triggering on subsequent decays into $\mu^+\mu^-$ and e^+e^- and also because they absorb Q-value which would otherwise produce pion multiplicity contributing to combinatorial background. It is predicted that "golden" exclusive decay modes such as $\Xi_{bc}^+ \to \Lambda_c^+ J/\psi$ or $\Xi_{bb}^0 \to \Lambda_b^0 J/\psi$ into triggerable modes have small total branching ratios between 10^{-5} and 10^{-7}, although the inclusive rate for all decays containing a J/ψ may be as high as 10^{-3} [94].

Decays without a distinctive J/ψ may still be accessible due to the abundance of cascading decays. These cascade decays can then result in triggerable decays either from jets containing multiple leptons due to sequences of semi-leptonic decays as discussed above or from many tracks with relatively large impact parameter significance.

A doubly-heavy baryon decaying into either a b-baryon or another doubly-heavy baryon will have a decay length that gives rise to a large number of high-impact parameter tracks that could allow the use of a vertex/silicon track trigger. A doubly-heavy baryon with a

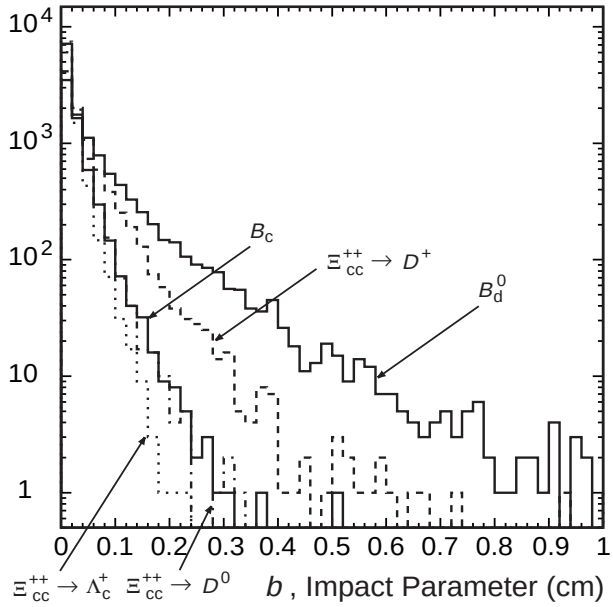

Figure 9.40: Impact distribution of all charged decay products in the cascade decays of Ξ_{cc}^{++} via Λ_c, D^0, and D^+ compared to the same distribution of the decay products from B_c and B_d^0.

short lifetime (e.g., $\tau(\Xi_{cc}^{++}) \approx 0.4$ ps, $\tau(\Xi_{bc}^0) \approx 0.3$ ps, and $\tau(\Xi_{bb}^0) \approx 0.7$ ps) can decay into a charm meson with a reasonably long lifetime (e.g., $\tau(D^+) = 1.06$ ps). The large mass of the doubly-heavy baryon parent can give substantial transverse momentum kick with respect to the original flight direction. Including a fairly long charm decay length, the final decay products can have impact parameters comparable to those of b hadrons with typical lifetimes of 1.5 ps. These decays can be found with reasonable efficiency using a vertex/silicon track trigger. To test this idea, a Monte Carlo study was made at the four-vector level. Ξ_{cc}^{++} baryons were generated with a p_T distribution according to Ref. [80] with a lifetime of 0.43 ps. This doubly-heavy baryon was allowed to decay to a singly-charmed meson or baryon in a two-body decay for simplicity. The impact parameters of the resultant decay products of the Λ_c, D^0, or $D^{\pm}$ were found. Distributions of these impact parameters are shown in Fig. 9.40 which, for the case of $\Xi_{cc}^{++} \to D^+$, is intermediate in extent between that of the products from B_c decay and from B_d^0 decay. Considering the earlier description of the efficiency of a typical vertex/silicon track trigger (see 9.3.4.3), there is potential promise in triggering on doubly-heavy baryons in cascade decays.

Finally, the decay mode $\Xi_{bc} \to D^{(*)}K^{(*)}N$ discussed in Section 9.4.3 shows promise due to its potentially relatively large rate and the nature of its decay products which allows a fairly clean reconstruction. If $N = p$, the proton would allow for the use of particle identification. The D^* can be identified by the standard procedure of cutting on the small value of $\Delta_m = m(D^*) - m(D)$, where $m(D^*)$ is the reconstructed mass of the D^* using the soft pion in $D^* \to D\pi$. Triggering would rely on a silicon track trigger as described above.

Decay modes containing a Λ_c in the cascade chain also have potential due to the possibil-

ity of the clean reconstruction of this charm baryon in the decay $\Lambda_c \to pK\pi$. Of note is that CDF cleanly reconstructed 197 signal events with Λ_c for a Λ_b lifetime measurement [95]. They used the lepton from the semileptonic decay $\Lambda_b \to \Lambda_c \ell\nu X$ as part of their trigger. Triggering certainly is a serious issue for any all-hadronic decay mode.

State	Lifetime [ps]	Mass [GeV]	Interesting Exclusive Decay Modes	Estimated Br
$\Xi_{cc}^{++}(ccu)$	0.43 [92]	3.651	$D^{*+}\pi^+\Lambda^0 \to p\pi^-$ $\hookrightarrow K^-\pi^+\pi^+$	9.4×10^{-4}
			$D^{*+}p\bar{K}^0 \to \pi^+\pi^-$ $\hookrightarrow K^-\pi^+\pi^+$	4.7×10^{-4}
			$\Lambda_c^+(cdu)\ \pi^+\ \bar{K}^0 \to \pi^+\pi^-$ $\hookrightarrow pK^-\pi^+$	4×10^{-4}
$\Xi_{cc}^{+}(ccd)$	0.11 [92]	3.651	$D^{*+}\ \Lambda^0 \to p\pi^-$ $\hookrightarrow K^-\pi^+\pi^+$	4×10^{-4}
			$D^0 p\bar{K}^0 \to \pi^+\pi^-$ $\hookrightarrow K^-\pi^+$	2×10^{-4}
			$\Lambda_c^+(cdu)\ \bar{K}^0 \to \pi^+\pi^-$ $\hookrightarrow pK^-\pi^+$	1.6×10^{-4}
$\Omega_{cc}^{+}(ccs)$	0.5 [61]	3.811	$\Lambda^0 K^0 D^+$	
$\Omega_{ccc}^{++}(ccc)$	0.3 [61]	4.925	Cascades to Ξ_{cc}^+	–

Table 9.18: Properties and interesting exclusive hadronic decay modes of multiple-charm baryons.

With these considerations, a list of potentially interesting exclusive hadronic decay modes for doubly-heavy baryons are collected in Tables 9.18 and 9.19. These decay modes, in addition to the semi-exclusive decays from semileptonic decays, deserve further study as possible discovery modes for doubly-heavy baryons.

9.5 Fragmentation

The fragmentation of quarks and gluons into hadrons involves confinement dynamics, and occurs at time scales that are long compared to those of the hard scattering that produced the quarks and gluons. Accordingly, in single-particle inclusive hard-scattering processes, the fragmentation process is factorized in perturbative QCD (see [126] and references therein) from the hard interaction and summarized in a nonperturbative fragmentation function (FF) $D_i^H(z,\mu)$ [127]. $D_i^H(z,\mu)$ is the probability density of a hadron H to form from parton i with momentum fraction z at factorization scale μ. Just as initial-state parton distribution functions (PDFs), fragmentation functions are not completely calculable in perturbation theory, although their evolution with μ is. The evolution equations for FFs are identical in form to those for PDFs, although the evolution kernels differ from second order

State	Lifetime [ps]	Mass [GeV]	Interesting Exclusive Decay Modes	Estimated Br
$\Xi_{bc}^{+}(bcu)$	0.33 ± 0.08 [91]	6.971	$\Lambda_c^+ \; J/\psi \to \mu^+\mu^-$ $\hookrightarrow pK^-\pi^+$ $D^{(*)0} \; p\bar{K}^0 \to \pi^+\pi^-$ $\hookrightarrow K^-\pi^+$ $D^{(*)+} \; pK^{(*)-}$ $\hookrightarrow K^-\pi^+\pi^+$	$< 2 \times 10^{-7}$ 2.1×10^{-5} 4×10^{-5}
$\Xi_{bc}^{0}(bcd)$	0.28 ± 0.07 [91]	6.971	$\Xi_c^0(csd) \; J/\psi \to \mu^+\mu^-$ $\hookrightarrow \Lambda^0\bar{K}^0$ $D^{(*)0} \; pK^{(*)-}$ $\hookrightarrow K^-\pi^+$ $D^{(*)+} \; p\pi^-K^{(*)-}$ $\hookrightarrow K^-\pi^+\pi^+$	$< 2 \times 10^{-7}$ 6.2×10^{-5} 4×10^{-5}
$\Omega_{bc}^{0}(bcs)$	–	7.095	$\Omega_c^0(ssc) \; J/\psi \to \mu^+\mu^-$ $\hookrightarrow \Omega^-\pi^+$	$< 1.44 \times 10^{-6}$
$\Xi_{bcc}^{+}(bcc)$	–	8.198	Cascades to above states	

Table 9.19: Properties and interesting exclusive hadronic decay modes of heavy baryons containing both a b and a c quark.

State	Lifetime [ps]	Mass [GeV]	Interesting Exclusive Decay Modes	Estimated Br
$\Xi_{bb}^{0}(bbu)$	0.79 [90]	10.235	$\Xi_{bc}^+(bcu) \; \pi^-$ $\hookrightarrow$ as in Table 9.19 $\Lambda_b^0(bdu) \; J/\psi \to \mu^+\mu^-$ $\hookrightarrow \Lambda_c^+\pi^-$	3×10^{-6} 2.4×10^{-7} if $\Lambda_b^0 \to \Lambda_c \ell\nu X$
$\Xi_{bb}^{-}(bbd)$	0.8 [90]	10.235	$\Xi_{bc}^0(bcd) \; \pi^-$ $\hookrightarrow$ as in Table 9.19 $\Xi_b^-(bsd) \; J/\psi \to \mu^+\mu^-$ $\hookrightarrow \Xi_c^0\pi^-$	6×10^{-5}
$\Omega_{bb}^{-}(bbs)$	0.8 [90]	10.385	Cascades to above states	
$\Xi_{bbc}^{0}(bbc)$	–	11.476	Cascades to above states	
$\Omega_{bbb}^{-}(bbb)$	–	14.76	Cascades to above states	

Table 9.20: Properties and interesting exclusive hadronic decay modes of heavy baryons containing two b quarks.

onwards [128–130]. Though nonperturbative, these FFs are universal and so, they may be determined for each hadron H in a few calibration experiments at some fixed scale μ_0, for subsequent use in other experiments and at other values of μ (see for example [131–135]).

The fragmentation of heavy quarks[4] is somewhat different. When the heavy quark is produced with an energy E not much larger than its mass m, the fragmentation process consists mainly of the nonperturbative transition of the heavy quark to the hadron H, which one assumes can be described by a nonperturbative FF. One may make a general ansatz for the functional form of this FF, the parameters of which are to be fixed by fitting to data. One may also be inspired by physical considerations in motivating a functional form. Within this philosophy, the best known form is that of Peterson et al. [136]. More recent forms are based on heavy-quark effective field theory. Both are described in section 9.5.2. When the heavy quark is produced with an energy E much larger than its mass m, large logarithms of E/m occur in the perturbative expression for the heavy-quark inclusive cross section, which must be resummed. These logarithms may be traced to the fragmentation stage of the reaction, and the resummation may be achieved using the formalism of perturbative FFs (PFFs). They describe the fragmentation process from scale E down to scale m. These PFFs are perturbative because, first, the coupling constant is small enough in the range from m to E and second, the heavy-quark mass regulates the collinear divergences, which would otherwise have to be absorbed into nonperturbative FFs. These perturbative and nonperturbative FFs must be properly matched together to avoid miscounting contributions and to enable a comparison with data.

Outside the context of factorization-based perturbative QCD, there is the successful string model of the Lund group. Yet other approaches to heavy-quark fragmentation exist [137,138], but for lack of space we shall not discuss them here.

We begin with a discussion of perturbative fragmentation and describe an attempt to learn more about the nonperturbative FF from the very precise SLD data. Next we examine what heavy-quark production data in $p\bar{p}$ collisions tell us about the nonperturbative FF. Then in section 9.5.2 we review and clarify the theory of the nonperturbative FFs. Next we discuss the phenomenon of beam drag in the context of the Lund string model, as (perhaps) observed at HERA in charm DIS and photoproduction, and present a study of the possible impact of this effect on CDF/D0 and BTeV studies. In section 9.5.4, we discuss various "systematic errors" in heavy quark FFs, and we conclude with observations on the experimental impact of the various issues in heavy-quark fragmentation.

We refer to the recent LHC Workshop report on bottom production [139] for additional studies involving heavy-quark fragmentation.[5]

[4] By heavy quarks we mean charm and bottom quarks. The top quark decays by the weak interaction before it has time to hadronize.

[5] In particular, in the context of section 9.5.4, one can find there a study by Frixione and Mangano on effective $z > 1$ support for fragmentation functions in certain event generators.

9.5.1 Perturbative fragmentation

9.5.1.1 Heavy-quark fragmentation in e^+e^- collisions †

A well-defined fragmentation function is a universal function, so that its study can be undertaken in the context of e^+e^- collisions without the complication due to initial state hadrons. We are interested in the situation where the scale E of the process is much larger than the heavy-quark mass m, a typical situation at the Tevatron. This requires the resummation of large logarithms $\ln(E/m)$ for a reliable computation of a differential cross section. This is achieved via the formalism of the perturbative FF (PFF), which we briefly review. The PFF satisfies the DGLAP [140–142] evolution equation:

$$\frac{dD_{i,\mathrm{pert}}(x,\mu)}{d\ln\mu} = \sum_j \int_x^1 \frac{dz}{z} P_{ij}\left(\frac{x}{z},\alpha_s(\mu)\right) D_{j,\mathrm{pert}}(z,\mu)\,, \tag{9.42}$$

where i,j label parton flavors. With initial condition at $\mu_0 \simeq m$, Eq. (9.42) determines the PFF at x,μ, and resums logarithms $\ln(\mu/\mu_0)$ to all orders. This initial condition for the PFF was first computed to NLO in [143] and is, for $i=Q$, given by the distribution

$$D_{Q,\mathrm{pert}}(z,\mu_0) = \delta(1-z) + \frac{\alpha_s(\mu_0)C_F}{2\pi}\left[\left(\frac{1+z^2}{1-z}\right)\left(\ln\left(\frac{\mu_0^2}{m^2}\right) - 1 - 2\ln(1-z)\right)\right]_+ . \tag{9.43}$$

For heavy quark production at $E \gg m$, the choice $\mu = E$ in the solution of (9.42) then resums terms containing $\ln^n(E/m)$ to all orders in α_s, to next-to-leading logarithmic (NLL) accuracy.

To study the PFF in the context of e^+e^- collisions at center-of-mass energy E

$$e^+\,e^- \to Z/\gamma(q) \to Q(p) + X, \tag{9.44}$$

one defines

$$x_E = x = \frac{2p\cdot q}{q^2}\,, \tag{9.45}$$

and factorizes the single heavy *quark* inclusive cross section as

$$\frac{d\sigma}{dx}(x,E,m) = \sum_i \int_x^1 \frac{dz}{z}\,\frac{d\hat{\sigma}_i}{dz}\,(z,E,\mu_F)\; D_{i,\mathrm{pert}}\left(\frac{x}{z},\mu_F,m\right)\,, \tag{9.46}$$

where $d\hat{\sigma}_i(x,E,\mu_F)/dx$ are the (scheme-dependent) partonic cross sections for producing the parton i, and $D_{i,\mathrm{pert}}(x,\mu_F,m)$ are the (scheme- but not process-dependent) perturbative fragmentation functions (PFFs) for parton i to evolve into the heavy quark Q. The factorization scale μ_F must be chosen of order E, to avoid the appearance of large logarithms $\ln(E/\mu_F)$ in the partonic cross sections.

The single-*hadron* inclusive cross section, including nonperturbative corrections, is then usually written as multiple convolution

†Author: C. Oleari

$$\frac{d\sigma^H}{dx}(x,E,m) = \sum_i \frac{d\hat{\sigma}_i}{dx}(x,E,\mu_F) \otimes D_{i,\mathrm{pert}}(x,\mu_F,m) \otimes D^H_{\mathrm{NP}}(x) \ . \tag{9.47}$$

Therefore the full fragmentation function requires the combination of the perturbative FF with a nonperturbative part which models the final hadronization. Note that for heavy-quark production in hadronic collisions at hadron transverse momentum $p_T \gg m$, one must replace the CM energy E with the boost-invariant p_T.

In Eq. (9.43) the initial condition is expressed as an expansion in terms of $\alpha_s(m)$. This is a beneficial property of heavy-quark fragmentation, but one should keep in mind that higher-order terms in this condition may be important. Moreover, irreducible, nonperturbative uncertainties of order Λ_{QCD}/m are present. We assume that all these effects are described by a nonperturbative fragmentation function D^H_{NP}, that takes into account all low-energy effects, including the final nonperturbative hadronization of the heavy quark. There are theoretical approaches to the fragmentation-function calculation that employ heavy-quark effective theory in order to study nonperturbative effects [144,145] more systematically. These will be discussed in the next subsection. Here we want to establish a connection with the most commonly used parameterizations, and thus we will use the Peterson form and the "Euler" form $x^\alpha(1-x)^\beta$.

9.5.1.2 Impact of SLD data

Let us first briefly review the present situation. Heavy-flavor production in e^+e^- collisions has been thoroughly studied both at fixed order [146–148] and in a combined fixed order plus next-to-leading logarithmic (here $\ln(E/m)$ with E the center of mass energy) resummed approach [149], using the Peterson function for the nonperturbative transition[6]. The results of this study [149], based on LEP [150,151] and ARGUS [152] data can be summarized as follows:

- Either increasing the order of the finite order perturbative expansion or including next-to-leading log (NLL) effects in a resummed approach reduces the Peterson parameter ϵ obtained from fitting to the data, corresponding to a harder nonperturbative fragmentation function.
- The differential cross section obtained by matching the α_s^2 fixed order and the NLL resummed expressions, the "NLL improved", is harder than pure NLL, so that the ϵ parameter needed in the nonperturbative part is, in general, larger, but only slightly so, than in the NLL case.
- At LEP energies, the importance of $\mathcal{O}(m/E)$ terms is found to be minor.

Let us now show some new results obtained from a fit to SLD [153] B-production data in e^+e^- collision at $E = 91.2$ GeV, in Fig. 9.41. The theoretical curves have been determined

[6] This combined approach is actually a variable flavor number scheme (VFNS) for heavy-quark fragmentation.

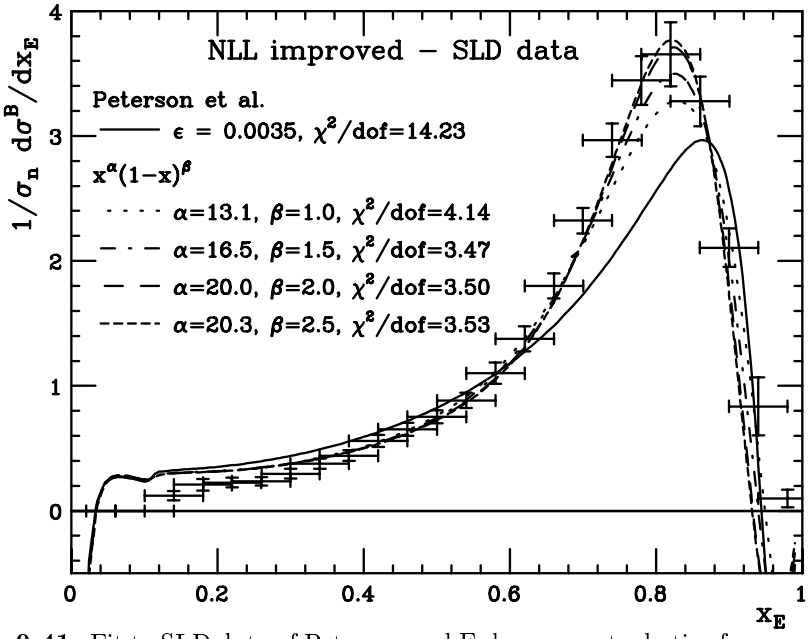

Figure 9.41: Fit to SLD data of Peterson and Euler nonperturbative fragmentation function via NLL improved calculation. The χ^2 are per degree of freedom.

from Eq. (9.47), at the same level of accuracy as used in [149]. We have used two families of nonperturbative FF: the Peterson form and the Euler form $x^\alpha(1-x)^\beta$. We have fitted the data by χ^2 minimization, keeping $\Lambda^{(5)}_{\rm QCD}$ fixed to 200 MeV. With this procedure we have fitted both the value of ϵ and the normalization (which was allowed to float) for the Peterson FF, and for the Euler form the value of α and the normalization, varying β in the range between 1.0 and 2.5, with an increment of 0.5.

We should caution at this point that the values of ϵ for the Peterson FF fitted above *cannot* be used for LEP studies, as the SLD and LEP collaborations use different values for some key input parameters such as the fraction of b quarks producing B^{**} mesons.

We find the Peterson form to have a very poor χ^2/d.o.f. The Euler form can accommodate the data better, at the values $\alpha = 16.5, \beta = 1.5$. To compare the fit results, we plot in Fig. 9.42 the nonperturbative FF at their best χ^2/d.o.f. values. We see that all curves are strongly peaked near $x = 1$, with the best fit value corresponding to a fairly hard fragmentation.

We note that in Ref. [154], and more recently in [155], the formalism used in the previous analysis of e^+e^- collisions has been applied to the Tevatron b-quark p_T cross section, for which the data exceed the central NLO-theory estimate by a factor of two[7]. At large p_T the theoretical uncertainty due to scale variations was found to be reduced with respect to the fixed-order approach, but the cross section decreased. At moderate p_T, the cross section gets somewhat enhanced, but not enough to explain the data-theory discrepancy. Another study involving FFs in heavy-quark hadroproduction, in the context of the so-called ACOT VFNS, was performed in [156]. The PFF formalism was also applied to γp [157] and $\gamma\gamma$ [158]

[7] This is somewhat less the case for the b-jet cross section, see section 1.3 in this chapter.

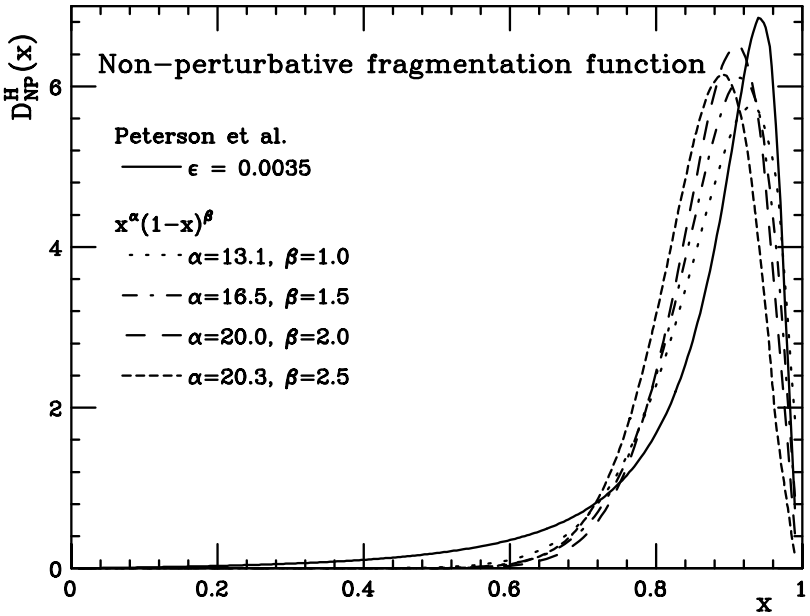

Figure 9.42: Functional forms of the nonperturbative fragmentation functions that produced the best fit to SLD data.

charm production. Similar conclusions were reached as for $p\bar{p}$ b-quark production.

9.5.1.3 Heavy-quark fragmentation in $p\bar{p}$ collisions †

It is well known that Tevatron data for the integrated transverse momentum spectrum in b production are systematically larger than QCD predictions. This problem has been around for a long time, although it has become less severe with time. The present status of this issue has been previously presented in Fig. 9.8. A similar discrepancy is also observed in UA1 data (see ref. [159] for details).

The theoretical prediction has a considerable uncertainty, which is mainly due to neglected higher-order terms in the perturbative expansion. In our opinion, it is not unlikely that we may have to live with this discrepancy, which is certainly disturbing, but not strong enough to question the validity of perturbative QCD calculations. In other words, the QCD $\mathcal{O}(\alpha_s^3)$ corrections for this process are above 100% of the Born term, and thus it is not impossible that higher order terms may give contributions of the same size. Nevertheless, it is conceivable that also nonperturbative effects contribute to enhance the cross section for this observable.

In this note, we present a study of the effects of b-quark fragmentation on the predicted single-inclusive p_T spectrum. In analogy with the case of charm production, the agreement between theory and data improves if one does not include any fragmentation effects. It is then natural to ask whether the fragmentation functions commonly used in these calculations are appropriate. The LEP [150,160,161] and SLD [153] measurements have shown

†Authors: P. Nason, G. Ridolfi

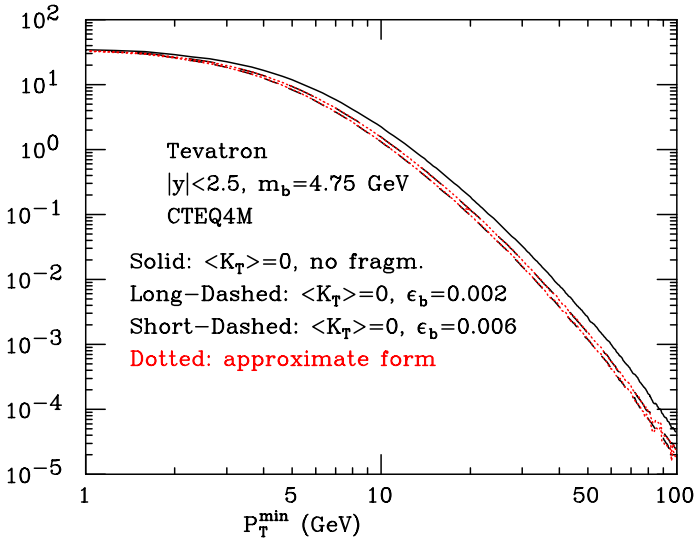

Figure 9.43: The effect of a Peterson fragmentation function [136] on the inclusive b cross section. The (red) dotted lines correspond to the approximation Eq. (9.50), and are almost indistinguishable from the exact results.

that fragmentation functions are harder than previously thought.

The effect of a nonperturbative fragmentation function on the p_T spectrum is easily quantified if one assumes a steeply-falling transverse momentum distribution for the produced b quark

$$\frac{d\sigma}{dp_T} = Ap_T^{-M}\,. \tag{9.48}$$

The corresponding distribution for the hadron is

$$\frac{d\sigma_{\rm had}}{dp_T} = A\int \hat{p}_T^{-M}\,\delta(p_T - z\hat{p}_T)D(z)\,dz\,d\hat{p}_T = Ap_T^{-M}\int_0^1 dz z^{M-1}D(z)\,. \tag{9.49}$$

We can see that the hadron spectrum is proportional to the quark spectrum times the $M^{\rm th}$ moment of the fragmentation function $D(z)$. Thus, the larger the moment, the larger the enhancement of the spectrum.

In practice, the value of M will be slightly dependent upon p_T. We thus define a p_T dependent M value

$$\frac{d\log\sigma(p_T > p_T^{\rm cut})}{d\log p_T^{\rm cut}} = -M(p_T^{\rm cut}) + 1 \tag{9.50}$$

and

$$\sigma_{\rm had}(p_T > p_T^{\rm cut}) = \sigma(p_T > p_T^{\rm cut}) \times \int_0^1 dz z^{M(p_T^{\rm cut})-1}D(z)\,. \tag{9.51}$$

This gives an excellent approximation to the effect of the fragmentation function, as can be seen from fig. 9.43.

Since the second moment of the fragmentation function is well constrained by e^+e^- data, it is sensible to ask for what shapes of the fragmentation function, for fixed $\langle z\rangle$, one

gets the highest value for $\langle z^{M-1} \rangle$. We convinced ourselves that the maximum is achieved by the functional form

$$D(z) = A\delta(z) + B\delta(1-z)\,, \tag{9.52}$$

which gives

$$\langle z \rangle = \frac{B}{A+B}\,; \quad \langle z^{M-1} \rangle = \frac{B}{A+B}\,. \tag{9.53}$$

This is however not very realistic: somehow, we expect a fragmentation function which is concentrated at high values of z, and has a tail at small z. We convinced ourselves that, if we impose the further constraint that $D(z)$ should be monotonically increasing, one gets instead the functional form

$$D(z) = A + B\delta(1-z)\,, \tag{9.54}$$

which gives

$$\langle z \rangle = \frac{A/2+B}{A+B}\,; \quad \langle z^{M-1} \rangle = \frac{A/M+B}{A+B}\,. \tag{9.55}$$

We computed numerically the M^{th} moments of the Peterson form:

$$D(z) \propto \frac{1}{z\left(1-\frac{1}{z}-\frac{\epsilon}{1-z}\right)^2}\,, \tag{9.56}$$

of the form

$$D(z) \propto z^{\alpha}(1-z)^{\beta}\,, \tag{9.57}$$

for $\beta = 1$ (Kartvelishvili [162]), for which

$$\langle z^{M-1} \rangle = \frac{\Gamma(\alpha+M)\Gamma(\alpha+\beta+2)}{\Gamma(\alpha+1)\Gamma(\alpha+\beta+M+1)}\,, \tag{9.58}$$

of the form of Collins and Spiller [163]

$$D(z) \propto \frac{\left(\frac{1-z}{z}+\frac{(2-z)\epsilon}{1-z}\right)(1+z^2)}{\left(1-\frac{1}{z}-\frac{\epsilon}{1-z}\right)^2}\,, \tag{9.59}$$

and of the form in Eq. (9.54), at fixed values of $\langle z \rangle$ corresponding to the choices $\epsilon_b = 0.002$ and 0.006 in the Peterson form. We found that the p_T distribution at the Tevatron, for p_T in the range 10 to 100 GeV, behaves like p_T^{-M}, with M around 5. Therefore, we present in Tables 9.21 and 9.22 values of the $4^{\rm th}$, $5^{\rm th}$ and $6^{\rm th}$ moments of the above-mentioned fragmentation functions. We thus find that keeping the second moment fixed the variation of the hadronic p_T distribution obtained by varying the shape of the fragmentation function among commonly used models is between 5% and 13% for both values of ϵ_b. Therefore, it seems difficult to enhance the transverse momentum distribution by suitable choices of the form of the fragmentation function. With the extreme choice of Eq. (9.54), one gets at most a variation of 50% for the largest values of ϵ_b and M. It would be interesting to see if such an extreme choice is compatible with e^+e^- fragmentation function measurements.

$\langle z\rangle = 0.879$	$M=4$	$M=5$	$M=6$
Peterson	0.711	0.649	0.595
Kartvelishvili	0.694	0.622	0.562
Collins-Spiller	0.729	0.677	0.633
Maximal (Eq. (9.54))	0.818	0.806	0.798

Table 9.21: Values of the $4^{\rm th}$, $5^{\rm th}$ and $6^{\rm th}$ moment, at fixed $\langle z\rangle$ (corresponding to $\epsilon_b = 0.002$ in the Peterson form), for different forms of the fragmentation function.

$\langle z\rangle = 0.828$	$M=4$	$M=5$	$M=6$
Peterson	0.611	0.535	0.474
Kartvelishvili	0.594	0.513	0.447
Collins-Spiller	0.626	0.559	0.505
Maximal (Eq. (9.54))	0.742	0.724	0.713

Table 9.22: Values of the $4^{\rm th}$, $5^{\rm th}$ and $6^{\rm th}$ moment, at fixed $\langle z\rangle$ (corresponding to $\epsilon_b = 0.006$ in the Peterson form), for different forms of the fragmentation function.

9.5.2 Fragmentation in the nonperturbative regime †

In this subsection we review the theory of the nonperturbative transition of a heavy quark into a heavy meson.

First, we examine the model of Peterson *et al.* [136] for the fragmentation of a fast-moving heavy quark Q with mass m_Q into a heavy hadron H (consisting of $Q\overline{q}$) with mass m_H and a light quark q with mass m_q. The basic assumption in this model is that the amplitude for the fragmentation is proportional to $1/(\Delta E)$, where $\Delta E = E_H + E_q - E_Q$ is the energy denominator for the process in old-fashioned perturbation theory. It follows that the probability for the transition $Q \to H + q$ is proportional to $1/(\Delta E)^2$. Taking the momentum of the heavy quark to define the longitudinal axis, one can express ΔE in terms of the magnitude of P_Q, the heavy-quark momentum, the fraction z of the heavy-quark momentum that is carried by the heavy hadron, and the transverse momentum $p_\perp$ of the heavy hadron or the light quark:

$$\begin{aligned}\Delta E &= \sqrt{m_H^2 + p_\perp^2 + z^2 P_Q^2} + \sqrt{m_q^2 + p_\perp^2 + (1-z)^2 P_Q^2} - \sqrt{m_Q^2 + P_Q^2} \\ &\approx \frac{m_H^2 + p_\perp^2}{2zP_Q} + \frac{m_q^2 + p_\perp^2}{2(1-z)P_Q} - \frac{m_Q^2}{2P_Q} + \cdots \\ &\approx -\frac{m_Q^2}{2P_Q}[1 - 1/z - \epsilon/(1-z)]. \end{aligned} \tag{9.60}$$

In the last line, we have set $m_H \approx m_Q$ and neglected $p_\perp^2$ relative to m_Q^2 and used the definition $\epsilon \equiv (m_q^2 + p_\perp^2)/m_Q^2$. Multiplying $1/(\Delta E)^2$ by a factor $1/z$ for the longitudinal

†Authors: G. Bodwin, B. Harris

phase space, one arrives at the following *ansatz* for the fragmentation function [136]:

$$D_Q^H(z) = \frac{N}{z[1-1/z-\epsilon/(1-z)]^2}, \tag{9.61}$$

where the normalization N is fixed by the condition

$$\sum_H \int dz D_Q^H(z) = 1, \tag{9.62}$$

and the sum extends over all hadrons that contain Q. Contrary to the claims in Ref. [136], we find that $D_Q^H(z)$ has a maximum at $z \approx 1-\sqrt{\epsilon}$ and a width of order $\sqrt{\epsilon}$. Previously it was believed that the shape of the Peterson et al. form is incompatible with results obtained from heavy-quark effective theory (HQET). However, as we shall discuss below, our new results for the maximum point and width are compatible with the HQET analysis.

Next we discuss the work of Jaffe and Randall [145], which provides a QCD-based interpretation of heavy-quark fragmentation in terms of the heavy-quark mass expansion. One begins with the standard Collins-Soper [127] definition of the fragmentation function for a heavy quark into a heavy hadron:

$$\hat{f}(z,\mu^2) = \frac{z}{4\pi}\int d\lambda e^{i\lambda/z}\frac{1}{2N_c}\mathrm{Tr}\,\not{n}\,\langle 0|\,h(\lambda n)\,|H'(P)\rangle\,\langle H'(P)|\,\overline{h}(0)\,|0\rangle\,, \tag{9.63}$$

where the trace is over color and Dirac indices, N_c is the number of colors, $h(x)$ is the heavy-quark field at space-time position x, P is the four-momentum of the heavy hadron, and n is defined by $n^2=0$ and $n\cdot p = 1$. The state $|H'(P)\rangle$ consists of the heavy hadron plus any number of additional hadrons. The matrix element is understood to be evaluated in the light-cone gauge $n\cdot A = 0$. We note that the definition (9.63) contains a factor z relative to the definition of the fragmentation function used in Ref. [145]. This factor z will be important in comparing with the work of Braaten *et al.* below.

Following the standard method for obtaining the heavy-quark mass expansion, one decomposes the field $h(x)$ into the sum of large $h_v(x)$ and small $\underline{h}_v(x)$ components:

$$h_v(x) = e^{-im_Q v\cdot x}P_+ h(x) \tag{9.64}$$

$$\underline{h}_v(x) = e^{-im_Q v\cdot x}P_- h(x), \tag{9.65}$$

with $P_\pm = (1\pm\not{v})/2$ and v the hadron's four velocity. The leading term in the mass expansion of $f(x,\mu^2)$ is contained in the large-large combination of fields:

$$\begin{aligned}\hat{f}(z,\mu^2) = \frac{z}{4\pi}\int d\lambda e^{i\lambda/z}\frac{1}{2N_c}\mathrm{Tr}\,\not{n}\\ \times\,\langle 0|\,P_+h(\lambda n)\,|H'(P)\rangle\,\langle H'(P)|\,\overline{P_+h(0)}\,|0\rangle\,e^{-im_Q\lambda n\cdot v}+\dots\,.\end{aligned} \tag{9.66}$$

In Ref. [145], it is argued that the matrix element in Eq. (9.66) is a dimensionless function $\mathcal{F}(\lambda\delta)$. This function may be written in terms of its Fourier transform:

$$\mathcal{F}(\lambda\delta) = 2\int_{-\infty}^{\infty} d\alpha e^{-i\alpha\lambda\delta}\,a(\alpha)\,, \tag{9.67}$$

where $\delta = 1 - m_Q/m_H$ which in terms of the parameter ϵ appearing in the Peterson et al. form is $\delta \approx \sqrt{\epsilon}$. Inserting Eq. (9.67) into Eq. (9.66), one can evaluate the integral, with the result

$$\hat{f}(z,\mu^2) = \frac{z}{\delta}\hat{a}\left(\frac{1/z - m_Q/m_H}{\delta}\right) + \dots \ . \tag{9.68}$$

A more complete analysis in Ref. [145] also yields the next-to-leading term in the hadron mass expansion:

$$\hat{f}(z,\mu^2) = z\left[\frac{1}{\delta}\hat{a}(y) + \hat{b}(y) + \cdots\right] , \tag{9.69}$$

where $y = (1/z - m_Q/m_H)/\delta$. The analysis in Ref. [145] does not yield a precise prediction for the functional form of a and b, but some general properties may be deduced. The function a describes, in the limit of infinite heavy-quark mass, the effects of binding in the heavy hadron on the heavy-quark momentum distribution. For a free heavy quark, $a(y)$ would be a δ-function at $y = 1$. In a heavy hadron, the binding smears the heavy-quark momentum distribution. It can be shown [145] that the distribution has a maximum at $z \approx 1 - \delta$ and a width of order δ. Using the fact the $\delta \approx \sqrt{\epsilon}$, we find that the maximum is at $z \approx 1 - \sqrt{\epsilon}$ and the width is of order $\sqrt{\epsilon}$ in agreement with the Peterson *et al.* model, as described above.

Braaten *et al.* [144] present a QCD-inspired model for the fragmentation of a heavy quark into an $S-$wave light-heavy meson. In this model, the fragmentation function is computed in perturbative QCD (Born level) in an expansion in inverse powers of the heavy-quark mass. For the projection of the Qq state onto the meson, Braaten *et al.* take the standard nonrelativistic-bound-state expression. For example, in the case of a $^1S_0$ meson, they assume the Feynman rule for the QqH vertex to be

$$\frac{\delta_{ij}}{\sqrt{3}}\frac{R(0)\sqrt{m_H}}{\sqrt{4\pi}}\gamma_5(1+\not{v})/2, \tag{9.70}$$

where $R(0)$ is the radial wave function at the origin. Braaten *et al.* make use of a definition of the fragmentation function that is equivalent to the Collins-Soper definition (9.63). From the terms of leading order in the heavy-quark mass expansion, they obtain, in the case of a $^1S_0$ meson,

$$\hat{f} \approx N\left[\frac{1}{\delta}\frac{(1-y)^2}{y^6}(3y^2+4y+8) - \frac{(1-y)^3}{y^6}(3y^2+4y+8)\right], \tag{9.71}$$

where $N = 2\alpha_s^2|R(0)|^2/(81\pi m_q^3)$. At first glance, this result may seem to contradict the Jaffe-Randall analysis, which shows that the terms of leading order in the heavy-quark mass expansion give a contribution that is contained entirely in the function $a(y)$ in Eq. (9.69). However, the factor z in the definition of the fragmentation function (9.63) is crucial here. From the definitions of y and δ, we have $z = 1/[1-\delta(1-y)]$, and, so, we can re-write Eq. (9.71) as

$$\hat{f}/z \approx \frac{N}{\delta}\frac{(1-y)^2}{y^6}(3y^2+4y+8), \tag{9.72}$$

which is of the form of $a(y)$ in Eq. (9.69).

There are several additional studies of the perturbative-QCD fragmentation function in the limit of a large heavy-quark mass. See the paper of Braaten *et al.* [144] for references.

9.5.3 Beam drag †

A puzzling situation has arisen in charm electroproduction and photoproduction at HERA. The data are well-described by NLO QCD [164,165] plus Peterson fragmentation [136], except at low p_t and large rapidity. To show this effect the charm electroproduction data of the ZEUS collaboration [166] is shown in Fig. 9.44. The figure shows the D^* meson cross sections

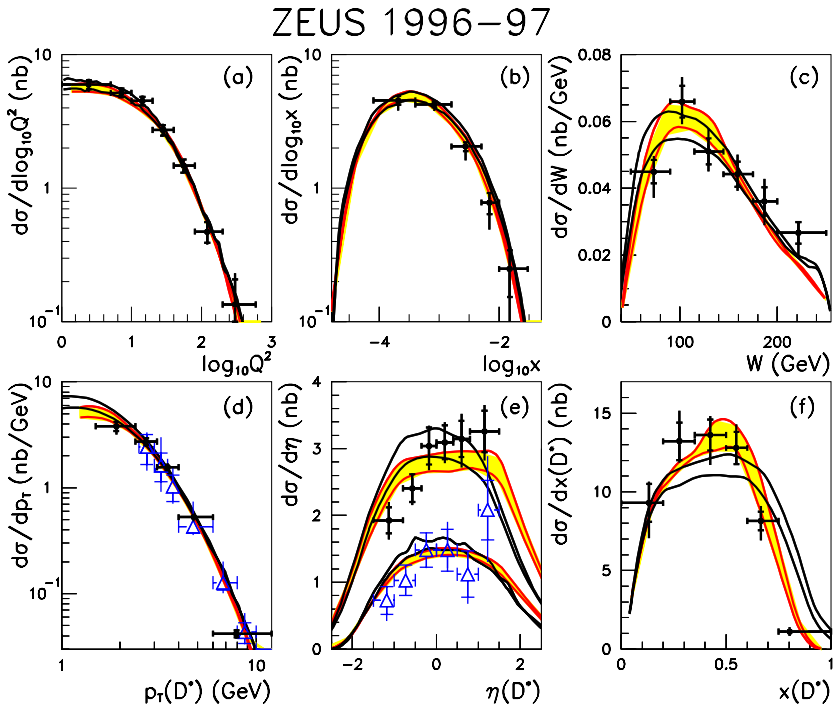

Figure 9.44: Effects of beam drag at HERA vs NLO theory and data from [166].

differential in momentum transfer Q^2, Bjorken x, hadronic energy W, transverse momentum p_t, pseudo-rapidity η, and D^* momentum fraction $x(D^*) = 2|\vec{p}_{\gamma P\mathrm{cms}}|/W$, compared with theory [164]. The boundaries of the bands correspond to varying the charm quark mass of 1.4 GeV by ± 0.1 GeV. The overall agreement is good, but the theory underestimates the data in the forward region and overestimates it in the backward region. Additionally, the D^* momentum fraction data, which is particularly sensitive to the charm hadronization process, is poorly described. Similar effects are seen in the D^* photoproduction data [167] at HERA. Variations of the parton distribution set, renormalization/factorization scale, charm mass, or fragmentation parameter ϵ are unable to account for the differences between data and theory. It also appears unlikely that an evolving fragmentation function would help since the p_t range covered is so small. A similar effect has been observed by the H1 collaboration in their charm electroproduction data [168].

One explanation [169] proposed for the photoproduction data [167] appears to work for the DIS data as well. One imagines a color string connecting the hadronizing charm quark

† Author: E. Norrbin

and the proton remnant which pulls (drags) the charmed meson to the forward region. This beam-remnant drag effect is made quantitative in the Lund String model modified for heavy-flavor production [170], as implemented in Pythia [171]. The shaded band in Fig. 9.44 shows that agreement is better when the Peterson *et al.* model is replaced by an effective fragmentation model extracted from the Pythia-based Monte Carlo RAPGAP [172].

Another way to improve the agreement between data and theory is to simply raise the minimum p_t of the events that are selected. Data from a slightly different decay chain, but higher minimum p_t cut are shown as open triangles. Here the Peterson and RAPGAP improved NLO predictions give essentially the same results, as expected from a power-suppressed effect. Note however that raising $p_t^{\rm min}$ may not be an option in some situations.

Let us adopt the view that beam remnant drag effects, which appear naturally in the string fragmentation model [173], exert influence here. This effect is closely related to the collapse of small strings, which is the most extreme case of string drag when all the energy and momentum of the remnant is taken up by the produced hadron. This latter effect has been used to describe the large charm asymmetries observed at several fixed target experiments [174,175]. It is important to understand this effect, as it affects $B - \bar{B}$ asymmetries at e.g. HERA-B [176], and thus CP violation measurements. An open problem is how to match the string model for beam drag to factorized QCD. In the rest of this section the Lund string fragmentation model is summarized and its influence on the distribution of final state hadrons in $p\bar{p}$ collisions is reviewed.

The Lund string fragmentation model provides a different approach to the problem of hadronization than the methods discussed so far. The Lund model in its basic form is simply a prescription for turning a partonic state (no matter how it was produced) into a hadronic final state. A string is the tube-like QCD force field stretched between a triplet and an anti-triplet color charge. In a high-energy process the string contains a lot of energy and decays into hadrons by the production of new $q\bar{q}$ pairs along the force field. The decay dynamics is constrained by a few physical assumptions such as Lorentz invariance, confinement and independence of the final state on the order in which string breaks are considered in the fragmentation process ('left-right symmetry'). This results in a fragmentation function with two free parameters, called the Lund symmetric FF [173]

$$f(z) \propto \frac{1}{z}(1-z)^a e^{-bm_\perp^2/z} \tag{9.73}$$

with a modification needed for heavy flavors [170]

$$f(z) \propto \frac{1}{z^{1+bm_Q^2}}(1-z)^a e^{-bm_\perp^2/z}, \tag{9.74}$$

where $m_\perp$ is the transverse mass of the produced hadron, m_Q is the heavy-quark mass and a and b are the two free parameters, which are common for all flavors and hadrons. The z variable represents the light cone fraction along the string direction and unlike 'stand alone' fragmentation functions no ambiguity is involved (cf. section 9.5.4).

To be practically useful, the Lund model must be hooked on to a perturbative description of the underlying hard process (such as $e^+e^- \to q\bar{q}$ or $gg \to q\bar{q}$). Normally a parton shower

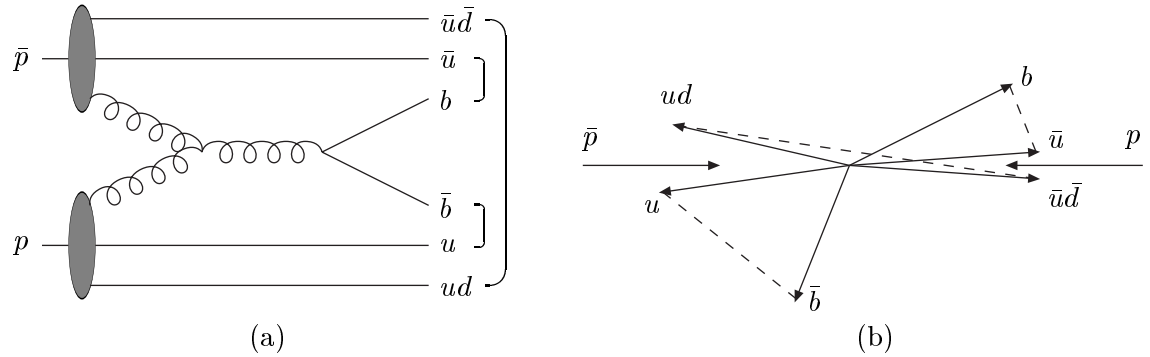

Figure 9.45: Example of a string configuration in a $p\bar{p}$ collision. (a) Graph of the process, with brackets denoting the final color singlet subsystems. (b) Corresponding momentum space picture, with dashed lines denoting the strings.

approximation is used, where the final state of a LO process is evolved down in virtuality by parton emission to some cut-off scale Q_0. Using a fixed lower scale for the perturbative treatment it has been possible in e^+e^- experiments to fit the two parameters of the Lund model to data and get excellent results. If the Q_0 scale is changed, the nonperturbative parameters of the Lund model will have to be re-tuned, so Q_0 can be seen as the scale at which perturbation theory is abandoned and replaced by the nonperturbative model. In the ideal case the value of Q_0 should not matter. In practice this is true only as long as it is at the order of 1 GeV. Any small change in Q_0 around this value is absorbed by a change of the fragmentation parameters. In a Monte Carlo program some additional parameters are needed to fully describe the process $e^+e^- \to$ hadrons, such as the transverse smearing along the string direction and the flavor composition of the new $q\bar{q}$ pairs [171].

When the model is carried over to hadron collisions several new aspects have to be considered. First of all, the particles entering the hard subprocess are not color singlets but quarks or gluons confined to hadrons. This problem is well known and solved by introducing PDFs which have been measured to good accuracy at e.g. HERA. Less well known is the consideration of color flow, beam remnants, small strings in the hadronization and beam drag. The remainder of this section will cover these aspects including a discussion of their possible implications in $p\bar{p}$ physics.

To be able to use the Lund string fragmentation model for hadronization, the strings in the event must be constructed. The string topology can be derived from the color flow of the hard process. For example, consider the LO process $u\bar{u} \to b\bar{b}$ in a $p\bar{p}$ collision. The color of the incoming u is inherited by the outgoing b, so the b will form a color-singlet together with the proton remnant, here represented by a color anti-triplet ud diquark. In total, the event will thus contain two strings, one b–ud and one $\bar{b}$–$\bar{u}\bar{d}$. In $gg \to b\bar{b}$ a similar inspection shows that two distinct color topologies are possible. Representing the proton remnant by a u quark and a ud diquark (alternatively d plus uu), one possibility is to have three strings b–$\bar{u}$, $\bar{b}$–u and ud–$\bar{u}\bar{d}$, Fig. 9.45, and the other is the three strings b–ud, $\bar{b}$–$\bar{u}\bar{d}$ and u–$\bar{u}$. When the remnant energy is to be shared between two objects, as e.g. in Fig. 9.45, further nonperturbative parameters are introduced, with a limited but not always negligible

impact on the uncertainty of the results [176].

Once the string topology has been determined, the Lund string fragmentation model [173] can be applied to describe the nonperturbative hadronization. Presupposing that the fragmentation mechanism is universal, i.e. process-independent, the good description of e^+e^- annihilation data should carry over. The main difference between e^+e^- and hadron–hadron events is that the latter contain beam remnants which are color-connected with the hard-scattering partons.

Depending on the invariant mass of a string, practical considerations lead to the need to distinguish three hadronization prescriptions:

1. *Normal string fragmentation.* In the ideal situation, each string has a large invariant mass. Then the standard iterative fragmentation scheme, for which the assumption of a continuum of phase-space states is essential, works well. The average multiplicity increases linearly with the string 'length', which means logarithmically with the string mass. In practice, this approach can be used for all strings above some cut-off mass of a few GeV.

2. *Cluster decay.* If a string is produced with a small invariant mass, maybe only two-body final states are kinematically accessible. The continuum assumption above then is not valid, and the traditional iterative Lund scheme is not applicable. We call such a low-mass string a cluster, and consider it separately from above. When kinematically possible, a Q–$\bar{q}$ cluster will decay into one heavy and one light hadron by the production of a light quark–antiquark pair in the color force field between the two cluster endpoints, with the new quark flavor selected according to the same rules as in normal string fragmentation. Close to the two-body threshold the decay is isotropic, while it should smoothly attach to the string picture of a preferential longitudinal direction for heavier clusters.

3. *Cluster collapse.* This is the extreme case of the above situation, where the string mass is so small that the cluster cannot decay into two hadrons. It is then assumed to collapse directly into a single hadron, which inherits the flavor content of the string endpoints. The original continuum of string/cluster masses is replaced by a discrete set of hadron masses, mainly D/B and D^*/B^* (or corresponding baryon states). In order to preserve overall energy and momentum, nearby string pieces have to absorb a recoil of the collapse, according to a procedure intended to minimize disturbances to the event. This mechanism plays a special rôle, in that it allows large flavor asymmetries in favor of hadron species that can inherit some of the beam-remnant flavor content.

Thus the cluster collapse mechanism tends to enhance the production of heavy hadrons which share its light flavor with the hadron beam. For charm this has been observed at several fixed-target experiments, where the effect is very large for large x_F [174]. This effect is yet to be studied for B mesons. It is expected to be fairly large at HERA-B [176] but small for the Tevatron, see [176] and below.

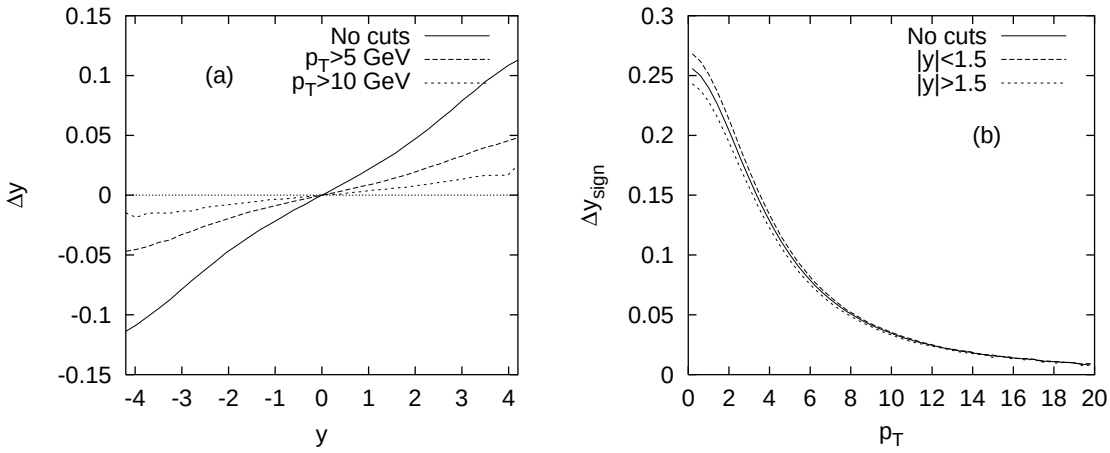

Figure 9.46: (a) Average rapidity shift Δy as a function of y for some different p_T cuts for a $p\bar{p}$ collider at 2 TeV. (b) Average rapidity shift Δy_{sign} as a function of p_T for some different rapidity cuts.

The color connection between the produced heavy quarks and the beam remnants in the string model gives rise to an effect called beam remnant drag. In an independent fragmentation scenario, a quark jet fragments symmetrically around the quark direction. The light cone (along the quark axis) energy-momentum of the quark is then simply scaled by some factor, picked from a fragmentation function, in order to give the momentum of the hadron. Thus, on the average, the rapidity would be conserved in the fragmentation process. This is not necessarily so in string fragmentation where both string ends contribute to the four-momentum of the produced heavy hadron. If the other end of the string is a beam remnant, the hadron will typically be shifted in rapidity in the direction of the beam remnant, often resulting in an increase in $|y|$. This beam-drag is shown qualitatively in Fig. 9.46, where the rapidity shift for bottom hadrons in a 2 TeV $p\bar{p}$ collision is shown as a function of rapidity and transverse momentum. We use two different measures of the rapidity shift. The first is the average rapidity shift $\Delta y = \langle y_B - y_b \rangle$. Here the heavy quark can be connected to a beam remnant on either side of the event, giving rise to shifts in both directions which tend to cancel in inclusive measures. A better definition is therefore

$$\Delta y_{sign} = \langle (y_B - y_b) \cdot sign(y_{other\ end}) \rangle, \tag{9.75}$$

which measures the rapidity shift in the direction of the other end of the string. This shift should almost always be positive. The rapidity shift is not directly accessible experimentally, only indirectly as a discrepancy between the shape of perturbatively calculated quark distributions and data. As can be seen from the figures this effect is large only at large rapidities and small p_T.

A possible observable consequence of the beam drag effect is the asymmetry between B^0 and $\bar{B}^0$ for large rapidities. Fig. 9.47 shows the distribution of bottom quarks and the hadrons produced from them, as well as the asymmetry between B^0 and $\overline{B}^0$ without any kinematic cuts, using pair production only. The asymmetry is antisymmetric because of the asymmetry of the initial state. Therefore the asymmetry is zero at $y = 0$ and increasing in different directions for increasing/decreasing rapidities. Consider the situation when the

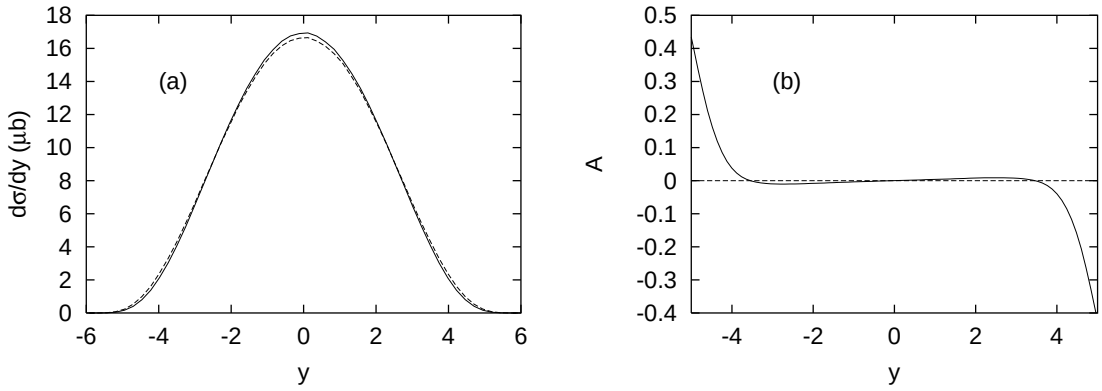

Figure 9.47: Bottom production at the Tevatron. (a) Rapidity distribution of bottom quarks (full) and the B hadrons produced from them (dashed). (b) The asymmetry $A = \frac{\sigma(B^0)-\sigma(\overline{B}^0)}{\sigma(B^0)+\sigma(\overline{B}^0)}$ as a function of rapidity. For simplicity, only pair production is included.

kinematic limit at large positive rapidities (the proton fragmentation region) is approached. Here the asymmetry changes sign for large rapidities because of the drag-effect; b quarks connected to diquarks from the proton beam remnant which carry most of the remnant energy often produce $\overline{B}^0$ hadrons which are shifted more in rapidity than the B^0's are. The $\overline{B}^0$ rapidity distribution is thus harder than for B^0. Cluster collapse, on the other hand, tends to enhance the production of 'leading' particles (in this case B^0) so the two mechanisms give rise to asymmetries with different signs. Collapse is the main effect at central rapidities while eventually at very large y, the drag effect dominates. The situation is reversed in the $\bar{p}$ fragmentation region. Despite the superficial differences between cluster collapse and beam drag it should be realized that they are simply two consequences of the same thing, namely the color connection between the products of the hard process and the beam remnants and the subsequent hadronization of the resulting string.

In Fig. 9.48 we introduce cuts in order to study the region of large (positive) rapidities and small p_T. The $\overline{B}^0$ spectrum is slightly harder than the B^0 one, but the size of the effect is quite small, approaching 4% at very large rapidities. Still, if large precision is desired in CP violation studies, this effect could be non-negligible. The effect is much larger at HERA-B because of the much smaller CM-energy, so the effect should be studied there first to assess its size. Further details and applications are given in [176].

9.5.4 Heavy-quark fragmentation ambiguities†

Unlike massless quarks, heavy quarks cannot have all of their four-momentum components degraded and stay on their mass shell simultaneously. Hence, only some components get scaled by z; which ones is to some degree a matter of choice, and a source of ambiguity. Moreover, the action of boosting between the parton-parton center-of-mass and the

†Authors: B. Harris, E. Laenen

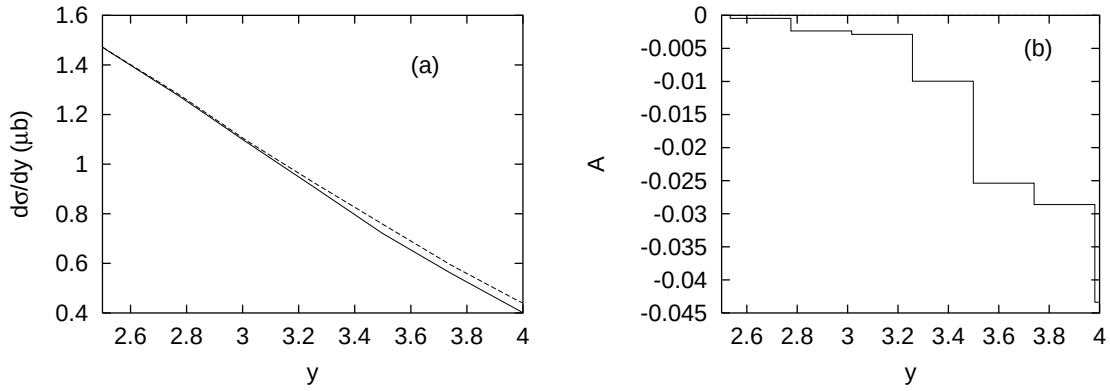

Figure 9.48: Bottom production at the Tevatron for $2.5 < |y| < 4$ and $p_T < 5$ GeV. (a) B^0 (full) and $\overline{B}^0$ (dashed) rapidity spectra. (b) The asymmetry $A = \frac{\sigma(B^0)-\sigma(\overline{B}^0)}{\sigma(B^0)+\sigma(\overline{B}^0)}$ as a function of rapidity. For simplicity, only pair production is included.

laboratory frame, and fragmenting do not commute for heavy quarks, generating another ambiguity. We have studied these ambiguities numerically at leading order, in the context of B-meson production at the Tevatron.

When fragmenting a heavy quark to a heavy hadron one must choose the momentum component to be scaled. Some common choices are

1. scaling the space component $\vec{p}_H = z\vec{p}_Q$ and adjusting the energy via the mass-shell condition $E_H = \sqrt{\vec{p}_H + m_H^2}$;

2. scaling the plus component $(E + p_{||})_H = z(E + p_{||})_Q$ and adjusting the minus component via the mass-shell condition $(E - p_{||})_H = m_H^2/(E + p_{||})_H$ (here $||$ refers to the Q direction, not the beam);

3. scaling the full four-momentum, ignoring the mass-shell requirement.

In Fig. 9.49 we show the effects of these choices on the P_T distribution of a generic B-meson in $p\bar{p}$ collisions at 1.8 TeV. We have taken $m_B = m_b = 5$ GeV, a Peterson et al. [136] fragmentation function with $\epsilon = 0.006$, and performed the fragmentation in the parton-parton center-of-mass. Choices 1 and 3 handle the p_x and p_y components in the same fashion so no effect is observed. The second method mixes the p_x and p_y components with the E and p_z components producing a pronounced difference at small p_T. All methods are identical in the limit of large p_T indicating that this is a source of power suppressed corrections.

There is also an ambiguity in the order in which the fragmentation of the heavy quark, and the boosting from the parton-parton center-of-mass to the lab frame is implemented. To see why this is so, one may compute, e.g. for the fragmentation choice $\vec{p}_H = z\vec{p}_Q$ with $m_H \simeq m_Q$, the difference in energy of a massive particle arising from the order of boosting

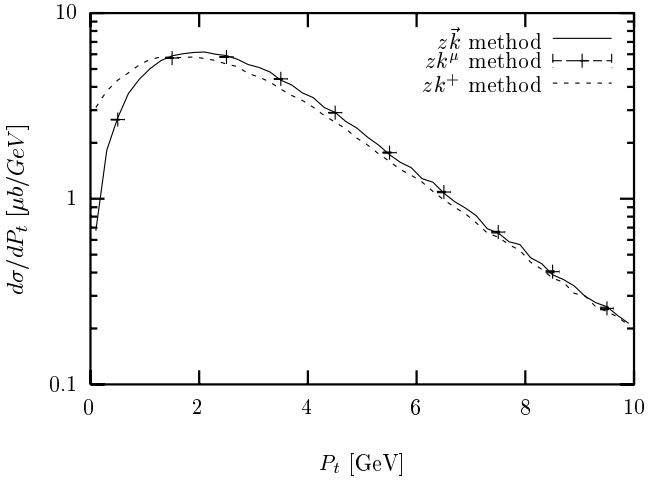

Figure 9.49: Effect of the different four-vector smearing methods on the P_T distribution of the B-meson.

(along z-axis with rapidity η) and fragmenting

$$\Delta E = \frac{m_Q^2}{2|\vec{p}_Q|}\sinh(\eta)\frac{1-z^2}{z} \tag{9.76}$$

for small $m_Q/|\vec{p}_Q|$.

The result of this non-commutativity (for the $\vec{p}_H = z\vec{p}_Q$ method) is shown in Figs. 9.50 and 9.51 for the pseudo-rapidity and transverse momentum distribution, respectively, of the $B-$meson. The interplay of such ambiguities with acceptance cuts is given in Table 9.23. For a transverse momentum above 5 GeV the effect is negligible.

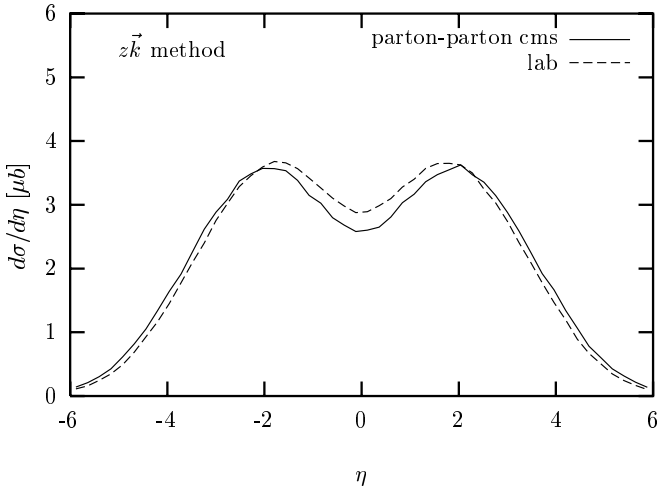

Figure 9.50: Commutativity of boosting and fragmenting for pseudo-rapidity distribution of the B-meson.

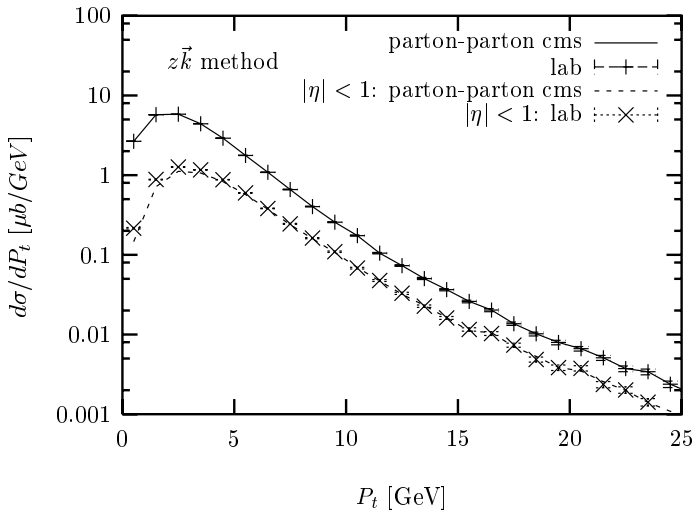

Figure 9.51: Commutativity of boosting and fragmenting for P_T distribution of the B-meson.

acceptance	$\sigma[\mu b]$ lab.	parton cms $\sigma[\mu b]$	difference
no cuts	26.24	26.24	-
$p_T > 0.5, \|\eta\| < 1.5$	9.66	8.87	8%
$p_T > 5, \|\eta\| < 1.5$	2.58	2.53	2%

Table 9.23: Interplay of boosting ambiguity with acceptance cuts.

9.5.5 Experimental impact†

In this section we shall try to address the extent to which fragmentation issues are relevant for heavy-quark studies at the Tevatron, specifically with respect to detector design and optimization.

The results from LEP and SLD on b fragmentation in e^+e^- collisions clearly indicate that the spectrum is harder than can be described by the standard Peterson *et al.* fragmentation function. This has little experimental impact other than in analyses which attempt to extract the b quark cross-section from the observed b hadron momentum spectrum. This could potentially have a small effect on the efficiency of 'same-side' tagging using the π from B^{**} decays. That is, a harder or softer fragmentation function will directly feed into the relation of this pion to the B from the decay.

There are some interesting correlations, both in b production and fragmentation, which feed, perhaps only weakly, into predictions of tagging efficiencies and strategies. The correlation of b and $\bar{b}$ directions in the forward and backward regions increases the "away-side" tagging power of a forward detector like BTeV since it implies that if one b is produced going forward (or backward) then most likely the other is also to be found in the same fiducial volume. On the other hand, 'same-side' tagging will be affected by the distribution of fragmentation particles produced along with the b hadron. This has been studied by

†Author: S. Menary

CDF who rely on data to extract efficiencies and tune the Monte Carlos.

The beam drag effect discussed in section 1.5.3 is potentially an issue for measurements in the very forward direction. The fact that BTeV is a two arm spectrometer can minimize this considerably since they can measure asymmetries in both the p and $\bar{p}$ arms and essentially subtract out the beam drag effect. In particular this can be done using very high statistics non-CP modes where an asymmetry is dominantly produced by this effect. This could be more problematic at LHCb which is a single arm spectrometer at a pp collider.

References

[1] P. Nason, S. Dawson and R. K. Ellis, Nucl. Phys. **B303**, 607 (1988).

[2] W. Beenakker, H. Kuijf, W. L. van Neerven and J. Smith, Phys. Rev. **D40**, 54 (1989).

[3] P. Nason, S. Dawson and R. K. Ellis, Nucl. Phys. **B327**, 49 (1989).

[4] W. Beenakker, W. L. van Neerven, R. Meng, G. A. Schuler and J. Smith, Nucl. Phys. **B351**, 507 (1991).

[5] M. L. Mangano, P. Nason and G. Ridolfi, Nucl. Phys. **B373**, 295 (1992).

[6] R. K. Ellis and D. A. Ross, Nucl. Phys. **B345**, 79 (1990).

[7] R. Bonciani, S. Catani, M. L. Mangano and P. Nason, Nucl. Phys. **B529**, 424 (1998) [hep-ph/9801375].

[8] S. Catani, M. Ciafaloni and F. Hautmann, Phys. Lett. **B242**, 97 (1990).

[9] J. C. Collins and R. K. Ellis, Nucl. Phys. **B360**, 3 (1991).

[10] S. Catani, M. Ciafaloni and F. Hautmann, Nucl. Phys. **B366**, 135 (1991).

[11] G. Camici and M. Ciafaloni, Phys. Lett. **B386**, 341 (1996) [hep-ph/9606427].

[12] G. Camici and M. Ciafaloni, Nucl. Phys. **B496**, 305 (1997) [hep-ph/9701303].

[13] S. P. Baranov and M. Smizanska, Phys. Rev. **D62**, 014012 (2000).

[14] R. D. Ball and R. K. Ellis, JHEP **0105**, 053 (2001) [hep-ph/0101199].

[15] E. L. Berger, B. W. Harris, D. E. Kaplan, Z. Sullivan, T. M. Tait and C. E. Wagner, hep-ph/0012001.

[16] DØ Collaboration, S. Abachi *et al.*, Phys. Rev. Lett. **74**, 3548 (1995).

[17] DØ Collaboration, Fermilab-PUB-99/144-E [hep-ex/9905024].

[18] CDF Collaboration, F. Abe *et al.* Phys. Rev. **D61**, 32001 (2000).

[19] S. Frixione, M. Mangano, Nucl. Phys. **B483**, 321 (1997).

[20] CDF Collaboration, F. Abe *et al.* Phys. Rev. **D53**, 1051 (1996).

[21] CDF Collaboration, F. Abe *et al.* Phys. Rev. Lett. **75**, 1451 (1995).

[22] M. Cacciari, M. Greco and P. Nason, JHEP **05**, 007 (1998) [hep-ph/9803400].

[23] CDF Collaboration, F. Abe *et al.*, Phys. Rev. Lett. **71** 500 (1993).

[24] P. Avery, K. Read, G. Trahern, Cornell Internal Note CSN-212 (1985) unpublished.

[25] F. Daghighian and D. Silverman, Phys. Rev. D **36**, 3401 (1987).

[26] E. Eichten, K. Gottfried, T. Kinoshita, K. D. Lane and T. M. Yan, Phys. Rev. D **21**, 203 (1980).

[27] E. Braaten, S. Fleming and A. K. Leibovich, hep-ph/0008091.

[28] G. P. Lepage *et al.*, Phys. Rev. D **46**, 4052 (1992).

[29] G. T. Bodwin, E. Braaten and G. P. Lepage, Phys. Rev. D **51**, 1125 (1995); erratum Phys. Rev. D **55**, 5853 (1997).

[30] F. Abe *et al.,* Phys. Rev. Lett. **79**, 572 (1997).

[31] F. Abe *et al.,* Phys. Rev. Lett. **79**, 578 (1997).

[32] P. Cho and A. K. Leibovich, Phys. Rev. **D53**, 6203 (1996); Phys. Rev. **D53**, 150 (1996).

[33] M. Beneke, M. Krämer, and M. Vänttinen, Phys. Rev. **D 57**, 4258 (1998).

[34] E. Braaten and J. Lee, Nucl. Phys. **B586**, 427 (2000).

[35] A. Petrelli et al., Nucl. Phys. **B514**, 245 (1998).

[36] F. Abe et al., Phys. Rev. Lett. **75**, 4358 (1995).

[37] J. L. Domenech and M. A. Sanchis-Lozano, Phys. Lett. **B476**, 65 (2000) [hep-ph/0012296].

[38] M. Cacciari, M. Greco, M.L. Mangano, and A. Petrelli, Phys. Lett. **B 356**, 553 (1995).

[39] B. A. Kniehl and G. Kramer, Eur. Phys. J. **C6**, 493 (1999); Phys. Rev. **D60**, 014006 (1999).

[40] A. Petrelli, hep-ph/9910274.

[41] E. Braaten, B. Kniehl and J. Lee, Phys. Rev. **D62**, 094005 (2000).

[42] M. A. Sanchis-Lozano and B. Cano-Coloma, Nucl. Phys. **B508**, 753 (1997).

[43] E. Braaten and T.C. Yuan, Phys. Rev. Lett. **71**, 1673 (1993).

[44] E. Braaten and S. Fleming, Phys. Rev. Lett. **74**, 3327 (1995).

[45] P. Cho and M. Wise, Phys. Lett. **B346**, 129 (1995).

[46] T. Affolder *et al.,* Phys. Rev. Lett. **85**, 2886 (2000).

[47] A. K. Leibovich, Phys. Rev. **D56**, 4412 (1997).

[48] M. Beneke and M. Kramer, Phys. Rev. **D55**, 5269 (1997).

[49] E. Braaten and J. Lee, hep-ph/0102130.

[50] E. Braaten, M.A. Doncheski, S. Fleming and M.L. Mangano, Phys. Lett. **B 333**, 548 (1994); M. Cacciari and M. Greco, Phys. Rev. Lett. **73**, 1586 (1994); D.P. Roy and K. Sridhar, Phys. Lett. **B339**, 141 (1994).

[51] M. Beneke and I. Z. Rothstein, Phys. Lett. **B372**, 157 (1996); **389**, 769(E) (1996).

[52] CDF Collaboration, F. Abe *et al.*, Phys. Rev. Lett. **81**, 2432 (1998); Phys. Rev. **D58**, 112004 (1998).

[53] S.S. Gershtein *et al.*, Sov. J. Nucl. Phys. **48**, 327 (1988).

[54] Y.-Q. Chen and Y. Kuang, Phys. Rev. **D 46**, 1165 (1992).

[55] V. V. Kiselev, A. K. Likhoded and A. V. Tkabladze, Phys. Rev. **D 51**, 3613 (1995).

[56] E. J. Eichten and C. Quigg, Phys. Rev. **D 49**, 5845 (1994).

[57] M. Baldicchi and G. M. Prosperi, Phys. Rev. **D 62**, 114024 (2000).

[58] W. Kwong and J.L. Rosner, Phys. Rev. **D 44**, 212 (1991).

[59] H. P. Shanahan, P. Boyle, C. T. Davies and H. Newton [UKQCD Collaboration], Phys. Lett. **B453**, 289 (1999).

[60] A.V. Berezhnoy, A.K. Likhoded, M.V. Shevlyagin, Yad. Fiz. **58**, 730 (1995); A.V. Berezhnoy, A.K. Likhoded, O.P. Yushenko, Yad. Fiz. **59**, 742 (1996); C.-H. Chang *et al.*, Phys. Lett. **B364**, 78 (1995); K. Kolodziej, A. Leike, R. Rückl, Phys. Lett. **B355**, 337 (1995); A.V. Berezhnoy, V.V. Kiselev, A.K. Likhoded, Z. Phys. **A356**, 79 (1996).

[61] J.D. Bjorken, 'Estimate of Decay Branching ratios for hadrons containing Charm and Bottom Quarks', draft report, 07/22/86 (1986) [unpublished]. (http://www-theory.fnal.gov/people/ellis/Bphysics/bjorken.PDF).

[62] M. Neubert, Phys. Rep. **245**, 259 (1994).

[63] I. Bigi, M. Shifman and N. Uraltsev, Ann. Rev. Nucl. Part. Sci. **47**, 591 (1997).

[64] G.T. Bodwin, E. Braaten, G.P. Lepage, Phys. Rev. **D51**, 1125 (1995); T. Mannel, G.A. Schuler, Z. Phys. **C67**, 159 (1995).

[65] M. Lusignoli, M. Masetti, Z. Phys. **C51**, 549 (1991); V.V. Kiselev, Mod. Phys. Lett. **A10**, 1049 (1995); V.V. Kiselev, Int. J. Mod. Phys. **A9**, 4987 (1994); V.V. Kiselev, A.K. Likhoded, A.V.Tkabladze, Yad. Fiz. **56**, 128 (1993); V.V. Kiselev, A.V. Tkabladze, Yad. Fiz. **48**, 536 (1988); G.R. Jibuti, Sh.M. Esakia, Yad. Fiz. **50**, 1065 (1989); Yad. Fiz. **51**, 1681 (1990); C.-H. Chang, Y.-Q. Chen, Phys. Rev. **D49**, 3399 (1994); D. Scora, N. Isgur, Phys. Rev. **D52**, 2783 (1995); A.Yu. Anisimov, I.M. Narodetskii, C. Semay, B. Silvestre–Bra, Phys. Lett. **B452**, 129

(1999);
A.Yu. Anisimov, P.Yu. Kulikov, I.M. Narodetsky, K.A. Ter-Martirosian, Phys. Atom. Nucl. **62**, 1739 (1999).

[66] P. Colangelo, G. Nardulli, N. Paver, Z. Phys. **C57**, 43 (1993);
E. Bagan *et al.*, Z. Phys. **C64**, 57 (1994).

[67] V.V. Kiselev, A.K. Likhoded, O.A. Onishchenko, Nucl. Phys. **B569**, 473 (2000);
V.V. Kiselev, A.K. Likhoded, A.E. Kovalsky, Nucl. Phys. **B585**, 353 (2000).

[68] V.V. Kiselev, A.V. Tkabladze, Phys. Rev. **D48**, 5208 (1993).

[69] I. Bigi, Phys. Lett. **B371**, 105 (1996);
M. Beneke, G. Buchalla, Phys. Rev. **D53**, 4991 (1996);
A.I. Onishchenko, hep-ph/9912424.

[70] C.-H. Chang, S.-L. Chen, T.-F. Feng and X.-Q. Li, Commun. Theor. Phys. **35**, 51 (2001) [hep-ph/0007162].

[71] C.-H. Chang, Y.-Q. Chen, G.-L. Wang and H.-Sh. Zong, hep-ph/010215, hep-ph/0103036.

[72] G. Chiladze, A.F. Falk, A.A. Petrov, Phys. Rev. **D60**, 034011 (1999);
C.H. Chang, J.P. Cheng, C.D. Lü, Phys. Lett. **B425**, 166 (1998);
T.M. Aliev, M. Savci, Phys. Lett. **B434**, 358 (1998); J. Phys. **G25**, 1205 (1999);
P. Colangelo, F. De Fazio, Mod. Phys. Lett. **A33**, 2303 (1999).

[73] M. Dugan and B. Grinstein, Phys. Lett. **B255**, 583 (1991);
M.A. Shifman, Nucl. Phys. **B388**, 346 (1992);
B. Blok, M. Shifman, Nucl. Phys. **B389**, 534 (1993).

[74] S.S. Gershtein *et al.*, hep-ph/9803433;
V.V. Kiselev, Phys. Lett. **B372**, 326 (1996) [hep-ph/9605451].

[75] O.N. Pakhomova, V.A. Saleev, Phys. Atom. Nucl. **63**, 1999 (2000).

[76] V.A. Saleev, hep-ph/0007352.

[77] D. Du, X. Li, Y. Yang, Phys. Lett. **B380**, 193 (1996);
S. Fajfer, D. Prelovsek, P. Singer, Phys. Rev. **D59**, 114003 (1999);
T.M. Aliev, M. Savci, Phys. Lett. **B480**, 97 (2000).

[78] M. Masetti, Phys. Lett. **B286**, 160 (1992);
Y.S. Dai, D.S. Du, Eur. Phys. J. **C9**, 557 (1999).

[79] C. Quigg, in Proc. of the Workshop on B Physics at Hadron Accelerators, Snowmass, Colorado, 1993, eds. P. McBride and C.S. Mishra [Fermilab, Batavia (1994)].

[80] S.S. Gershtein *et al.*, hep-ph/9803433.

[81] OPAL Collaboration, K. Ackerstaff *et al.*, Phys. Lett. **B420**, 157 (1998);
ALEPH Collaboration, R. Barate *et al.*, Phys. Lett. **B402**, 213 (1997);
DELPHI Collaboration, P. Abreu *et al.*, Phys. Lett. **B398**, 207 (1997).

[82] V.V. Kiselev, A.E. Kovalsky, A.K. Likhoded, hep-ph/0002127;
V.V. Kiselev, A.A. Likhoded, A.I. Onishchenko, Nucl. Phys. **B569**, 473 (2000);
A. Abd El-Hady, J.H. Munoz, J.P. Vary, hep-ph/9909406;
C.H. Chang, Y.Q. Chen, Phys. Rev. **D49** 3399 (1994).

[83] P. Avery *et al.*, MCFAST: A Fast Simulation Package for Detector Design Studies, FERMILAB-CONF-97-151, June 1997, to be published in the proceedings of Computing in High-energy Physics (CHEP 97), Berlin, Germany, 7-11 Apr. 1997.

[84] P. Grannis and A. Lucotte, 'Extending the sensitivity to $\sin 2\beta$ in the $B^0/\bar{B}^0$ system using a low p_t $J/\psi \to e^+e^-$ trigger at D0 for Run II', D0 Note 3596, 10 Feb. 1999.

[85] R. Akers *et al.*, Z. Phys. **C67**, 27 (1995);
R. Akers *et al.*, Phys. Lett. **B353**, 545 (1995).

[86] S.S. Gerstein *et al.*, Phys. Atom. Nucl. **63**, 274 (2000).

[87] V. V. Kiselev, A. K. Likhoded and A. I. Onishchenko, Phys. Rev. D **60**, 014007 (1999);
V.V. Kiselev, A.K. Likhoded, A.I. Onishchenko, Eur. Phys. J. **C16**, 461 (2000);
A.K. Likhoded, A.I. Onishchenko, hep-ph/9912425.

[88] A.I. Onishchenko, private communication;
X.-H. Guo, H.-Y. Jin, X.-Q. Li, Phys. Rev. **D58**, 114007 (1998).

[89] V. V. Kiselev, A. E. Kovalsky and A. K. Likhoded, Nucl. Phys. **B585**, 353 (2000).

[90] A. K. Likhoded and A. I. Onishchenko, hep-ph/9912425.

[91] V. V. Kiselev, A. K. Likhoded and A. I. Onishchenko, Eur. Phys. J. **C16**, 461 (2000) [hep-ph/9901224].

[92] V. V. Kiselev, A. K. Likhoded and A. I. Onishchenko, Phys. Rev. **D60**, 014007 (1999).

[93] A. I. Onishchenko, hep-ph/0006295.

[94] A. K. Likhoded, private communication, (25 Feb. 2000).

[95] CDF Collaboration, F. Abe *et al.*, Phys. Rev. Lett. **77**, 1439 (1996).

[96] M. J. Savage and R. P. Springer, Int. J. Mod. Phys. **A6**, 1701 (1991).

[97] B. Guberina, B. Melic and H. Stefancic, hep-ph/9911241.

[98] C. H. Chang, Y. Q. Chen and R. J. Oakes, Phys. Rev. **D54**, 4344 (1996).

[99] P. Nason, S. Dawson, R. K. Ellis, Nucl. Phys. **B327**, 49 (1988).

[100] C. Peterson *et al.*, Phys. Rev. **D27**, 105 (1983).

[101] Particle Data Group, Eur. Phys. J. **C15**, 1 (2000).

[102] W. Hao, V. Papadimitriou, internal CDF note 4884, March 1999, (unpublished).

[103] T. Keaffaber, Ph.D. Thesis, Purdue University, May 2000.

[104] C. H. Chang, Y. Q. Chen, Phys. Rev. **D49**, 3399 (1994).

[105] S. S. Gershtein *et al.*, "Physics of B_c mesons", Phys. Usp. **38**, 1 (1995).

[106] S. S. Gershtein *et al.*, "Theoretical Status of the B_c meson", hep-ph/9803433.

[107] V.V. Kiselev and A.K. Likhoded, these proceedings, section (9.3.3)

[108] F. Abe *et al.*, Phys. Rev. Lett. **77**, 5176 (1996).

[109] "Summary or B Physics Prospects with the CDF II Detector", CDF Collaboration, internal CDF note 5045, June 1999 (submitted to the Fermilab PAC).

[110] F. Abe *et al.*, Phys. Rev. Lett. **77**, 1945 (1996).

[111] J.D. Bjorken, 'Is the *ccc* a new deal for baryon spectroscopy', Fermilab-Conf-85/69.

[112] D. Ebert, R. N. Faustov, V. O. Galkin, A. P. Martynenko and V. A. Saleev, Z. Phys. **C76**, 111 (1997) [hep-ph/9607314].

[113] J. Richard, hep-ph/9407224.

[114] D. B. Lichtenberg, R. Roncaglia and E. Predazzi, Phys. Rev. D **53**, 6678 (1996) [hep-ph/9511461].

[115] S. Fleck and J. M. Richard, Prog. Theor. Phys. **82**, 760 (1989).

[116] D. U. Matrasulov, M. M. Musakhanov and T. Morii, Phys. Rev. C **61**, 045204 (2000) [hep-ph/0004147].

[117] M. A. Moinester, Z. Phys. **A355**, 349 (1996) [hep-ph/9506405].

[118] E. Bagan, M. Chabab and S. Narison, Phys. Lett. **B306**, 350 (1993).

[119] S. S. Gershtein, V. V. Kiselev, A. K. Likhoded and A. I. Onishchenko, Mod. Phys. Lett. **A14**, 135 (1999) [hep-ph/9807375].

[120] S. S. Gershtein, V. V. Kiselev, A. K. Likhoded and A. I. Onishchenko, Phys. Rev. **D62**, 054021 (2000).

[121] M. L. Stong, hep-ph/9505217.

[122] V. V. Kiselev and A. I. Onishchenko, Nucl. Phys. **B581**, 432 (2000) [hep-ph/9909337].

[123] M. A. Sanchis-Lozano, Nucl. Phys. **B440**, 251 (1995) [hep-ph/9502359].

[124] S.S. Gershtein, V.V. Kiselev, A.K. Likhoded, A.I. Onishchenko, Mod. Phys. Lett. **A14**, 135 (1999) [hep-ph/9807375];
Heavy Ion Phys. **9**, 133 (1999) [hep-ph/9811212].

[125] A. De Rujula, H. Georgi and S. L. Glashow, Phys. Rev. **D 12**, 147 (1975).

[126] J. C. Collins, D. E. Soper and G. Sterman, in: *Perturbative QCD*, ed. A. H. Mueller (World Scientific, 1989).

[127] J. C. Collins and D. E. Soper, Nucl. Phys. **B194**, 445 (1982).

[128] W. Furmanski and R. Petronzio, Phys. Lett. **97B**, 437 (1980).

[129] G. Curci, W. Furmanski, and R. Petronzio, Nucl. Phys. **B175**, 27 (1980).

[130] R. K. Ellis, W. J. Stirling and B. R. Webber, *QCD and collider physics*, *Cambridge, UK: Univ. Pr. (1996).*

[131] J. Binnewies, B. A. Kniehl, and G. Kramer, Z. Phys. **C65**, 471 (1995) [hep-ph/9407347].

[132] M. Greco and S. Rolli, Phys. Rev. **D52**, 3853 (1995), [hep-ph/9409356].

[133] B. A. Kniehl, G. Kramer and B. Potter, Nucl. Phys. **B582**, 514 (2000) [hep-ph/0010289].

[134] S. Kretzer, Phys. Rev. **D62**, 054001 (2000) [hep-ph/0003177].

[135] L. Bourhis, M. Fontannaz, J. P. Guillet and M. Werlen, hep-ph/0009101.

[136] C. Peterson, D. Schlatter, I. Schmitt, and P. Zerwas, Phys. Rev. **D27**, 105 (1983).

[137] A. V. Berezhnoy, V. V. Kiselev, and A. K. Likhoded, hep-ph/9901333.

[138] A. V. Berezhnoy, V. V. Kiselev, and A. K. Likhoded, hep-ph/9905555.

[139] P. Nason *et al.*, hep-ph/0003142.

[140] G. Altarelli and G. Parisi, Nucl. Phys. **B126**, 298 (1977).

[141] V. N. Gribov and L. N. Lipatov, Yad. Fiz. **15**, 781 (1972).

[142] Y. L. Dokshitzer, Sov. Phys. JETP **46**, 641 (1977).

[143] B. Mele and P. Nason, Nucl. Phys. **B361**, 626 (1991).

[144] E. Braaten, K. Cheung, S. Fleming, and T. C. Yuan, Phys. Rev. **D51**, 4819 (1995), [hep-ph/9409316].

[145] R. L. Jaffe and L. Randall, Nucl. Phys. **B412**, 79 (1994), [hep-ph/9306201].

[146] P. Nason and C. Oleari, Nucl. Phys. **B521**, 237 (1998), [hep-ph/9709360].

[147] G. Rodrigo, M. Bilenky, and A. Santamaria, Nucl. Phys. **B554**, 257 (1999), hep-ph/9905276.

[148] W. Bernreuther, A. Brandenburg, and P. Uwer, Phys. Rev. Lett. **79**, 189 (1997), [hep-ph/9703305].

[149] P. Nason and C. Oleari, Nucl. Phys. **B565**, 245 (2000), [hep-ph/9903541].

[150] ALEPH, D. Buskulic *et al.*, Phys. Lett. **B357**, 699 (1995).

[151] OPAL, R. Akers *et al.*, Z. Phys. **C67**, 27 (1995).

[152] ARGUS, H. Albrecht *et al.*, Z. Phys. **C52**, 353 (1991).

[153] SLD, K. Abe *et al.*, Phys. Rev. Lett. **84**, 4300 (2000), [hep-ex/9912058].

[154] M. Cacciari and M. Greco, Nucl. Phys. **B421**, 530 (1994), [hep-ph/9311260].

[155] M. Cacciari, M. Greco, and P. Nason, JHEP **05**, 007 (1998), [hep-ph/9803400].

[156] F. I. Olness, R. J. Scalise, and W.-K. Tung, Phys. Rev. **D59**, 014506 (1999), [hep-ph/9712494].

[157] M. Cacciari and M. Greco, Z. Phys. **C69**, 459 (1996), [hep-ph/9505419].

[158] M. Cacciari *et al.*, Nucl. Phys. **B466**, 173 (1996), [hep-ph/9512246].

[159] S. Frixione, M. L. Mangano, P. Nason, and G. Ridolfi, hep-ph/9702287, published in *Heavy Flavours II*, eds. A.J. Buras and M. Lindner, (World Scientific, Singapore).

[160] DELPHI, P. Abreu *et al.*, Z. Phys. **C57**, 181 (1993).

[161] OPAL, G. Alexander *et al.*, Phys. Lett. **B364**, 93 (1995).

[162] V. G. Kartvelishvili, A. K. Likhoded, and V. A. Petrov, Phys. Lett. **B78**, 615 (1978).

[163] P. D. B. Collins and T. P. Spiller, J. Phys. **G11**, 1289 (1985).

[164] B. W. Harris and J. Smith, Phys. Rev. **D57**, 2806 (1998), [hep-ph/9706334].

[165] S. Frixione, M. L. Mangano, P. Nason and G. Ridolfi, Nucl. Phys. **B412**, 225 (1994), [hep-ph/9306337].

[166] ZEUS, J. Breitweg *et al.*, Eur. Phys. J. **C12**, 35 (2000), [hep-ex/9908012].

[167] ZEUS, J. Breitweg *et al.*, Eur. Phys. J. **C6**, 67 (1999), [hep-ex/9807008].

[168] H1, C. Adloff *et al.*, Z. Phys. **C72**, 593 (1996), [hep-ex/9607012].

[169] E. Norrbin and T. Sjostrand, hep-ph/9905493.

[170] M. G. Bowler, Zeit. Phys. **C11**, 169 (1981).

[171] T. Sjostrand, Comput. Phys. Commun. **82**, 74 (1994).

[172] H. Jung, Comp. Phys. Commun. **86**, 147 (1995).

[173] B. Andersson, G. Gustafson, G. Ingelman, and T. Sjostrand, Phys. Rept. **97**, 31 (1983).

[174] WA82 Collaboration, M. Adamovich *et al.*, Phys. Lett. **B305** 402 (1993); WA92 Collaboration, M. Adamovich *et al.*, Nucl. Phys. **B495** 3 (1997); E769 Collaboration, G.A. Alves *et al.*, Phys. Rev. Lett. **72** 812 (1994); E791 Collaboration, E.M. Aitala *et al.*, Phys. Lett. **B371** 157 (1996).

[175] E. Norrbin and T. Sjostrand, Phys. Lett. **B442**, 407 (1998), [hep-ph/9809266].

[176] E. Norrbin and T. Sjostrand, Eur. Phys. J. C **17**, 137 (2000) [hep-ph/0005110].